SPIN-GLASS BEHAVIOR IN DILUTE ALLOYS WITH ATOMIC ORDER-DISORDER TRANSITIONS

By

James Stephen Shell

A DISSERTATION

Submitted to
Michigan State University
in partial fulfillment of the requirements
for the degree of

DOCTOR OF PHILOSOPHY

Department of Physics

1982

ABSTRACT

SPIN-GLASS BEHAVIOR IN DILUTE ALLOYS WITH
ATOMIC ORDER-DISORDER TRANSITIONS

By

James Stephen Shell

An experimental investigation of the influence of binary host atomic order-disorder transitions on the spin-glass behavior of dilute alloys has been conducted. The investigation was carried out with the use of a homebuilt vibrating sample magnetometer (VSM), a commercial squid based susceptometer, and an AC mutual inductance bridge apparatus. These instruments were used to study the magnetic susceptibility of three host alloy systems with the emphasis on $(Cu_3Pt)_{1-x}Mn_x$.

An overview of general spin-glass theory and a discussion of experimental considerations including the design, calibration, and operation of the VSM are presented. The nature and reliability of the samples is discussed prior to the presentation of experimental results. The observed experimental behavior is presented and discussed in light of mean field theories, free electron RKKY couplings, mean free paths, Brillouin zones, and Fermi momentum effects. None of the above approaches can explain the results in even a qualitative

fashion. Finally, preliminary investigations were started on Cu_3AuMn alloys and the hysteresis behavior of Cu_3PtMn alloys.

Perhaps this work will help make clear to them
why I chose to do physics. In any case, I would like
to dedicate this dissertation to my parents.

I w

be the

of the

search

Profess

ge to t

thesis

I would

rent d

ultip

nical

Mr. Ca

lay id

Yukon

Mr. Do

for sa

Koski

Patter

cellen

to Mrs

like t

Suscep

ACKNOWLEDGMENTS

I would like to thank Professor Carl L. Foiles for suggesting the thesis topic and providing expert guidance throughout the course of the research. His clarity of thought and patience made this research most enjoyable. I would also like to express my appreciation to Professor Jerry Cowen for many fruitful discussions and for introducing me to the S.H.E. susceptometer. The AC susceptibility data in this thesis is due largely to the efforts of Professors Foiles and Cowen. I would like to thank Professor Gerald Pollack for constant encouragement during the course of this work, especially as my outside interests multiplied. I am also deeply grateful to various members of the technical staff for their support. In particular, I would like to thank Mr. Daniel Edmunds, without whose help much of the electronics would lay idle or never have been built. Thanks are also due to Mr. John Yurkon for assistance in troubleshooting the magnet power supply, Mr. Donn Schull for general electronics assistance, Mr. Boyd Shumaker for sample preparation assistance and Mr. Bob Cochrane, Mr. Dick Hoskins, and Mr. Floyd Wagner for their assistance in machine shop matters. I am also grateful to Mrs. Peri-Anne Warstler for her excellent typing of this thesis especially under such short notice and to Mrs. Carol Edmunds for many a fine home-cooked meal. I would also like to thank the Chemistry Department for the use of their Squid susceptometer.

The

Science

The financial support of the Physics Department and the National Science Foundation has been appreciated.

Oracle

LIST O

LIST O

I. IN

A.

B.

C.

II. O

A.

B.

III.

A

B

C

D

E

F

G

H

I

J

TABLE OF CONTENTS

LIST OF TABLES

LIST OF FIGURES

I. INTRODUCTION

A. Why Study Magnetism?

To the uninitiated, the topic of this thesis and the field of magnetism in general may seem either esoteric and without application, or an old field of study whose prime is long past. In fact, just the opposite is true and it is the purpose of this section to discuss the role of magnetism and dilute alloys in the field of condensed matter physics. Historically, many important developments in condensed matter physics and many-body physics first appeared in the theory of magnetism. The reason for this may lie with the relative ease with which magnetic systems can be visualized, as compared with other interacting many-body systems. The flexibility of being able to work both classically and quantum mechanically, as well as in spaces (spin or real) of arbitrary dimension is most certainly an important aid.

In fact, one might argue that the modern era of many-body theory actually began in the 1950's when the theory of spin waves in metallic ferromagnetic materials was developed. Even the Kondo problem has provided an excellent many-body system which can be checked experimentally. It was also one of the first problems to be attacked using the powerful, newly developed theory of the renormalization group.[1] It has recently been solved exactly.[2]

Another example of an important concept whose origin lay in the

theory of magnetism is that of broken symmetry. This idea arose from early attempts to understand anti-ferromagnetism.[3] The problem was this. The conventional alignment of spins is an acceptable idea within mean field theory. However, such a state is not an eigenstate of the system and therefore cannot be the true ground state. More serious is the problem that such a state does not satisfy the symmetry requirements of quantum mechanics. A ground state of a quantum mechanical system must be an eigenstate of any symmetry which the Hamiltonian possesses. The Heisenberg Hamiltonian has rotational symmetry in spin space. A single Neel state does not. The true ground state must therefore be a symmetric linear combination of all the orientationally degenerate Neel states. This symmetry has definite consequences for the energy level spectrum. It requires the existence of anti-ferromagnetic spin waves, which are probably the first example of the use of Goldstone bosons in theoretical physics. This introduction of Goldstone bosons is currently being used in certain Lagrangian field theories of elementary particle physics.

Another area where magnetism has made important inroads is in the field of phase transitions and critical phenomena. The first example of an interacting many-body system which is completely solvable and undergoes a phase transition was probably the 2-D Ising model in zero field solved by Onsager in 1944.[4] Magnetic systems were natural systems to consider because the order parameter is generally quite transparent and very physical. Most of the phase transitions to date have dealt with systems in which the ordered phase has simple long range order. These include ferromagnets,

antiferromagnets, ferrimagnets, helical and canted structures. The dilute magnetic alloys studied in this thesis do not order into such simple geometrical arrangements. Rather, the spins appear to freeze in random directions. This may be an example of a new, more subtle, form of phase transition to an ordered phase where the spins are strongly correlated but exhibit no simple long range order. A currently investigated system, the 2-D XY model, shows some promise towards explaining the spin-glass transition, the helium superfluid transition, and a possible mechanism for quark confinement.[5]

It is also possible that the new field of dynamic critical phenomena will enter the picture. The dynamic properties of a system (transport coefficients, relaxation rates, etc.) all depend on the equations of motion and are not simply determined by the equilibrium distribution of the particles at a given instant of time. The static properties of a system (thermodynamic coefficients, linear response to time independent phenomena) are determined by the equilibrium distribution of particles at a single time. The modern field of dynamic critical phenomena may be necessary to explain spin-glass behavior since the spin-glass transition does appear to be cooperative and yet time dependent.[6] Finally, condensed matter physics has entered the new field of disordered systems, and magnetic systems are once again playing an important role, and will certainly aid in establishing fundamental concepts about these systems. It is likely that other areas of physics will draw on this knowledge, because often the magnetic analogs are the simplest systems that can be checked experimentally.

B. Preface of Thesis Content

The measurements described in this thesis are an attempt to shed further light on the nature of impurity-impurity interactions in dilute magnetic alloys. Our studies have dealt with metallic spin-glass systems in general, and the low temperature behavior of the magnetic moments in order-disorder binary alloys. By controlling the degree of order of the host we have a nice way of modifying the interactions between impurities in a systematic fashion. The goal of the research was to determine the effect of the host condition on the paramagnetic and spin-glass properties of the alloys.

Since the alloys under study exhibit spin-glass behavior at sufficiently low temperatures, a general introduction to these systems is in order. In the context of this thesis, the following definition of a spin-glass can be given. A spin-glass is a random, metallic, magnetic system characterized by a random freezing of the magnetic moments without long range order. Whether or not this freezing occurs gradually or suddenly is a question not easily answered, but certain thermodynamic measurements do show a sharp behavior. The discontinuity in the slope of χ versus T is often associated with this transition, and defines what we shall call the freezing temperature T_f (or the spin-glass temperature T_{sg}). The most common metallic spin-glasses are typically transition metal impurities in non-magnetic hosts. Usually the spin-glass regime exists for only a limited concentration range of the impurity. We can picture the situation roughly as follows. See Figure 1.

In the very dilute regime the isolated impurity-conduction electron

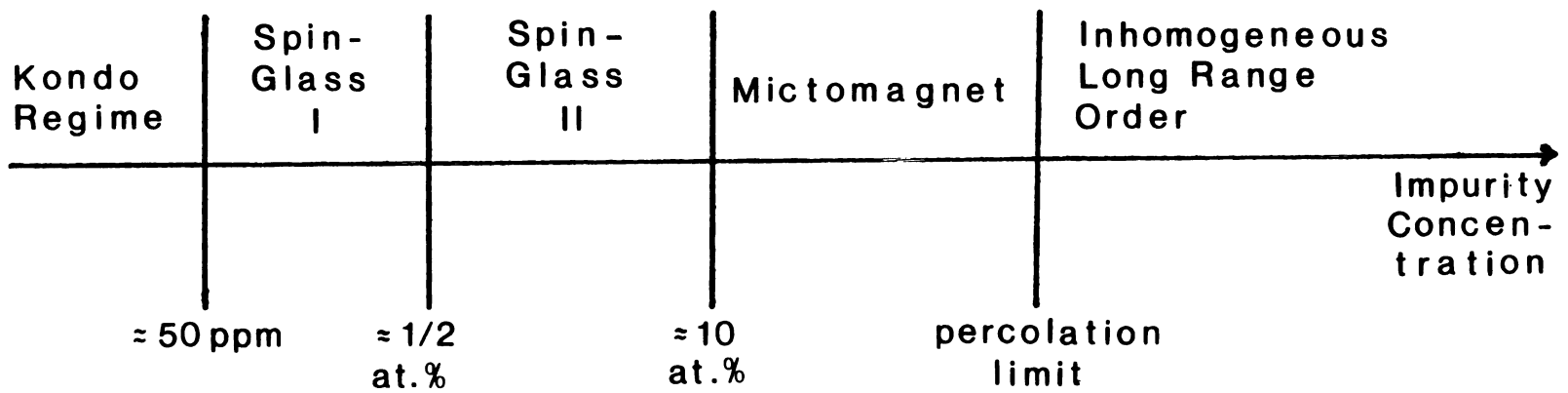

Figure 1. Concentration dependence of magnetic phases in metallic alloys.

interaction is the dominant effect. It results in the well-known Kondo effect. This interaction causes a weakening or fluctuation of the d or f electron spin at the so-called Kondo temperature T_K, given by

$$T_K = \frac{D}{k_B} e^{-\frac{1}{N|J|}}$$

where D = bandwidth, N = density of states at the Fermi level, and J is the effective exchange parameter. For $T < T_K$, the Kondo effect prevents strong impurity-impurity interactions. For CuMn, $T_K \simeq 30$ mK.

In the 50 ppm to 1/2 at.% concentration range, a scaling approach based on RKKY exchange seems to work. Physically it is assumed that essentially single spins are interacting in this regime. Here one finds the first evidence of spin-glass freezing and $T_f \propto C$. The random molecular field approximation also seems to work best here. In the 1/2 at.% to 10 at.% concentration range we begin to see the breakdown of scaling, and small cluster formation is possible - mostly pairs and triplets. Some indication of this could be the non-linear concentration dependence of T_f. The interactions are thought to be RKKY plus short range interactions.

Above 10 at.% and up to the percolation limit the dilute alloys form mictomagnets. Here the observed behavior is dominated by cluster formation. Above the percolation limit one sees inhomogeneous long range order with definite signs of ferromagnetic behavior (at approximately 15 at.%) and antiferromagnetic behavior

(at approx

the subjec

nigh conce

nsurity c

In this re

ost insign

In the cas

as at 'ea

for the in

Thus, in t

robabili

about 6 o

neighbors

same numb

from the

clusters

Final

spin-glas

temperatu

oments wh

relate.

One m

The data

(See Table

others sho

difficult

(at approximately 45%) for FCC latices. The materials that are the subject of this thesis are probably best thought of as in the high concentration region of the spin-glass I phase. We deal with impurity concentrations of the order of 1/4 at.% to about 3 at.%. In this regime clusters are not thought to play a role, and yet a not insignificant fraction of the impurities have nearest neighbors. In the case of an FCC lattice, the probability that a given impurity has at least one nearest neighbor is shown in Table 1. The numbers for the inclusion of next nearest neighbors are also presented. Thus, in the case where we have nominally 1/2 at.% impurities, the probability of finding clusters of two or more impurities is only about 6 or 8 percent if you allow nearest neighbors and next nearest neighbors respectively. However, for the 3 percent samples, these same numbers are 31% and 42%, respectively. So, although we are far from the single isolated impurity limit, the probability of having clusters with greater than 2 atoms falls off very quickly.

Finally, let us comment on the temperature dependent behavior of spin-glasses. For temperatures much greater than the freezing temperature the general experimental evidence indicates that the moments which are statistically close to other moments begin to correlate.

One might say that some form of short range order begins to grow. The data near the freezing temperature is somewhat of a puzzle. (See Table 2). Sharp discontinuities are found in some measurements, others show only broad changes of behavior. Other experiments are difficult to interpret either way. At still lower temperatures

Table 1. Cluster Probabilities for Specific Dilute Concentrations.

Impurity Concentration	Probability an impurity has at least 1 n.n. (a)	Probability an impurity has at least 1 n.n. or 1 n.n.n. (b)
1/2 at %	0.058	0.086
1 at %	0.114	0.166
2 at %	0.215	0.305
3 at %	0.306	0.422

a. See Reference 7.

b. See Reference 8.

Table 2. Summary of Experimental Results Relating to the Freezing Temperature.

Well-Defined T_{sg}	Broad T_{sg}
Mossbauer Effect	Specific Heat
Susceptibility	Resistivity
$^{+}$-precession	Thermoelectric Power
Anomalous Hall Effect	Nuclear Magnetic Resonance
Remanence	Ultrasonic Velocity
Irreversibility	
? Neutron Scattering ?	

we see the existence of various types of excitations. These include diffuse non-coherent spin fluctuations, localized magnetic excitations, and others.

C. Magnetic Behavior in Order-Disorder Alloys

This thesis is in some ways a natural extension of some earlier work on magnetic interactions in atomic order-disorder alloys. The earlier work was carried out by T. W. McDaniel and C. L. Foiles[9] (hereafter denoted by MF). Their study was essentially a high temperature (77°K to 300°K) magnetic investigation of CuPdMn alloys. This thesis is essentially a low temperature (4.2°K to 77°K) magnetic investigation of Cu_3PtMn and CuPdMn alloys with the emphasis on the former alloy system. The reasons for the change in temperature regime of interest and principle alloy of interest are as follows:

(1) The temperature range from 4.2°K to 77°K affords one the general advantage of increased sensitivity in the measurement of magnetic parameters which can be of great aid when studying dilute alloys.

(2) The low temperature regime is particularly useful in this case because Cu_3PtMn and CuPd(17)Mn and CuMn all order into the spin-glass phase for an appropriate manganese concentration.

(3) The decision to focus on Cu_3PtMn rather than CuPd(17)Mn alloys was primarily a matter of technical convenience. First of all, because platinum is a 5d transition metal and palladium is a 4d

transitio

that much

metal.

most with

order can

rents, th

spectrum

x-ray sca

ductile ef

domains.

The s

the latti

$Cu_{0.33}Pd_{0}$

to note w

intensity

atomic pe

composit

in the e

lation.

of the C

fact, slo

gonal dis

a = 3.70

this reas

into the

quite as

transition metal, its atomic x-ray scattering form factor is just that much more different from copper, which is a 3d transition metal. This allows one to determine the degree of order in the host with better precision. Although indications of the amount of order can be estimated from indirect means such as transport measurements, the presence or absence of superlattice lines in the x-ray spectrum is certainly the most conclusive. Greater clarity in the x-ray spectrum is also desirable if one is going to worry about subtle effects such as the existence or period of anti-phase domains.

The second matter of technical convenience is concerned with the lattice structure of the alloys. MF concentrated mostly on $Cu_{0.83}Pd_{0.17}$ which we have denoted by CuPd(17). It is interesting to note why Cu_3Pd was not chosen. It was discovered that the maximum intensity of the superlattice lines occurs at approximately 17 atomic percent palladium and not 25 atomic percent which is the composition of maximum order for the Cu_3Au structure. The minimum in the electrical resistivity also occurs at 17 atomic percent palladium. All this indicates that the ordered phase of Cu_3Pd is not of the Cu_3Au structure, but differs in some essential way. In fact, slow cooling below the critical temperature leads to a tetragonal distortion.[10] The lattice spacings in angstroms are $a = 3.703$ and $c = 3.655$ yielding a c/a ratio of 0.987.[11] For this reason, the host chosen by MF was CuPd(17) which does order into the Cu_3Au structure. Of course, this ordered phase isn't quite as nice as the Cu_3Au ordered phase because there are not

enough palladium atoms to occupy all the corners of the unit cell. The problem of tetragonal distortion is essentially non-existent in the Cu_3Pt system.

As I mentioned earlier, this thesis is in some ways a natural extension of earlier work. Although the principle phenomena of interest, that is, spin-glass behavior, is unique to this thesis, some of the results gleaned from the MF study have direct relevance to this research. It is assumed by the author that the reader of this thesis will not have a working knowledge of the MF study. In the spirit of continuity, I will present a brief synopsis of the MF study. Some of their results have direct relevance to this thesis. A more concise account of their work can be found in Reference 12.

The MF study concerned itself with the influence of order-disorder transitions upon the paramagnetic Curie temperature, θ, of alloys with dilute concentrations of manganese. Most of their results are based on the $(Cu_{0.83}Pd_{0.17})_{1-x}Mn_x$ system. Their measurements include (1) room temperature measurements of magnetization versus field up to approximately 4.7 Koe and (2) magnetization versus temperature measurements at 3 KOe from 80 to 290°K. All the data was taken with a homebuilt vibrating sample magnetometer.

The susceptibility in both states of order obeyed a Curie-Weiss Law. This is generally written as

$$\chi = \frac{C}{T-\theta} \qquad \text{where } C = \frac{Ng^2\beta^2 S(S+1)}{3k} \qquad \text{is called}$$

the Curie

g, Θ and k

to as the

moment is

operationa

$(\frac{3kC}{N g^2})^{1/2}$.

the experi

is simplif

of the dat

The di

tially inc

a more neg

= -10 °K/a

dΘ/dc = +

moment on

netons inc

order of t

usually fo

study atte

Θ(c) for c

of dΘ/dc f

They c

tration ha

(1) S

low mangan

lattice wo

the Curie constant, N is the number of magnetic atoms, the symbols g, β and k have their standard meanings, and θ is usually referred to as the paramagnetic Curie temperature. The effective magnetic moment is theoretically defined as $P_{eff} = g(S(S+1))^{1/2}$ and is operationally determined from the Curie-Weiss Law using $P_{eff} = (\frac{3kC}{N\beta^2})^{1/2}$. Incidentally, if the comparison is made by converting the experimental data to molar values so that $N = N_0$, the calculation is simplified. This is because $\frac{3k}{N_0\beta^2}$ is almost exactly 8.0. Most of the data presented in this thesis will be in molar values.

The disordered samples displayed a θ very near zero and essentially independent of concentration. The ordered samples displayed a more negative θ which was linear in Mn concentration with $d\theta/dc \simeq -10$ °K/at.% Mn. This should be compared with CuMn which has $d\theta/dc \simeq +10$°K/at.% Mn. Within experimental error the magnetic moment on the manganese ion was a constant 5.5 ± 0.1 Bohr magnetons independent of manganese concentration and the state of order of the CuPd host. For Mn in copper the effective moment is usually found to be 4.9 Bohr magnetons. Two of the problems the MF study attempted to resolve were (1) the very different behavior of $\theta(c)$ for ordered and disordered CuPdMn and (2) the opposite signs of $d\theta/dc$ for CuMn and CuPd(17)Mn.

They concluded that the dependence of θ upon manganese concentration has three possible origins.

(1) Some form of long range antiferromagnetism may occur. The low manganese concentration coupled with its random placement in the lattice would tend to discount this hypothesis. However, the large

Pd concentration may change things drastically. PdMn yields weak ferromagnetic behavior which is destroyed by anti-parallel couplings near 5 atomic percent manganese.

(2) A coupling between impurities via the RKKY interaction. The experimentally observed dependence on concentration and host condition is very close to that predicted by Kok and Anderson.[13] There is a problem, however, with the sign of $d\theta/dc$. Although ordered CuPd forms a simple cubic lattice with a unit cell having a basis of 4 atoms, the array of lattice sites is still face-centered cubic. Thus, any lattice sum over all sites should yield the same result as copper. The number of electrons per atom in a free electron model ranges from 0.83 to 1.0 as the valence of palladium changes from zero to one. The lattice sum for an FCC structure is near an extremum for e/a equal to 1.0. Thus one expects only minor changes in the lattice sum as the valence of palladium is allowed to vary. A change in sign of $d\theta/dc$ therefore bodes some difficulty for a free-electron RKKY theory. However, there may exist a redeeming possibility. The sign of $d\theta/dc$ can be changed simply by adding a 180° phase shift in the RKKY exchange. DeGennes[14] found that by introducing a mean free path into the RKKY coupling, the oscillations in spin polarization are attenuated and shifted in phase.

As far as an interpretation of the disordered host data is concerned, the situation is encouraging but by no means conclusive. The fact that θ and $d\theta/dc$ are small is what one would expect from a Kok and Anderson argument, but the equivalence of a disordered

host and an amorphous or liquid host is by no means obvious.

The introduction of atomic order must certainly change the Fermi surface and this opens the door to possible anisotropies in the RKKY coupling. By examining $\underline{Cu_3AuMn}$ (0.01) and $\underline{Cu_3PtMn}$ (0.01), MF found the change in θ as a function of order was 5 times smaller than for the $\underline{CuPdMn}$ system. MF argue that the sharp contrast in θ behavior rules out anisotropy effects in the Fermi surface as the primary cause of the sign of θ.

The possible ogre of preferential occupancy of certain lattice sites by the impurities must also be considered. This behavior could have drastic effects on the lattice sum. Some work on this problem has been done on the Cu_3Pt alloys which are the main interest of this thesis. To my knowledge, no clear evidence for the $\underline{CuPd(17)}$ system was presented in the MF study.

The final possibility considered by MF was that of local environment effects. Work by Kouvel and Owen suggest that the Mn impurities interact via a form of super-exchange through the copper atoms. MF argue that if the coupling element is changed from Cu to Au to Pt to Pd, a systematic change in the super-exchange might account for their experimental results. In fact, they conclude that this is the most likely explanation.

Several of the questions raised in the MF study continue to persist for the $\underline{Cu_3PtMn}$ alloys.

(1) There still exists the difference in θ versus concentration behavior for the ordered and disordered alloys with the added

wrinkle that the θ dependence for the disordered alloys is not quite independent of concentration, but considerably weaker than that of the ordered samples.

(2) The discrepancy in the sign of θ compared with CuMn still persists since Cu_3Pt also has an FCC lattice structure.

Two additional questions raised in this study are the following:

(3) Why are the spin-glass freezing temperatures for this alloy roughly linear with manganese concentration with $(dT_{sg}/dc)_{DOS} > (dT_{sg}/dc)_{OS}$?

(4) There are also weak indications that $\theta(c)$ may change sign for the Cu_3PtMn alloys for sufficiently dilute amounts of manganese. Is this sign reversal real and how does it relate to an analogous sign reversal in CuMn?

II. GENERAL SPIN-GLASS THEORY

The purpose of this section is to give a brief introduction to the general theory of spin-glasses. It should be noted that there does not exist any generally accepted theoretical understanding of these systems. There has been a great deal of theoretical activity in recent times, but no unifying thread has emerged thus far. The discussion will be presented in two parts. First, a discussion of mean field theories will be presented. The utility of mean field theories resides primarily in their simple physical interpretation and ease with which one can calculate physical properties. Thus it is logical that this be the first step in probing a theoretically complex topic. The second part of the discussion will touch on some of the other non-mean-field approaches, especially virial expansions and high temperature expansions. The discussion is intended to present the topic from a somewhat historical/logical approach and is certainly a reflection of the author's personal viewpoint. This will also serve as a brief introduction to some of the ideas and models that will be used to interpret the experimental results.

Before I begin the discussion of mean-field theories proper, let me comment on why the spin-glass problem has been one of such great difficulty. It is the goal of equilibrium statistical mechanics to calculate the free energy $F_N(\beta)$ of a system of N particles. Then the thermodynamic limit ($N \to \infty$) is taken to find the free

energy per particle $f(\beta) = \lim_{N \to \infty} F_N(\beta)/N$. Now the thermodynamic limit is often needed in the evaluation of the partition function Z_N before the logarithm is taken. This allows one to neglect factors in Z_N of lower than exponential order in N. This particular convenience is upset by the introduction of randomness. A random system is described by a Hamiltonian which contains random parameters which usually represent the interactions in the random quenched configuration. To calculate the physical properties we must average over all possible configurations. This is achieved by averaging $F_N(\beta)$ over some probability distribution for the random parameters. This average must be computed after taking the logarithm, but before taking the thermodynamic limit. That is, we must calculate

$$-\beta f(\beta) = \lim_{N \to \infty} \frac{1}{N} \langle \ell n \, Z_N(\beta) \rangle_{\text{randomness}} \tag{2.1}$$

Notice that the thermodynamic limit can no longer be used directly in the evaluation of Z_N. In addition, averaging over the random parameters is difficult because the logarithm prevents any useful factorization into a product of one parameter averages. In short, the primary difficulty in these theories stems from the quenched nature of the disorder.

Two methods of attack have been formulated within mean-field theory. One is the $n \to 0$ replica method of Edwards and Anderson. They remove the disorder at the outset and are left with performing a thermal trace over the exponential of some effective Hamiltonian.

The second approach is typified by the work of Thouless-Anderson and Palmer. They perform the thermal averages at the outset and are left with averaging over the disorder. These theories will be considered in a bit more detail shortly. Neither of these methods allows us to use the thermodynamic limit in the evaluation of Z. In the case of the replica method, statistical mechanics demands that we calculate

$$\lim_{N \to \infty} \lim_{n \to 0} \frac{\langle Z^n \rangle - 1}{n} ,$$

but most theoreticians would prefer to interchange the limits. The legality of this interchange is by no means obvious. Because the non-equilibrium nature of this problem is so important, I would like to say a few more words about it. As shown in Equation (2.1), the desired free energy involves the calculation of $\langle \ell n \langle Z \rangle_s \rangle_c$ when $\langle \ \rangle_s$ denotes a thermal trace over the spins and $\langle \ \rangle_c$ denotes a configuration average. In fact, if we were to do the simpler calculation $\ell n \langle Z \rangle_{s,c}$, what would we have? We must have in that case a system where the positions of the particles are in thermal equilibrium as well as the spins. That is, we have described a gas of paramagnetic particles interacting with spin-dependent exchange forces. And in this case there is a real correlation between the relative spins of the particles and their positions. But in the spin-glass systems of interest, the atoms have condensed into the solid state and are no longer free to move. The former systems are referred to as annealed, the latter are called quenched. In

the spin-glass case the randomness is immobile. Therefore, the averaging must be carried out over a physical observable. The free energy is such an observable, the partition function is not. There is undoubtedly still some correlation between the spin and spatial configurations in the condensed systems, but it is certainly different from the case of the paramagnetic gas.

Rather than go through a detailed discussion of any one particular mean-field theory, a general overview of the work to date will be given. This overview is certainly not complete, but is designed to show how the various models fit into the overall scheme of things. See the flowchart in Figure 2.

Before the first actual development of mean field theories for random systems, the problem was being attacked with diagrammatic expansions. The formalism of cumulants (or semi-invariants) was already in place due to work by J. G. Kirkwood in 1938. He used the theory of cumulants to expand the free energy in power of kT.

$$\text{i.e.)} \quad F(\beta) = \sum_{n=1}^{\infty} \frac{\beta^n}{n!} \, Mn \tag{2.2}$$

The primary contribution of Brout [B] was to rearrange the terms in the Kirkwood expansion. He abandoned the expansion in powers of 1/kT in favor of expansion in powers of 1/Z. Here Z is the effective number of spins interacting with a given spin. This is useful because in the limit $Z \to \infty$ the mean field theory becomes exact. Therefore, the mean field theory results should coincide with the leading order term in Brout's expansion. Horwitz and Callen [HC]

Abbreviation	Reference
B	15
HC	16
E	17
RMF	18
PP	19
MRF	20
EA	21
SK	22
TAP	23
VP	24
BGG	25
S	26
KSS	27
AT	28
BM	29
P	30

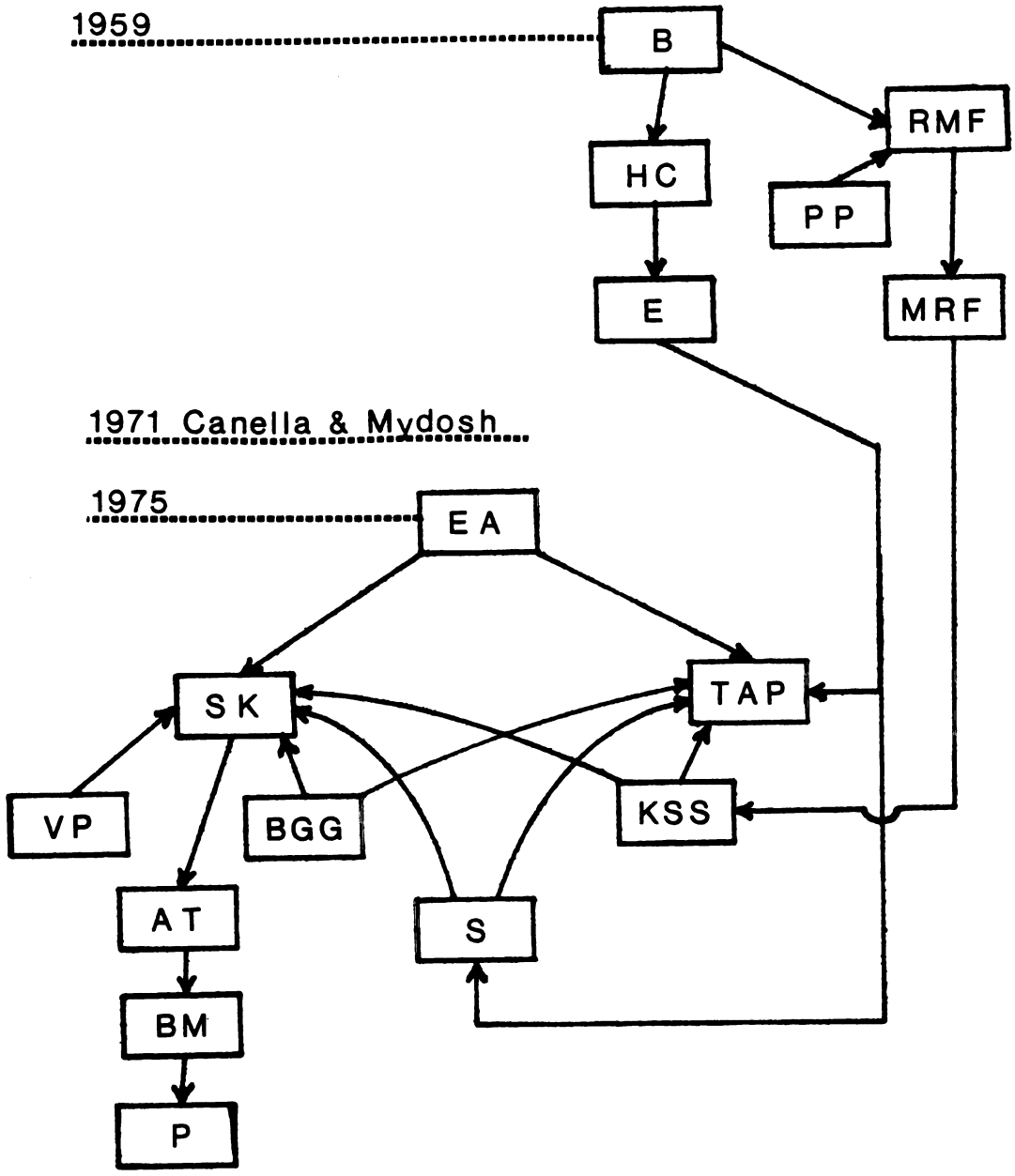

Figure 2. Mean field theory development flowchart.

extended Brout's method by regrouping the cumulants in such a way that certain restrictions in the summation of indices could be lifted. This, plus an expansion in terms of spin-deviation operators $\sigma_i = \bar{S} - S_{iz}$ led to the development of vertex renormalization. With vertex renormalization one can eliminate all reducible diagrams. (Reducible diagrams are linked diagrams which can be separated into unlinked parts by a single cut.) This renormalization procedure led to an irreducible linked diagram expansion for the Ising model. Englert [E] extended these ideas further by exploiting the similarities between the semi-invariant expansion of the partition function and the methods of propagators in quantum field theory. This opened the door to the use of some of the more powerful many-body theory techniques. These 1/Z expansions are useful as a means of verifying mean-field theory and suggesting higher order corrections to them.

About the same time as Brout's work, the first mean-field theory was being developed by Klein and Brout. The statistical problem that needed to be solved was the calculation of

$$Z = \sum_{\substack{\text{all} \\ \text{states}}} e^{-\beta H}$$

where

$$H = \sum_{i<j} v_{ij} S_i S_j$$

and v_{ij} is the Rudermann-Kittel-Kasuya-Yosida exchange potential (RKKY). This is in all probability an impossible task. So the

approach was to first ignore all spin-spin correlations and try and calculate the effective field distribution for a random distribution of impurities with random spin orientations. It is clear that a new type of molecular field theory is necessary. Since each impurity has a different environment, each impurity experiences a different effective Weiss molecular field. Since the positions of the impurities are random, so is the molecular field and thus the name Random Molecular Field [RMF]. So the problem is to obtain the probability distribution P(H) of this random molecular field. Once this is known, the thermodynamic variables of the system can be found by integrating the expression for the thermodynamic variable of a single spin in a fixed molecular field over the distribution of the fields. The mean free energy per particle can then be calculated according to

$$\ell n\ Z(\beta) = \int_{-\infty}^{\infty} P(H)\ \ell n\ Z(\beta,H)dH.$$

It should be re-emphasized that spin-glasses show many features that are not explainable by a single generalization from an ordered to a random molecular field. But it is a good way to start thinking about the static properties. So for models of this type, the physics is largely buried in the functional form of $P(c,T.H_{ext})$. Comparison between models will be made on that basis.

The first guess as to the form of P(H) was done by Marshall in 1960. His model predicted that P(H,T) at high temperatures should be a cut-off Lorentzian, i.e.,

$$P(H,T) = \frac{\Delta}{\pi} \frac{1}{H^2 + \Delta^2} \qquad |H| < \alpha$$

$$= 0 \qquad |H| > \alpha$$

where

$$\langle H^2 \rangle = 2\Delta\alpha/\pi \qquad \langle H^4 \rangle = 2\Delta\alpha^3/3\pi.$$

At low temperatures Marshall argued that P(H,T) should approach the form shown in Figure 3a. At low temperatures the correlation between spins is larger and the total energy of the system must go down. But this can only be done by arranging for the spins to sit in fields of larger magnitude. Thus the mean values of H must get pushed out to larger values. Klein and Brout find more or less agreement with Marshall. They find P(H) to be a Lorentzian with width proportional to the impurity concentration. If they properly exclude large fields from impurities close to the origin, the distribution changes from Lorentzian to Gaussian. They also tackle the problem of including spin-spin correlations. They express the 2-particle correlation function $g(r_{12})$ as a power series in $cz(r)$ where c is the impurity concentration and z(r) is the number of sites included within some radius $r = R_c$. For $r > R_c$ the cluster expansion breaks down. Thus they conclude that the impurities are fully or partially correlated to the spin at the origin if they are located within some correlation radius R_c and are approximately

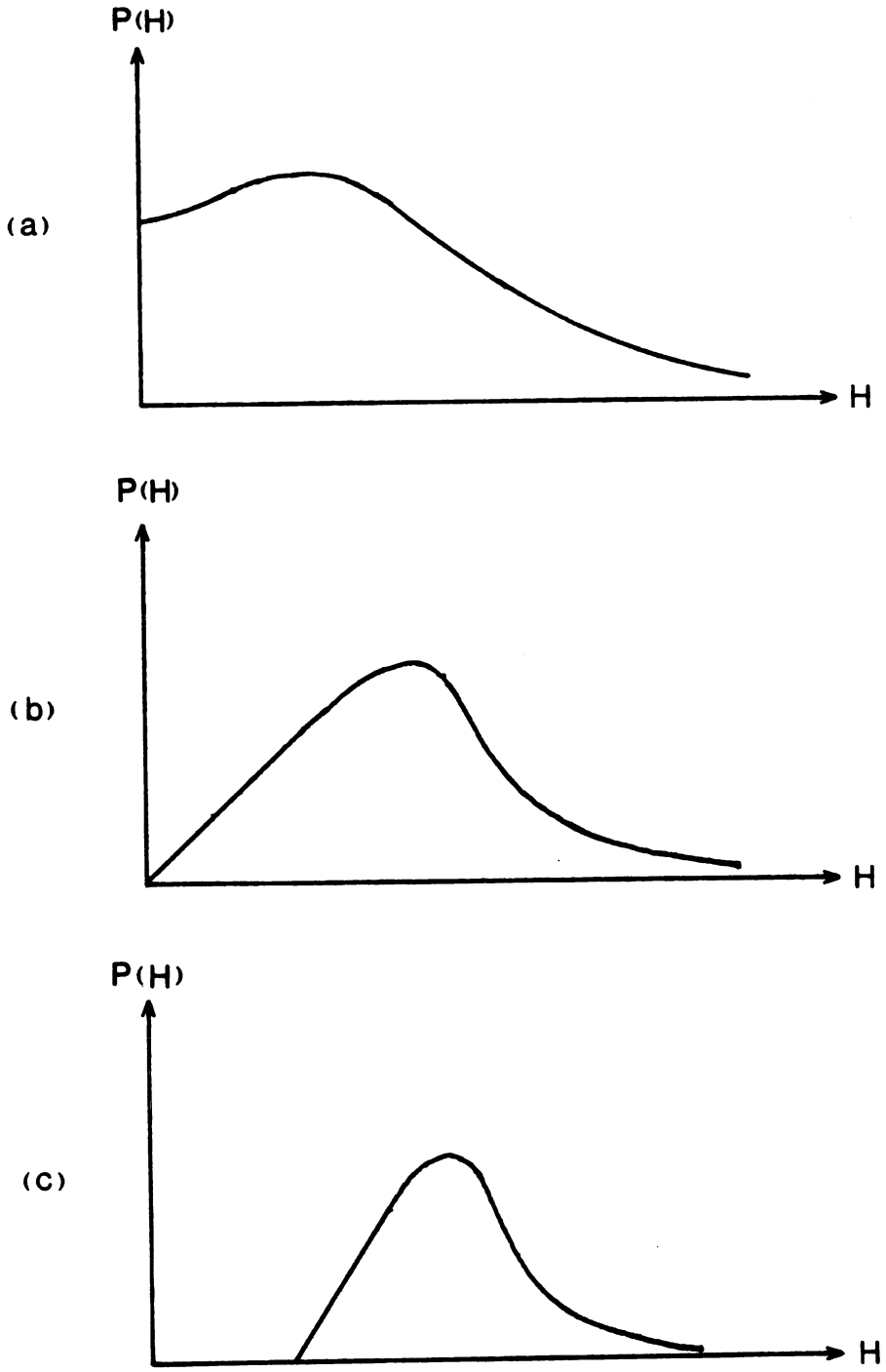

Figure 3. P(H) for different models.

randomly oriented if located outside R_c. So P(H) is the sum of 2 contributions. For $r < R_c$, P(H) is the field obtained from the correlated spins and for $r > R_c$ the field distribution is essentially Gaussian. The next development was the mean-random field approximation [MRF]. The idea here is straight forward. When calculating the probability distribution of the internal field at a particular site, replace all functions of the internal field at the other sites by their mean values. Continue to neglect spin-spin correlations and use the random molecular field approximation. In principle $P(H_j)$ could be different at each site. If one imposes the self-consistency requirement which says that each $P(H_j)$ has the same functional form, then an integral equation for the probability distribution is generated. This model was reasonably successful in explaining experimental low temperature properties as long as one used Ising spins. The Heisenberg mean random field predictions disagree with experiment. This is unfortunate since the actual spin systems studied experimentally were Heisenberg-like.

The probability distribution P(H) in the Sherrington-Kirkpatrick model (to be discussed shortly) is shown in Figure 3b and 3c for one and two dimensional spins respectively as computed using numerical simulations by Palmer and Pond [PP]. They find P(H) to be linear in h for small h for Ising spins, and find a "hole" in the 2-dimensional spin case. Muon spin depolarization or Mossbauer studies may be able to choose among these models.

In 1971 Canella and Mydosh published their now famous low field ac susceptibility measurements and this caused theoretical activity

to greatly increase. In 1975 a new kind of spin-glass theory was developed by Edwards and Anderson [EA]. Their model consists of a set of spin variables on a periodic lattice interacting via exchange bonds that are randomly ferromagnetic and anti-ferromagnetic. They obtain some of the experimentally observed behavior of real spin-glasses (like a cusp in the susceptibility) and some behavior which isn't observed experimentally. It is not clear how well the [EA] approach is withstanding the test of time. Some high temperature series expansion work of Fisch and Harris leads to the conclusion that the spin-glass phase cannot exist below 5 dimensions. Bray, Moore and Reed have performed numerical simulations which they interpret as evidence that the spin-glass phase has no frozen in order but only very long relaxation times. They argue that the frozen in magnetization results from the mean field approximation, and that in systems with fewer than 4 spatial dimensions, this state does not persist.

Nevertheless, its useful to examine the 3 crucial elements on which the EA model is based.

(1) They perform an average over configurations of random bonds in such a way that all spatial inhomogeneities are averaged out. Recall

$$Z = e^{-\beta F(T)} = \mathrm{Tr} e^{-\beta H},$$

therefore

$$e^{-\beta nF} = (\mathrm{Tr} e^{-\beta H})^n = Z^n \quad \text{for any } n$$

so

$$(\mathrm{Tr} e^{-\beta H})^n = \mathrm{Tr}_n e^{-\beta \sum_{ij} J_{ij} \sum_{\alpha=1} S_i(\alpha) S_j(\alpha)}$$

and

$$\langle (\mathrm{Tr} e^{-\beta H})^n \rangle_{P(J_{ij})} = \mathrm{Tr} e^{\sum_{ij} \frac{\beta^2 \overline{J_{ij}^2}}{2} \left(\sum_{\alpha=1} S_i(\alpha) S_j(\alpha) \right)^2}$$

or

$$e^{-\beta nF} = \mathrm{Tr} e^{-\beta \sum_{\alpha\beta} H_{\alpha\beta}}$$

where

$$H_{\alpha\beta} = \sum_{ij} \overline{\beta J_{ij}^2} \, S_i(\alpha) S_j(\alpha) S_j(\beta) S_i(\beta)$$

The random interaction J_{ij} has been eliminated and replaced by its mean which is translationally invariant. Anderson argues that the only limit in which this average is safe is the limit $n \to 0$ when it becomes $\langle \log Z \rangle_{J_{ij}}$. So the trick is to do the problem for all integer n to get an expression for F(n) and take the limit $n \to 0$ when finished. This formal structure is a coupling between different replicas .

(2) The second element is the characterization of the spin-glass phase by the order parameter $q = \langle\langle \vec{S}(x) \rangle \cdot \langle \vec{S}(x) \rangle\rangle_J$ where $\vec{S}(x)$

is the spin variable at the lattice site x and the inner brackets correspond to a spin-average for a fixed configuration of bonds. The outer brackets $< >_J$ denote an average over the bonds. This order parameter was introduced because many people interpreted the cusp in χ as evidence for a phase transition. Edwards and Anderson thought about the transition in the following way. Since there is not thought to be any long range order in space, perhaps there is still long range order in time. This idea led them to suggest the following order parameter. $q = \lim_{t' \to \infty} \langle\langle S_i(t = 0) S_i(t') \rangle\rangle$. The connection with the replica method is that the replica-replica correlation $q_{\alpha\beta} = \langle S_i^{\alpha} S_i^{\beta} \rangle$ seems to behave in exactly the same manner as the long time correlations $\langle S_i(0) S_i(\infty) \rangle$. Apparently 2 replicas α, β can be considered as the same system at two times t_1 and t_2 with $|t_1 - t_2| \to \infty$. Using a variational method, EA were able to show the existence of a critical temperature below which q is non-zero. See Figure 4. The parameter q is then given by a self-consistent equation and one can deduce the thermodynamic and magnetic properties of the system.

(3) The third crucial element is their use of replication techniques to allow the bond and spin averages to be performed interchangeably. A bit more on this shortly. The appealing aspect of the EA model is the following. If ε_{ij} is the probability of finding a pair of spins at sites i and j, and $\Sigma J_{ij} \varepsilon_{ij} \neq 0$ then one can have ferromagnetic or antiferromagnetic ordering at sufficiently low temperatures. In their model, $\Sigma J_{ij} \varepsilon_{ij}$ can equal zero on any scale, and the mere existence of a ground state is sufficient to cause a transition and a consequent cusp in the susceptibility.

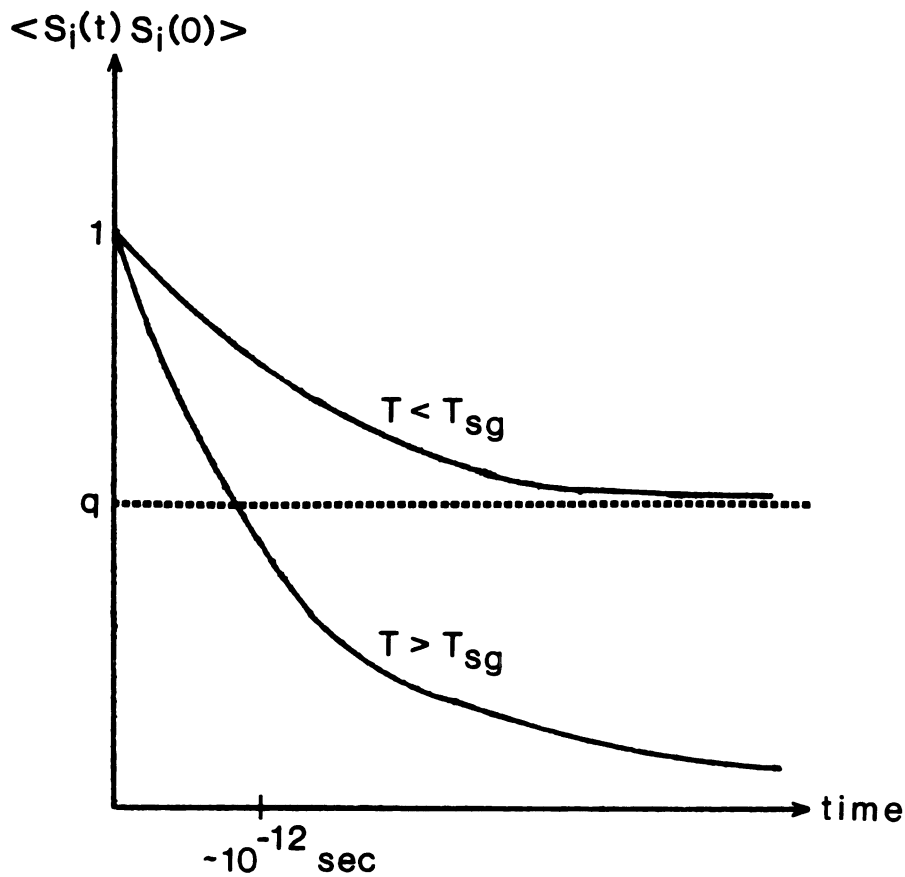

Figure 4. EA order parameter.

Because the replica trick has enjoyed widespread use, let's discuss it briefly. The goal of the replica trick is straightforward. It allows one to interchange the bond and spin averages. Recall that when the randomness is quenched, the averaging must be carried out over the free energy and not the partition function. The replica method essentially transforms the free energy average to a partition function average in the following way.

$$\text{Recall, } \ell n\, \chi = \lim_{n \to 0} \frac{(\chi^n - 1)}{n}$$

$$\text{for integral } n, \quad Z^n = \prod_{\alpha=1}^{n} Z^{\alpha}$$

$$\text{therefore} \quad \ell n Z = \lim_{n \to 0} \frac{Z^n - 1}{n}$$

$$\text{implies} \quad \langle \ell n Z \rangle = \lim_{n \to 0} \frac{\langle Z^n \rangle - 1}{n}$$

Notice this transformation was not achieved without sacrifice. We have, as pointed out earlier, increased the effective spin dimensionability of the problem and have been forced to introduce limit-procedures. Van Hemmen and Palmer [VP] present a very thorough analysis of the replica trick using a slightly different form

$$\langle \ell n Z \rangle = \frac{d}{dn} \ell n \langle Z^n \rangle \Big|_{n = 0}$$

and conclude that the fatal error in the method is the analytic continuation from integer n to real n. There is not universal

agreement on this point.

An infinite-ranged model for which the mean-field approximation of EA should be exact was formulated by Sherrington and Kirkpatrick [SK]. Their solution agreed with that of EA but also contained a pathology. The entropy becomes negative at sufficiently low temperatures. This is not possible for a discrete Ising-type model. Since they used the replica method, this may be due to passage from integer n to $n \to 0$ as pointed out by van Hemman & Palmer. However, there are other possibilities:

(1) Reversal of the limits $N \to \infty$ and $n \to 0$.

(2) The steepest descent method.

(3) The stability of the SK stationery point in the steepest descent calculation.

The third possibility has led to the development of several new theories. It begins with the work of deAlmeida and Thouless [AT]. They found the stationery point chosen by SK to be a maximum of the integrand at high temperatures, but not at low temperatures in the spin-glass and ferromagnetic phases. They consider the SK spin-glass and ferromagnetic phases to be unstable. They restore the stability using the concept of replica symmetry breaking. This comes about in the following way. SK derive the following result for the configuration averaged n-replica partition function

$$\overline{Z^n} = e^{\frac{1}{4}nN\beta^2\tilde{J}^2} \int_{\alpha<\beta} \prod \frac{dq_{\alpha\beta}}{\sqrt{2\pi}} \; e^{-Nf\{q\}} \tag{2.3}$$

where

$$f\{q\} = \tfrac{1}{2}\beta^2\tilde{J}^2 \sum_{\alpha<\beta} q_{\alpha\beta}^2 - \ell n \, \mathrm{Tr}\, e^{\beta^2\tilde{J}^2 \sum_{\alpha<\beta} q_{\alpha\beta} S^\alpha S^\beta}$$

Because of the factor N in the exponent in Equation (2.3), the integral is dominated in the thermodynamic limit by that set $\{q_{\alpha\beta}\}$ which give the absolute minimum of $f\{q\}$. This leads to the mean field equations

$$\frac{\partial f}{\partial q_{\alpha\beta}} = 0 = \beta^2\tilde{J}^2(q_{\alpha\beta} - \langle S^\alpha S^\beta \rangle)$$

SK assumed the absolute minimum of $f\{q\}$ occurs when $q_{\alpha\beta} = q$ for all pairs (α,β), but AT showed this was not the case. The idea behind replica symmetry breaking is just to divide the replicas in different groups and allow the order parameter to be different for each group. A great deal of work in this area has been done by Bray and Moore [BM]. Parisi [P] takes the idea one step further. He argues that the order parameter for spin-glass is a zero by zero matrix having the diagonal elements equal to zero. This can be parameterized by a function on the interval [0,1]. This would seem to imply the need for an infinite number of order parameters to characterize the spin-glass transition. Parisi also finds that there are an infinite number of eigenvalues which accumulate toward zero. He speculates that this infinite set of first order transitions is likely connected to remanence and is related to a breakdown of linear response theory. Bray and Moore also suspect that linear response theory breaks down.

Because of the subtle difficulties involved using replication theory, Thouless, Anderson, and Palmer [TAP] looked for a solution that did not require its use. They found a solution of the SK model which did behave reasonably at low temperatures (no negative entropies), and also confirmed the SK solution at and above the critical temperature. Above T_c they use a high temperature expansion. Below T_c they use a mean field theory which takes into account not only the average spin at each site, but also the fluctuations from this average. They performed a diagrammatic sum where the diagrams were classified according to powers of 1/Z. The largest contributions (single chains) give the SK high temperature result. The ring diagrams of order N/Z are negligible if they converge, but TAP found they diverge at $T_c \simeq \tilde{J}$. Below T_c, the only way to make the diagram series converge was to introduce a random mean spin at every site which satisfied the following mean field equations.

$$m_i = \tanh h_i/T \tag{2.4}$$

$$h_i = \sum_i J_{ij} m_j - \frac{m_i}{T} \sum_j J_{ij}^2 (1 - m_j^2) \tag{2.5}$$

Those can in fact be derived from the following free energy,

$$F = \sum_{(ij)} J_{ij} m_i m_j - \tfrac{1}{2}\beta \sum_{(ij)} J_{ij}^2 (1-m_i^2)(1-m_j^2) +$$

$$\tfrac{1}{2} T \sum_i [(1+m_i)\ell n\tfrac{1}{2}(1+m_i) + (1-m_i)\ell n\tfrac{1}{2}(1-m_i)]$$

The first term is the internal energy of a frozen lattice. The second term is the correlation energy of the fluctuations. The last term is the entropy of a set of Ising spins constrained to have means m_i. Equations 2.4 and 2.5 can be rewritten as

$$m_i = \tanh(\beta \sum_j J_{ij} m_j - \beta^2 \sum_j J_{ij}^2 (1-m_j^2) m_i)$$

The meaning of this equation is fairly transparent. The term $\beta \sum_j J_{ij} m_j$ is the total mean field h_i experienced by the spin S_i. From this is subtracted the contribution which is induced by the spin S_i itself. This can easily be seen. A mean moment m_i at site i produces a mean field $J_{ij} m_i$ at site j. This induces a mean moment $J_{ij} \chi_{jj} m_i$ at site j (here $\chi_{jj} = \partial m_j / \partial h_j$). This in turn produces a mean field $J_{ij}^2 \chi_{jj} m_i$ at site i. This is the field which must be subtracted from the total mean field at site i, since the field which orients a given spin is that due to only the other moments in the system. The final step involves the use of linear response theory to derive $\chi_{jj} = \beta(1-m_j^2)$. This may be a weak link in the theoretical development. This added term can be thought of as a kind of feedback term. It may be able to explain blocking or remanent phenomena. Since the TAP equations involve N simultaneous mean field equations for N spins, they can only be solved numerically, and then only near $T \sim 0$ and $T \sim T_c$. Their theory leads to the startling prediction that not only at the transition temperature T_c, but all temperatures $T < T_c$ have some of the fluctuation properties of a critical point.

This completes my brief introduction to the mean field theories of spin-glasses except for a brief mention of a few other approaches which lend support to some of the previously noted theories. For example, Sommers [S] solves the EA model by summing a renormalized diagrammatic expansion. His high temperature phase is identical with the SK solution, and his low temperature phase is similar to a particular solution of the TAP equations. Klein, Schowalter, and Shukla [KSS] study Ising spins interacting via random potentials in the Bethe-Peierls-Weiss approximation. They claim as the effective number of neighbors approaches infinity, the magnetic properties arising from the BPW approximation, the mean random field (MRF) and the SK replica treatment are identical. They are also able to obtain the microscopic free energy derived by TAP. Blandin, Gabay and Garel [BGG] derive a mean field theory using a Landau theory approach. To third order they obtain a solution similar to TAP (saddle point in the free energy). In fourth order this saddle point breaks into a maximum (which they identify as the SK result) and a minimum. Kosterlitz, Thouless and Jones solve the spherical model of a spin-glass in the limit of infinite ranged interactions. They use the properties of large, random matrices and show that the results are identical to those obtained by the $n \to 0$ replica trick.

Finally, as we close this section on mean field theories let's briefly examine the predictions they make for the magnetic susceptibility. In the Edwards-Anderson model for example, one finds

$\chi = \chi_c(1-q)$ where $\chi_c = \frac{c}{T}$ is the usual Curie Law and q

is the previously mentioned EA order parameter. Thus $\chi = \chi_c$ above $T = T_c$.

Below T_c,

$$q = -\tfrac{1}{2}(1-(\frac{T_c}{T})^2)$$

therefore,

$$\chi = \frac{c}{T_c}[1-(\frac{T_c-T}{T_c})]\{1 + (\frac{T_c-T}{T_c}) + o(T_c-T)^2\}$$

or

$$\chi = \frac{c}{T_c} - o(T_c-T)^2$$

Thus, the cusp is linear on the high temperature side of T_c and quadratic on the low temperature side. This is an artifact of the molecular field approximation since experimentally the cusp is symmetric.

If one allows a non-zero mean for the Gaussian distribution of exchange interactions, (such as the Sherrington-Kirkpatrick model) then one finds

$$\chi(T) = \frac{[1-q(T)]}{\{kT-\tilde{J}_0(1-q(T))\}} = \frac{\chi^{(0)}}{1-\tilde{J}_0\chi^{(0)}}$$

where $\chi^{(0)}$ is the result for $J_0 = 0$. Therefore, above the ordering

temperature (when q = 0) we have a Curie-Weiss Law.

In the spin-glass phase fluctuations decrease $\chi^{(0)}$ and χ giving rise to a cusp. Positive $\tilde{J}_0$ enhances χ at all temperatures. More conventional mean field theories, such as the mean random field predict the high temperature behavior to be almost Curie-Weiss like. They predict

$$\chi(T) = \frac{N_0 C p_{eff}^2 \mu_B^2}{3k_B(T-\theta)} \left[1-\left(\frac{2}{\pi}\right)^3 \frac{\Delta(T)}{k_B T}\right]$$

(See Appendix I). Typically, one does begin to see deviations away from Curie-Weiss behavior some distance above T_{sg}, in contradiction with the EA mean field theories. Mydosh,[31] for example, would argue that significant deviations occur as high as 5 T_{sg}.

B. Virial and High Temperature Expansions

Most of the theories presented in the previous pages are based on the concept of a mean field. Approaches which do not use this concept generally take the form of expansions (density or temperature) or computer simulations. For completeness, we will briefly examine two expansions. In 1970 Larkin and Khmelnitskii[49] introduced a virial expansion which is valid at high temperatures and low concentrations. In order to obtain a virial expansion they introduced the recurrence relations:

$$(1)\quad f_i = F_i$$

$$(2)\quad F_{ij....n} = \sum_k f_k + \sum_{kr} f_{kr} + \sum_{kr...m} f_{kr...m} + f_{ij...n}$$

where the summations are carried out over different sets of the indices. The nature of the series becomes clear if a few of the terms are worked out.

$$f_{ij} = F_{ij} - (f_i + f_j) = F_{ij} - (F_i + F_j)$$

$$f_{ijk} = F_{ijk} - (F_{ij} + F_{ik} + F_{jk}) + (F_i + F_j + F_k)$$

A simpler way to write it might be

$$f_i = F^{(1)}$$

$$f_{ij} = F^{(2)} - \Sigma F^{(1)}$$

$$f_{ijk} = F^{(3)} - \Sigma F^{(2)} + \Sigma F^{(1)}$$

$$f_{ijk} = F^{(4)} - \Sigma F^{(3)} + \Sigma F^{(2)} - \Sigma F^{(1)}$$

where the superscript refers to free energies of clusters of that size. The terms in the expression for $f_{ij...n}$ alternate in sign with the first term always positive. This leads to cancellation of terms in the proper fashion if you simply sum the $f_{ij...n}$. Larkin and Khmelnitskii assume a Hamiltonian of the form

$$H = \sum_{ij} v_{ij} \vec{S}_i \vec{S}_j - \mu \vec{H} \sum_i \vec{S}_i$$

where $\vec{H}$ is the external magnetic field and v_{ij} is the asyomptotic form of the RKKY interaction (i.e., $V(R) = V_0 \cos\frac{2k_0R}{R^3}$). Thus, indirect interactions only are considered. Since the distribution of impurities doesn't depend on temperature, one must calculate the thermodynamic functions for a given configuration of impurities, and then average over all configurations. The first term is just the free energy of non-interacting spins given by

$$F^{(1)} = -NT \ln \sinh(\mu H(S+\tfrac{1}{2})/T)/\sinh(\mu H/2T)$$

The second term in the expansion takes the form

$$F^{(2)} = -\frac{4}{3} NnV_0[S(2S+1)\ln \frac{V_0 n}{T(a^3 n)} + \Phi_2 (\frac{\mu H}{T})]$$

The physical quantities do not depend on the cut-off parameter a. The general form of the m-cluster free energy is

$$F^{(m)} = -NT (\frac{nV_0}{T})^{m-1} \Phi_m(\frac{\mu H}{T})$$

Summing all such terms, LK argue that the free energy is of the form

$$F = -NT\Phi(\frac{nV_0}{T}, \frac{\mu H}{T}).$$

So in the range of temperatures larger than the Kondo temperature but smaller than V_0, the free energy does not depend on the three parameters n, H, T, but only on their ratios. This is essentially

what Souletie and Tourner[95] argue using only RKKY interactions. The important point to be made here is that for $H >> T$, the series represents an expansion in terms of the parameter nV_0/H. Thus in very strong magnetic fields and low temperatures we have a way of estimating the magnitude of V_0. Using the expression for $F^{(2)}$ and making the assumption $H >> T$ one can derive

$$m = \mu SN[1 - \frac{2}{3}\frac{V_0 n}{\mu H}(2S+1)] .$$

This expression is applicable when the second term in parenthesis is small.

This approach allows us to try and estimate the magnitude of V_0 from magnetization data at high fields. Larkin and Khmelintskii also derive an expression for the magnetic susceptibility at high temperatures in weak fields. They find[33]

$$\chi^{-1} = \frac{3(T+C_s nV_0)}{N\mu^2 S(S+1)}$$

$$C_s = \frac{4}{3}\int \frac{dy}{y^2}[1 - \frac{M(y)}{Z(y)}]$$

where

$$M(y) = \tfrac{1}{2}\sum_{J=0}^{2S} J(J+1)(2J+1)^{-y\varepsilon_J}$$

$$Z(y) = S(S+1)\sum_{J=0}^{2S}(2J+1)e^{-y\varepsilon_J} \quad \text{and} \quad \varepsilon_J = J(J+1)/2.$$

The numerical values of C_s are equal to:

C(1/2) = 0.667	C(1) = 0.85	C(3/2) = 0.984	C(2) = 1.09
C(5/2) = 1.17	C(3) = 1.25	C(7/2) = 1.31	C(4) = 1.36

Thus, for spin 1/2 $T^* = C_s n V_0 = 0.667\ nV_0$.

For large S, $T^* = 8/9 \ell n V_0$ nS. This work is in contrast to Klein's mean field approach where the Curie-Weiss constant is put in by hand. Thus LK find θ to be a linear function of the concentration.

It is also worth mentioning the work of K. Matho[51] which is in some ways an extension of the LK approach. For example, LK evaluate Φ_2 only in the limit $\mu H >> T$, except for S = 1/2 when they do the calculation analytically. Matho extends this work by evaluating $F^{(2)}$ in the limit $T << T_1$ but for arbitrary quantum spin S and magnetic field H. According to Matho the second virial contribution is given by

$$\beta f^{(2)} = - \frac{c}{z} \int dW D(W) \ell n \{ Z_{12}(\beta W, z) / A_s^2(z) \}$$

when Z_{12} is the partition function of isolated pairs coupled by an exchange energy W. The distribution of couplings is given by D(W) and is assumed to be symmetric. Matho assumes $D(W) = W_1/W^2$ for $|W| \leq kT$ and D = 0 outside. The high energy cut-off is related to the second moment of the full RKKY distribution by $D^{(2)}/W_1 = 2T_1$. Matho argues that the exact formula for the Curie-Weiss temperature T_s^* of LK is given by $kT_s^* = cW_1\theta_s$ where θ_s is given in terms of the

trigamma function

$$\theta_s = \frac{-1}{4\pi i S(S+1)} \sum_{j,\lambda} \{\psi^{(1)}(\tfrac{1}{2} + \frac{y_{j,\lambda}(0)}{2\pi i}) - \psi^{(1)}(\tfrac{1}{2} - \frac{y_{j,\lambda}(0)}{2\pi i})$$

where

$$y_{j,\lambda} = \ell n\ (-\chi_{j,\lambda})$$

$$\chi_{j,\lambda}(z) = \left(\frac{A_{j-1}(z)}{A_j(z)}\right)^{1/j} e^{i\pi(2\lambda-1)/j} \qquad \text{for } j = 1, \ldots 2S, \quad \lambda = 1, \ldots j$$

where the $A_j(z)$ are the coefficients of the polynomial $P(x,z)$ given by

$$P(x,z) = \sum_{j=0}^{2S} A_j(z) x^{\frac{1}{2}j(j+1)}$$

and are given explictly by

$$A_s(z) = \frac{\sinh(S+\frac{1}{2})z}{\sinh(\frac{1}{2}z)}, \qquad Z = \beta g \mu_B H$$

Numerical values for $S \leq 7/2$ are given approximately by $\theta_s \simeq 2S/(2S+1)$. The freezing temperature is estimated to be $kT_{sg} \simeq S^2 CW_1$. Thus $T_{sg} \sim T_S^*$ for $S = 1/2$, but $T_{sg} >> T_S^*$ for large spin values. This is in agreement with other authors[34] who claim that in order for the spin glass state to be stable, T_{sg} must be greater than θ. If one looks ahead briefly at our $\underline{Cu_3PtMn}$ data, one finds this to be nearly the case for the disordered state alloys but is certainly not the case for the ordered state alloys if we interpret $T_S^* = |\theta_N|$. (See

Figure 5).

One might argue that those results are based on an expansion of the free energy which up to now only includes pair contributions. How good an approximation this is depends to some extent on how well the near neighbor spins effectively screen out the more distant spins.

Finally, Matho[35] points out the relationship between virial and high temperature expansions. He argues that the high temperature expansion is valid only for temperatures higher than all the bond energies. For $T >> T_1$, the second virial corrections reduce to the 1/T expansion with the moments $D^{(1)}$ and $D^{(2)}$ as coefficients. Here T_1 is the high energy cut-off in the exchange distribution. For $T << T_1$, the corrections depend only on the central amplitude W_1 through the parameter CW_1/kT_1.

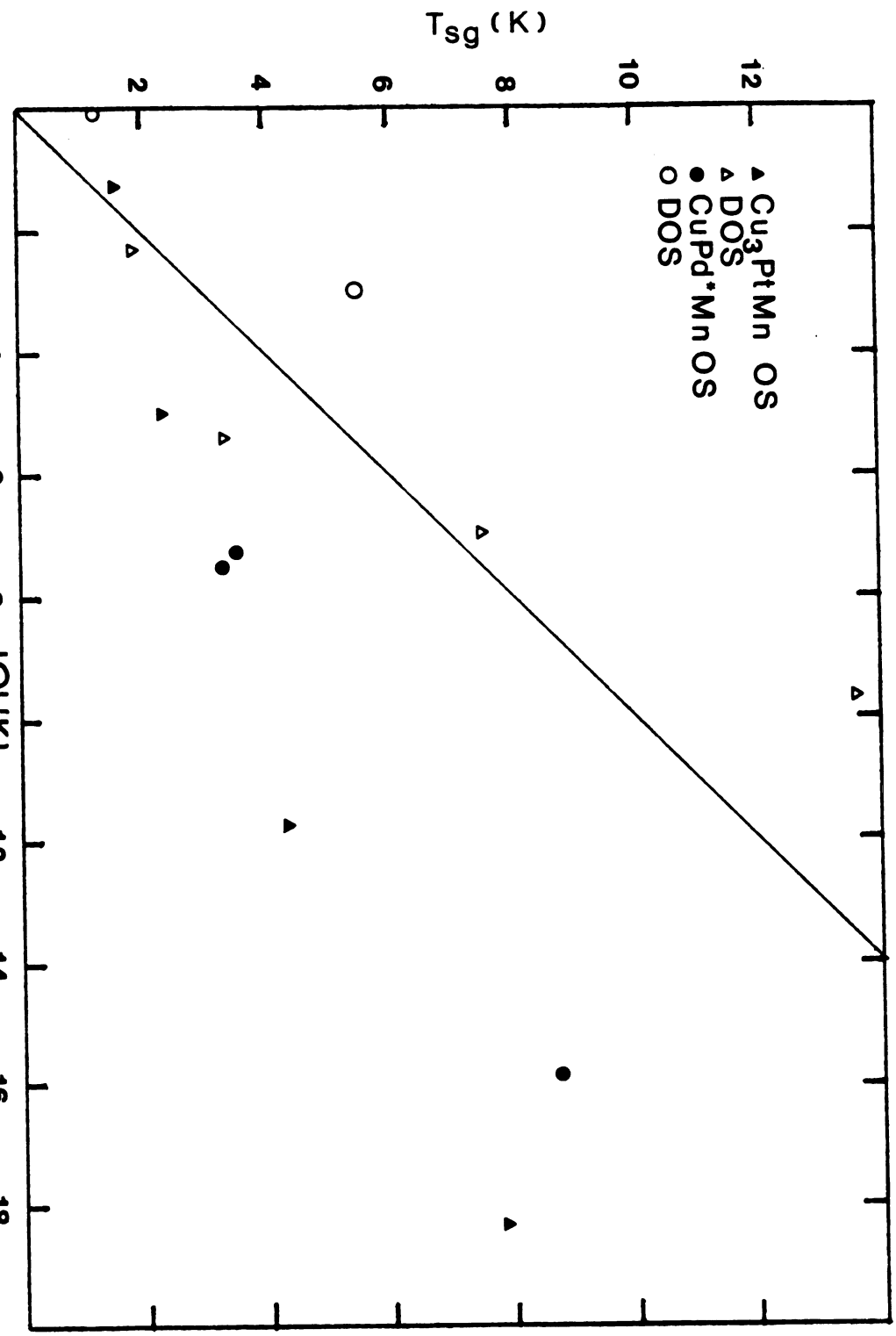

Figure 5. T_{sg} vs θ for $\underline{Cu_3PtMn}$ and $\underline{CuPd(17)Mn}$

III. INSTRUMENTATION

A. General Magnetometer Systems

The data presented in this thesis were obtained with the use of three distinct magnetometers. Most of the data used to determine θ for the alloys of interest were taken with a homebuilt vibrating sample magnetometer (VSM). Details of its construction and operation will be presented in succeeding sections. Most of the samples with low freezing temperatures were examined with an AC susceptibility apparatus employing a mutual inductance bridge. The samples with high freezing temperatures were examined with a commercial SQUID-based fluxmetric apparatus. These three approaches are all essentially induction measurement systems. In order to better understand the relationship between these methods of measurement and their advantages and disadvantages over older more conventional methods, the following short introduction to magnetic measurement methods is presented.

The measurement of bulk magnetic properties is typically performed using one of two general methods. One type of measurement I refer to as force methods since it involves the measurement of the force exerted on the sample. These methods are generally static (the measured signal is DC) and require a spatial inhomogeneity in either the field or sample-field geometry. The second class of measurements I refer to as induction type measurements. These

measurements require a dynamic setting. Either the sample or field or both exhibit a time dependence. In addition, there are methods which attempt to combine some of the desirable features of both. (See Figure 6).

The two most common force techniques are the Guoy and Faraday methods. The Faraday method works on the principle that a sample of magnetic material in a non-uniform magnetic field experiences a force. If the field gradient is along one direction only (the z-direction, for example) one can easily show that

$$F_z = -\chi \cdot \text{vol} \cdot \vec{H} \cdot \frac{\partial \vec{H}}{\partial z} \quad .$$

It is advantageous to measure the magnetization of a material in a uniform field because such a measurement makes no requirement on the field dependence of the magnetization. Force measurements which require a field gradient are limited to situations where the magnetization either varies linearly with the field or is field independent. If one has the situation $\vec{m} = \chi(H)\vec{H}$, then the force on the sample will also include contributions from the derivatives of χ with respect to H.

In the Guoy method the magnetic field is uniform. The spatial inhomogeneity arises because one uses a long sample which is only partially immersed in the magnetic field. If the sample has its extent primarily in the z-direction then one can easily show that

$$F_z = -\tfrac{1}{2}\chi A(H_2^2 - H_1^2)$$

Figure 6. Basic Techniques for Bulk Susceptibility Measurements.

AFM = Alternating Force Magnetometer

NCPM = Null Coil Pendulum Magnetometer

VSM = Vibrating Sample Magnetometer

VCM = Vibrating Coil Magnetometer

MIB = Mutual Inductance Bridge

FM = Fluxmetric Magnetometer

SQUID = Superconducting Quantum Interference Device

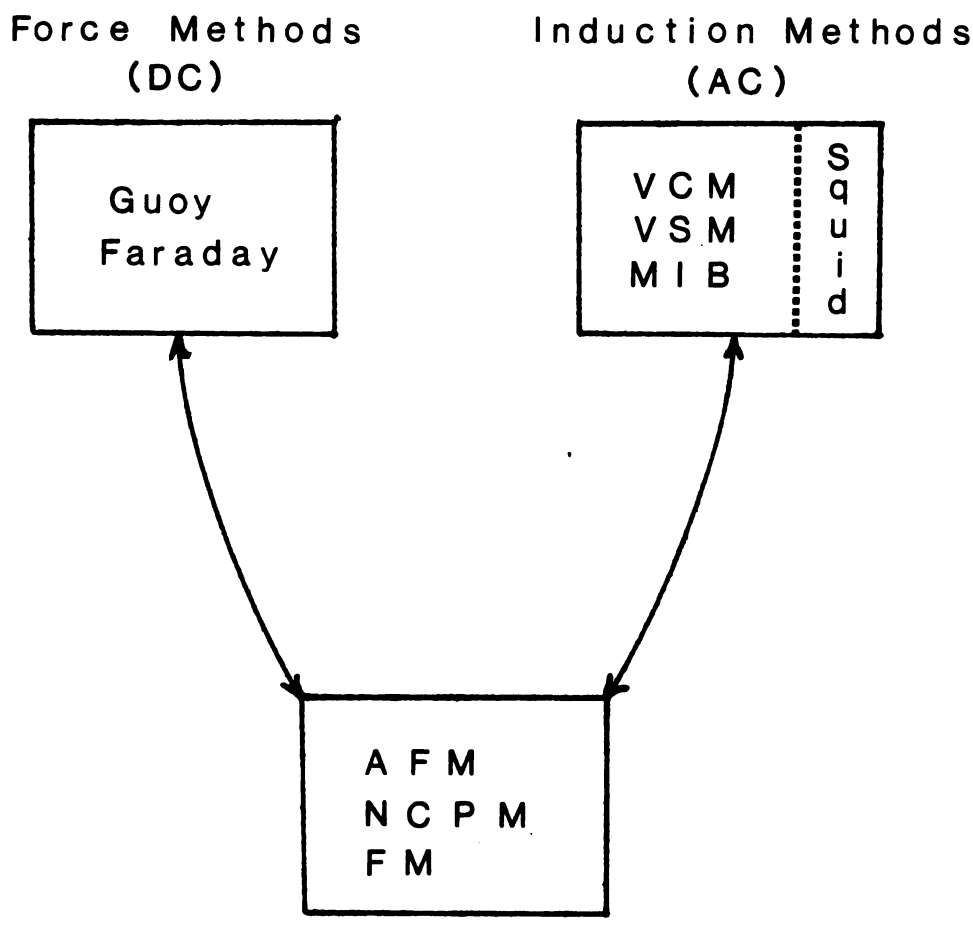

Figure 6. Basic techniques for measuring bulk susceptibility.

where A is the cross-sectional area of the sample.

The three techniques in the middle box straddle the ground between force and induction techniques. The fluxmetric method is usually an induction approach but doesn't quite use all the power of other AC techniques. The idea is to immerse the sample and a pick-up coil in the magnetizing field so that the dipole field from the sample is coupled to the coil. Then the sample is gradually removed from the vicinity of the pick-up coils and the change in flux induces a voltage in the pick-up coil. This induced voltage can be integrated by using a Ballistic galvanometer or an electronic integrator. Modern systems measure the flux change itself with unprecedented accuracy by using SQUID electronics. More on this later.

The next two methods to be described are fundamentally force methods, but show some AC characteristics and also demonstrate null techniques. The first is the null-coil pendulum magnetometer used by C. A. Domenicali. In this apparatus, the sample is placed in an inhomogeneous magnetic field inside a "null coil" of known geometry. The current through the coil is adjusted so as to make the net magnetic moment of coil plus sample equal to zero. The coil is rigidly attached to the lower end of a sensitive pendulum and the null position of the pendulum is observed with the aid of a projection microscope. This approach has two distinct advantages over conventional force methods, (1) the necessity for measuring the force on the sample is eliminated and (2) knowledge of the magnetic field gradient is not required. If the effective field gradients

acting on the coil and sample are equal, then the return to equilibrium implies $m_{sample} = m_{coil} = iAn$, where i is the current through the coil, A is its effective cross-sectional area, and n is the number of turns on the coil. If the effective gradients acting on the coil and sample are not equal, then even if the forces are equal, the magnetic moments are not necessarily equal and opposite. There are two ways around this problem. (1) the pendulum magnetometer may be calibrated with a standard of known magnetic properties and the same size and shape as the samples to be studied. (2) One may try and establish a magnetic field geometry in which the effective gradient is the same for sample and coil. The first method is in general much simpler.

In the case of our VSM, both the coil and sample were in a uniform magnetic field, so this problem did not arise. Nevertheless, we chose to calibrate the system by using a similar standard specimen. One can also worry about the small magnetic field generated by the null coil itself. This field will be negligible except for measurements in very small fields. This was not a problem in our measurements since the VSM typically operated in the 5 KOe to 9 KOe range. One can, however, make this correction arbitrarily small by using two concentric null-coils connected in series opposition.

A more complete discussion of null determinations of magnetization and its implications for cryogenic measurements can be found in Reference 36. In general, the introduction of the sample into a uniform field will produce a nonuniformity in the field. This difficulty can be overcome if the sample is an ellipsoid of

revolution, for then the demagnetizing field is uniform. Even in this case there will be images induced if the magnet is an electromagnet, and the image will change with changes in the permeability of the pole faces. Since our samples were essentially cyclindrical with a diameter of approximately 2 mm and a length of about 14 mm, there will exist a distortion of the field due to both the images and the non-uniformity of the demagnetizing field. However, if a Domenicali coil is wound around the sample, it is easy to show that the B field at every point in space will be unchanged and the magnetization will be uniform throughout the sample and directly proportional to the current per unit length in the Domenicali coil. Another advantage of null coils not directly related to the measurement process is that it gives the experimenter a way to create a variable magnetic moment at the sample location which can be very useful for checking general system operation and for fine tuning or alignment just before a series of measurements is to be taken.

Another variation of the force method is the so-called alternating force magnetometer.[37] The principle behind this instrument is to use AC techniques to improve the sensitivity beyond conventional force methods. The idea is to subject the sample to a small oscillating magnetic field gradient in addition to the steady uniform field which magnetizes the sample. The sample is held in position on the end of a rod which moves back and forth horizontally because of the alternating force on the sample. This motion is detected and is the desired signal. This instrument can also be designed to operate in a null fashion by putting a current carrying coil on the other end of the rod immersed in its own field gradient. The

direct current in the coil is adjusted until the vibration detector indicates zero.

Let's turn now to a discussion of some of the induction methods. An interesting example is the vibrating coil magnetometer.[38] Here the sample is fixed in a uniform magnetic field and some signal detection coils are vibrated back and forth with respect to the sample. This is in contrast to the VSM where the sample is vibrated and the coils are held rigidly. The advantage of the VCM is its greater flexibility in the setting of sample environment conditions. Temperature variation and control are somewhat easier, as compared to a VSM, and measurements under high pressure for example, are possible only in a VCM arrangement. The principle difficulty in producing a practical VCM is the elimination of the signal induced by curvature in the magnetizing field. Since our pressures were never to exceed one atmosphere absolute, the VSM was the logical choice.

At this stage I would like to briefly discuss the mutual inductance bridge[39] technique since it was used to experimentally determine some of the spin-glass freezing temperatures. The basic idea behind the mutual inductance technique rests on the fact that the mutual inductance of two concentric solenoids depends on the magnetic characteristics of the material within the solenoids. The change in mutual inductance upon introduction of a sample of mass m is given by

$$\Delta(\text{mutual inductance}) = K\, m\, \chi$$

where K is a constant characteristic of the coils. In this particular case, the susceptibility coils used consisted of a primary and two oppositely wound secondaries. These were wound so as to make the total mutual inductance approximately zero. The change in mutual inductance produced by inserting the sample into one of the secondaries was measured with a Cryotronics Model 17B mutual inductance bridge operating at 17 Hertz. Since the coils were not exactly balanced without a sample, and the balance was temperature and field dependent, readings with the sample in and out of the coils were taken and subtracted.

Since the operating temperature range of this system was limited to the interval 1.2°K to 4.2°K, a way to measure T_{sg} for those samples where $T_{sg} > 4.2$°K had to be found. One approach would have been to measure hysteresis loops as a function of temperature and look for the onset of irreversibility. This is a long, inaccurate and tedious process. The best solution was to gain access to an S.H.E. Corporation VTS 800 Series Susceptometer. Since this is a squid-based device, accurate data could be taken in low dc fields (≈25 gauss). These fields were low enough that the spin-glass transition was not severely rounded out. Nogata and Keesom[40] demonstrated that low field dc susceptibility was a practical way to determine T_{sg}. The instrument developed by S.H.E. Corporation is essentially a state of the art version of the fluxmetric magnetometer. Instead of using a ballistic galvanometer or electronic integrator to integrate the voltage induced in a pick-up coil, a squid sensor is used. A rough block diagram of the system is shown in Figure 7.

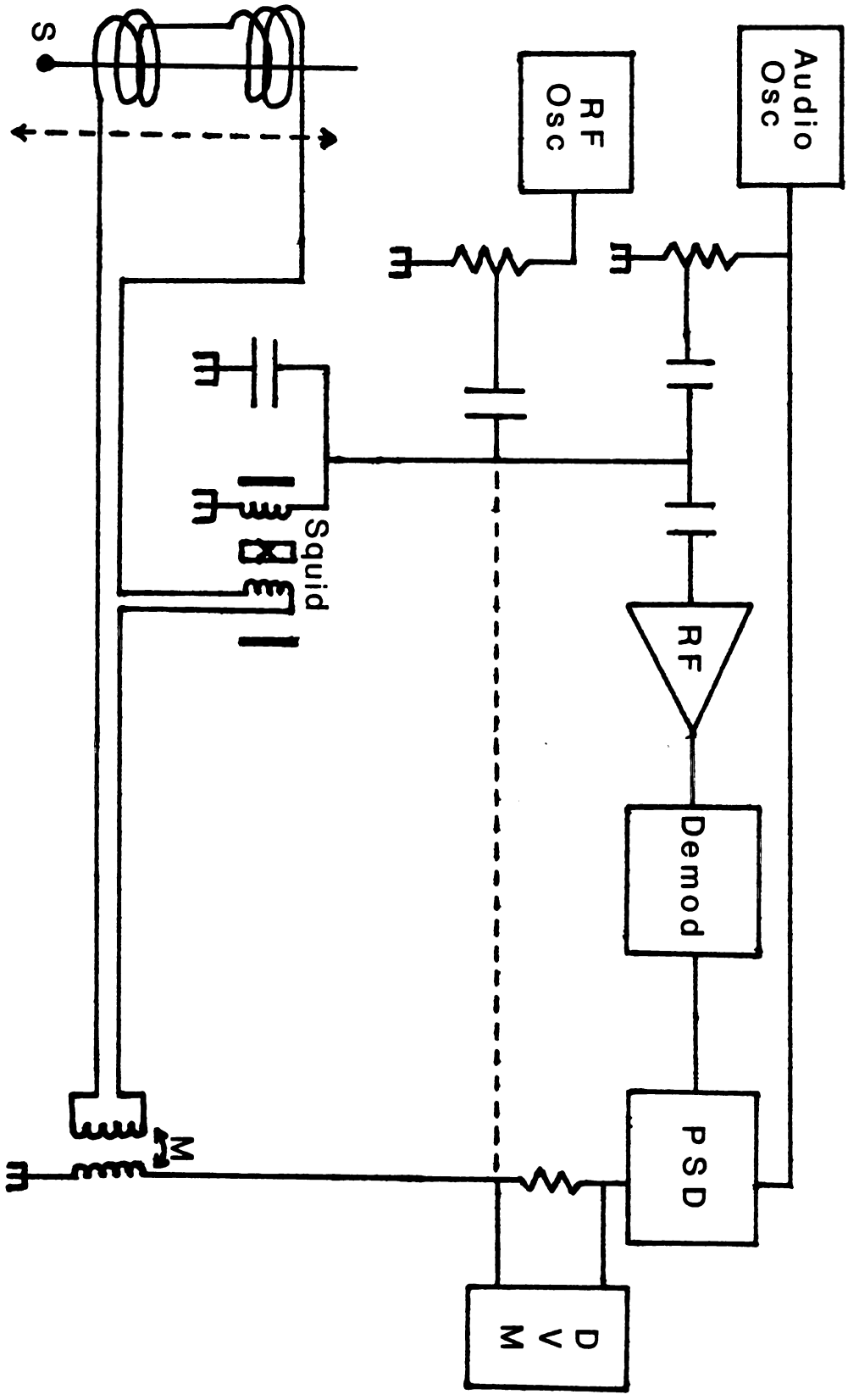

Figure 7. Squid based magnetometer.

The sample and its holder are suspended on the end of a long titanium ribbon and they are cycled back and forth through two pairs of Helmholtz coils. The flux change caused by the movement of the sample induces an EMF in the coil pairs. This causes a current to flow through the signal coil of the squid. It is the job of the squid and associated electronics to detect this current and, if operated in a feedback mode, to keep it approximately constant. This is known as flux-locked loop operation. The current induced in the signal coil causes a flux change in one part of the squid cylinder. It is this flux change which is detected in the following manner. (For a good discussion of squid devices see Reference 41.) The RF oscillator supplies an RF signal to the squid tank circuit. This generates an RF supercurrent through the squid point contact. If the RF amplitude is great enough, the critical current of the weak link will be exceeded and it will go normal. This allows a readjustment of the flux between the two holes in the squid such that the point contact again goes superconducting. It should be noted that this RF induced transition takes place about the average DC flux in the squid cylinder which is constant since the rest of the squid cylinder is always in a superconducting state. Thus, if the average dc flux within one hole of the squid body should change due to the presence of current in the signal coil, a flux change will also appear in the hole containing the RF coil due to the constant shuffling back and forth of flux. Now the average dc flux in the RF hole is slowly modulated (at approximately 1000 Hz) by an audio signal introduced via the same RF coil. Thus the amplitude of the 1 KHz frequency component of the RF detector is a

measure of the average dc flux in the RF hole of the squid which is constantly communicating with the average flux in the signal hole of the squid. Thus the lock-in output is a dc voltage directly proportional to any small dc flux change in the squid body. To ensure that the change experienced by the RF coil is small, a dc current is fed back to the squid signal coil via a mutual inductance. The voltage caused by this current flowing through a standard resistance is the actual measured quantity. It varies linearly with the flux change in the signal coil. Flux changes as small as 2×10^{-7} gauss-cm^2 can be detected. The dotted line indicates that many times this feedback current is fed back directly to the RF coil.

B. General VSM Considerations

If one "inverts" the alternating force magnetometer, one arrives at essentially the vibrating sample magnetometer. That is, rather than driving the sample with an alternating magnetic field gradient and measuring the vibration of the rod, one could drive the rod (with say a loudspeaker) and measure the magnetization of the sample by measuring the induced voltage in a system of pick-up coils mounted in the vicinity of the sample. That is precisely what is done and Figure 8 shows the basic idea behind the VSM.[42]

Here the system is designed to operate in a null comparison mode. The signal derived from the oscillation of the reference sample in the upper set of coils is first phase shifted so as to be 180° out of phase with respect to the sample signal. Then it

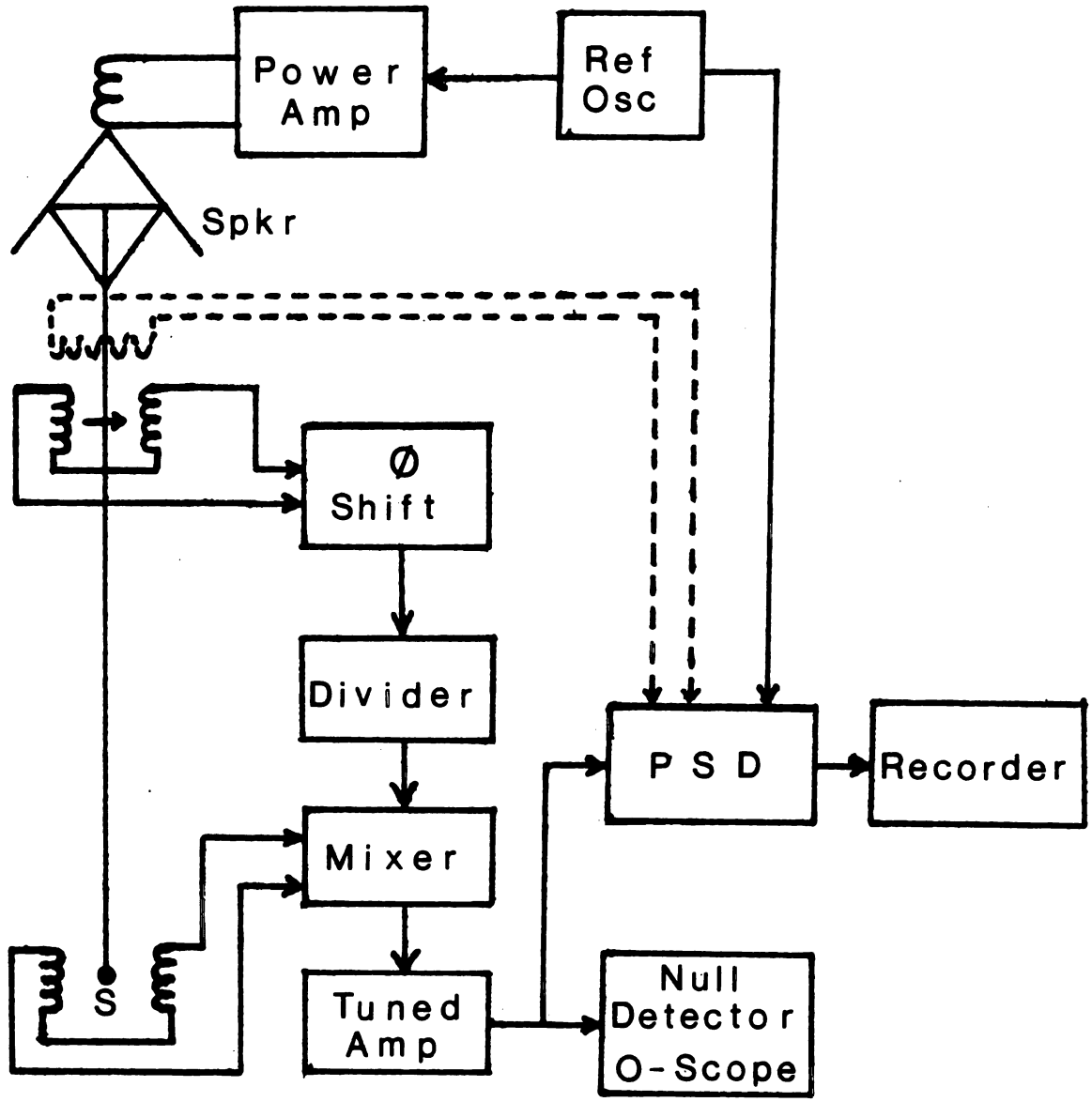

Figure 8. Conventional Foner style VSM.

is attenuated with a precision divider and mixed with the sample signal. The combined signal is fed to the primary of a well shielded audio transformer. At balance, there is no current flow in the transformer primary. Any inbalance is amplified by a high-gain narrow bandpass amplifier and fed to the input of a phase sensitive detector. The reference signal for the phase sensitive detector is derived from the oscillator used to drive the loud-speaker. Balance is achieved when the lock-in output reads zero. The magnetic moment of the sample is proportional to the reference voltage divider setting. Because it's a null measurement, the divider settings are independent of vibration amplitude, frequency and the electronic circuitry following the mixer. One could also implement an automatic null balancing approach by taking the dc output from the phase sensitive detector and using it to drive a coil which replaces the permanent magnet (see dotted line in Figure 8). The machine described above is essentially the design of the magnetometer used in the MF study.

The magnetometer used by the author was similar, but significant modifications were made (see Figure 9). Again, a null measurement was made, but in this case a Domenicali type coil was used and the signal was nulled out at the sample. This eliminates the need for phase shifters, dividers, and mixers. It also greatly reduces image effects. Of course, this approach has some drawbacks. Often times fairly large currents ($\sim$100 mA) would be needed to null the sample moment and this large current caused problems in two ways. Since the Domenicali coil has a finite resistance even at 4.2°K, the

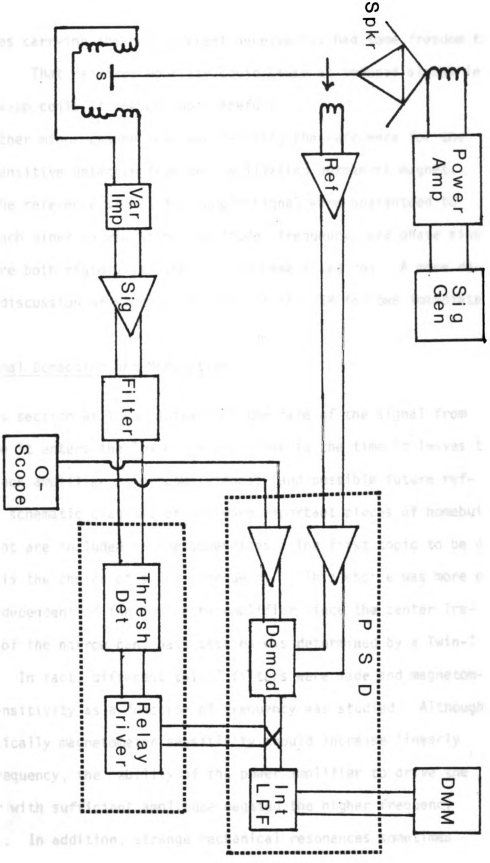

Figure 9. VSM used in this study.

nulling coil would raise the sample temperature slightly. Secondly, the wires carrying the null current necessarily had some freedom to vibrate. That required mobility could cause an induced signal in the pick-up coils if one was not careful.

Another minor change involved deriving the reference for the phase sensitive detector from the oscillating permanent magnet. Thus, the reference signal and sample signal were guaranteed to track each other in vibration amplitude, frequency, and phase since they were both rigidly attached to the same fixed rod. A more detailed discussion of specific aspects of the VSM follows immediately.

C. Signal Detection and Modulation

This section will concentrate on the fate of the signal from the time it enters the low noise amplifier to the time it leaves the phase lock amplifier. For completeness (and possible future reference) schematic diagrams of the more important pieces of homebuilt equipment are included in the appendices. The first topic to be discussed is the choice of signal frequency. This choice was more or less independent of the low noise amplifier since the center frequency of the narrow band pass section was determined by a Twin-T filter. In fact, different twin-T filters were made and magnetometer sensitivity as a function of frequency was studied. Although theoretically magnetometer sensitivity should increase linearly with frequency, the ability of the power amplifier to drive the speaker with sufficient amplitude negated the higher frequency choices. In addition, strange mechanical resonances sometimes

occurred at the higher frequencies.

A vibration frequency of 33 Hz was finally selected. The speaker responded well at this frequency. The choice of operating frequency was further dictated by an examination of the ambient noise with a spectrum analyzer. What was found was rather to be expected. There was a 1/f noise component which essentially vanished by 50 Hz. At 60 Hz and all higher harmonics there was also considerable noise. This suggested the possibility of operating as close as possible to 30 Hz, that is, the first even subharmonic of 60 Hz. One gains some degree of immunity to ambient 60 Hz interference if one operates at 30 Hz. A simple analysis shows why.

Let the frequency we wish to detect be called ω. Then its period is $T = 2\pi/\omega$. Now assume the amplifier delivers to the detector a voltage $V(t) = \sum_n \hat{V}_n \sin(n\omega t + \psi_n)$ where $\hat{V}_n$ is the peak value of the n^{th} harmonic and ψ_n is the phase of the n^{th} harmonic relative to the reference (chopper) frequency. It is assumed that the switching action of the demodulator takes place in a time negligible compared with T. Now the n^{th} harmonic component of V(t) (i.e., $V_n(t) = \hat{V}_n \sin(n\omega t + \psi_n)$) represents a spurious input to the demodulator for all $n \neq 1$. The average value $\langle V_n \rangle$ at the detector output due to $V_n(t)$ at the detector input is

$$\langle V_n \rangle = \frac{1}{T}\left[\int_0^{T/2} V_n(t)dt - \int_{T/2}^{T} V_n(t)dt\right]$$

$$= \frac{\omega V_n}{2\pi}\left[\int_0^{\pi/\omega} \sin(n\omega t + \psi_n)dt - \int_{\pi/\omega}^{2\pi/\omega} \sin(n\omega t + \psi_n)dt\right]$$

The integral is written in two parts because of the sign reversal introduced by the demodulator during the interval $T/2 < t < T$. Therefore,

$$\langle V_n \rangle = \frac{\hat{V}_n}{n\pi} [1 - (-1)^n] \cos\psi_n$$

Since the filter is linear, superposition applies, and the average of the combination of N signals harmonically related is

$$\langle V \rangle = \frac{1}{\pi} \sum_{n=1}^{N} \frac{\hat{V}_n \cos\psi_n}{n} [1 - (-1)^n] \qquad n = 1,2,3,....N$$

Thus, for $n = 2$, $\langle V_2 \rangle = 0$ regardless of the phase ψ_2.

Once the signal frequency is chosen, in a null measurement it is the job of the electronics to detect amidst all the noise background, the presence or absence of the known signal. In a system like the one used, the ac signal from the detection coils is first applied by a high-gain, narrow band-pass low noise amplifier.

The amplifier gain is of the order of 10^6. The amplified ac signal is converted to a dc signal by the synchronous demodulator. The demodulator is driven by a reference voltage which maintains a constant phase relationship with the input signal voltage. Typically, the dc signal is then fed directly to a low pass filter. In our case, provision was made to break that connection at certain times. This will be discussed in more detail later.

The output of the filter is the average value of the signal which appeared at the output of the demodulation. It is the average

value that is of interest, not the peak or RMS value. For random noise signals the peak and RMS values depend on the amplitude of the noise, while the average value tends to zero as the averaging time increases. This affords another means of distinguishing between signal and noise.

The detection coil signal, which may be only a few nanovolts, must first be sufficiently amplified in order to drive the input amplifier of the lock-in.

I will not give a detailed description of the electronics, but will mention some general practices relating to low level signal amplification. It is generally known that for an amplifier consisting of several stages in cascade, the overall noise figure (NF = $10 \log \frac{S_i/N_i}{S_o/N_o}$) is determined primarily by the noise figure of the first stage, provided this stage has a reasonable power gain. If the signal can be sufficiently amplified, then the noise generated in succeeding stages will have a negligible effect. Therefore, in the input stage, center frequency gain and low noise are more important than narrow bandwidth.

In our particular application, the detection coils are electrically floating and connected to the input terminals of a Triad G10 transformer. The transformer serves as a differential input. Any common mode voltage between the coils and the copper shield which encloses the input stage is not seen by the transformer. Problems can arise if the two input lines are not equally balanced with respect to ground. In that case, some fraction of the AC voltage between ground and the coils would be seen by the transformer.

If we assume that the characteristics of the signal source (i.e., the pick-up coils) are fixed and not alterable, then the design problem is to choose the parameters of the amplifier so that the output is an amplified replica of the input, and the output signal to noise ratio is optimized. If we desire that the amplifier respond to the signal voltage generator in such a way that it is independent of the source impedance, then we must require the amplifier input impedance to be much larger than the source impedance.

The optimum signal to noise ratio is achieved by properly matching source-amplifier impedances with the Triad transformer. The transformer secondary is connected to the control grid of a high-gain grounded cathode pentode. The plate voltage output is passed through a 60 Hz notch filter and further amplified by two triode stages. The narrow band section of the amplifier is simply an operational amplifier (White Model 212 A) with a 33 cycle Twin-T rejection filter in the feedback loop. This is followed by a cathode follower stage to lower the output impedance. The final stage is a low pass filter with a frequency cut-off of $\sim$100 Hz. This signal is now appropriate to send to the phase-lock-amplifier. This same signal is mointored on an oscilloscope to assist in rapidly finding the proper value of null current and to keep watch on the signal from the magnetometer.

D. Signal Detection Coils

The detection coils employed in our VSM were #986 Miller air core RF chokes configured in a standard four coil Mallinson array.

That is, all coil axes are parallel to the field and each pair is connected in series opposition and both pairs are connected in series opposition. The question of which coil size and configuration is optimal is very complex. Some degree of experimentation in this area was carried out by the author. A description of that work and a derivation of the induced EMF for a given coil-sample configuration is presented in Appendix A.

E. Field Noise

One of the major experimental problems facing users of VSM's is the ambient magnetic field noise. This problem was also given serious attention by the author. When the ambient magnetic field suddenly changed value, some voltage was induced in the pick-up coils because they are not perfectly balanced. This voltage impulse would eventually work its way to the tuned circuitry in the pre-amplifier. The amplifier would ring with a sizeable component at the tuned frequency. Even though its phase might be different from the signal of interest, and it presumably decayed away experimentally, it would often overload the lock-in amplifier.

The original idea was to build a precision clipper and insert it just before the tuned circuitry. If the signal of interest was say 5 nV, one would have to amplify it by 10^6 to get into the 5-10 mV level before you could reliably clip it. There are commercially available voltage comparators with 1 mV sensitivity and repeatability.[1]

---

[1] Calex Model 540 Voltsensor (Calex Mfg. Co., Inc. Pleasant Hill, CA).

The next step was to investigate the effect of the clipping on the frequency spectrum of the signal. This was done by assuming the signal of interest to be $\cos\omega t$ and the added signal due to the ringing to be of the form $ce^{-dt}\cos(\omega t+\psi)$.

In particular, if one assumes a signal of the form

$$V(t) = \cos 10t + 5e^{-0.7t}\cos(10t)$$

so that the ringing is in-phase, and the burst is initially 5 times the signal amplitude and has a time constant of 1.4 seconds, the frequency spectrum is as shown in Table 3. Also shown are the same values if the signal is clipped with an amplitude of (1.2). Also shown are the results for the same signal with the noise pulse shifted by 1 radium relative to the signal.

One can see that for the in-phase noise signal, it appears as though the true measurement signal has more than doubled in amplitude. If the waveform is clipped with an amplitude of 1.2, the in-phase signal appears to have grown by only 17%. In both cases the quadrature component is very small. From Table 2 the in-phase component of the "true" signal seems to grow by 59%. The clipped version of this shows only a 2% increase. However, in both cases, there is a sizeable quadrature component. This isn't a problem if the lock-in phase is properly adjusted (see Appendix E for some discussion of this point). Overall it appears that some use might arise from such a precision clipper. However, about this time, a simpler and better idea was devised. It really doesn't matter

Table 3. Quadrature and In-Phase Components of Clipped Sine Waves.

$V(t) = \cos(10t) + te^{-0.7t}\cos(10t)$

	$V(t)$		$V^{clipped}$	
Freq.	cosine coeff.	sine coeff.	cosine coeff.	sine coeff.
0	0.018	0.0	-0.0003	0.00
10	2.15	0.038	1.17	0.0020
20	0.031	0.102	0.0004	0.009
30	0.026	0.055	-0.20	0.0013

$V(t) = \cos(10t) + 5e^{-0.7t}\cos(10t + 1)$

	$V(t)$		$V^{clipped}$	
Freq.	cosine coeff.	sine coeff.	cosine coeff.	sine coeff.
0	-0.056	0.0	-0.013	0.0
10	1.59	-0.92	1.02	-0.44
20	0.061	0.051	0.014	-0.009
30	0.032	0.029	0.043	0.14

if the tuned amplifier rings (provided it doesn't ring too long) so long as the final data readings don't reflect this fact. So the idea was to monitor the output of the tuned amplifier with comparators. If a noise burst suddenly appeared, then we would race ahead of the signal and disconnect the demodulator output from the integrator-low pass filter input. The capacitors in the low-pass filter are quite capable of holding their potential until the system reconnects. This scheme allowed one to use the full amplification and narrow bandpass characteristics of the tuned amp, and did not require any modification of the incoming signal. This idea was considered feasible and the circuitry was constructed. A schematic diagram of the device (called the "interrupter") appears in the Appendix B.

The operation of the circuit is straightforward. The signal passes through a non-inverting variable gain follower and is examined by two comparators in parallel. If the absolute value of the signal exceeds a set amount, a 555 timer configured as a one-shot is triggered. The positive output pulse from the 555 eventually turns off the transitor which is keeping the reed relay closed, and the relay opens breaking the connection between the demodulator and the integrator.

F. Holder Design

Next to the detection coil design, the construction of the sample holder is probably the most crucial design element. Many holders

were built and tested during the course of this work, but we shall discuss only those three which were used to take most of the data in the thesis. The oldest of the three incorporated the following features: (See Figure 10)

(1) A bifilar wound platinum resistance thermometer with a room temperature resistance of approximately 10 ohms. This was wound on a thin aluminum cylinder. Aluminum was chosen because many magnetic impurities (especially iron) do not retain their magnetic moments in aluminum. Aluminum is also easily machined and etched. The platinum wires were insulated from the aluminum with GE varnish and cigarette paper.

(2) Next a Domenicali coil consisting of approximately 250 turns of #38 copper wire was wound.

(3) Then approximately one inch of Evanohm wire (resistance ≈30 ohms) was twisted together and varnished to the holder and connected to a twisted pair set of leads.

(4) Finally a AuFe (7%) versus Chromel thermocouple was attached directly to the holder. This thermocouple was quite long as it had to run the full length of the cryostat and exit through a wax seal and then move on to a liquid nitrogen reference bath.

The other two holders were slight modifications of this design. The second holder was developed to measure hysteresis. Because the field strength was only several hundred gauss, the contribution from the holder had to be made as small as possible. This was accomplished by winding a single turn of wire on a plastic form,

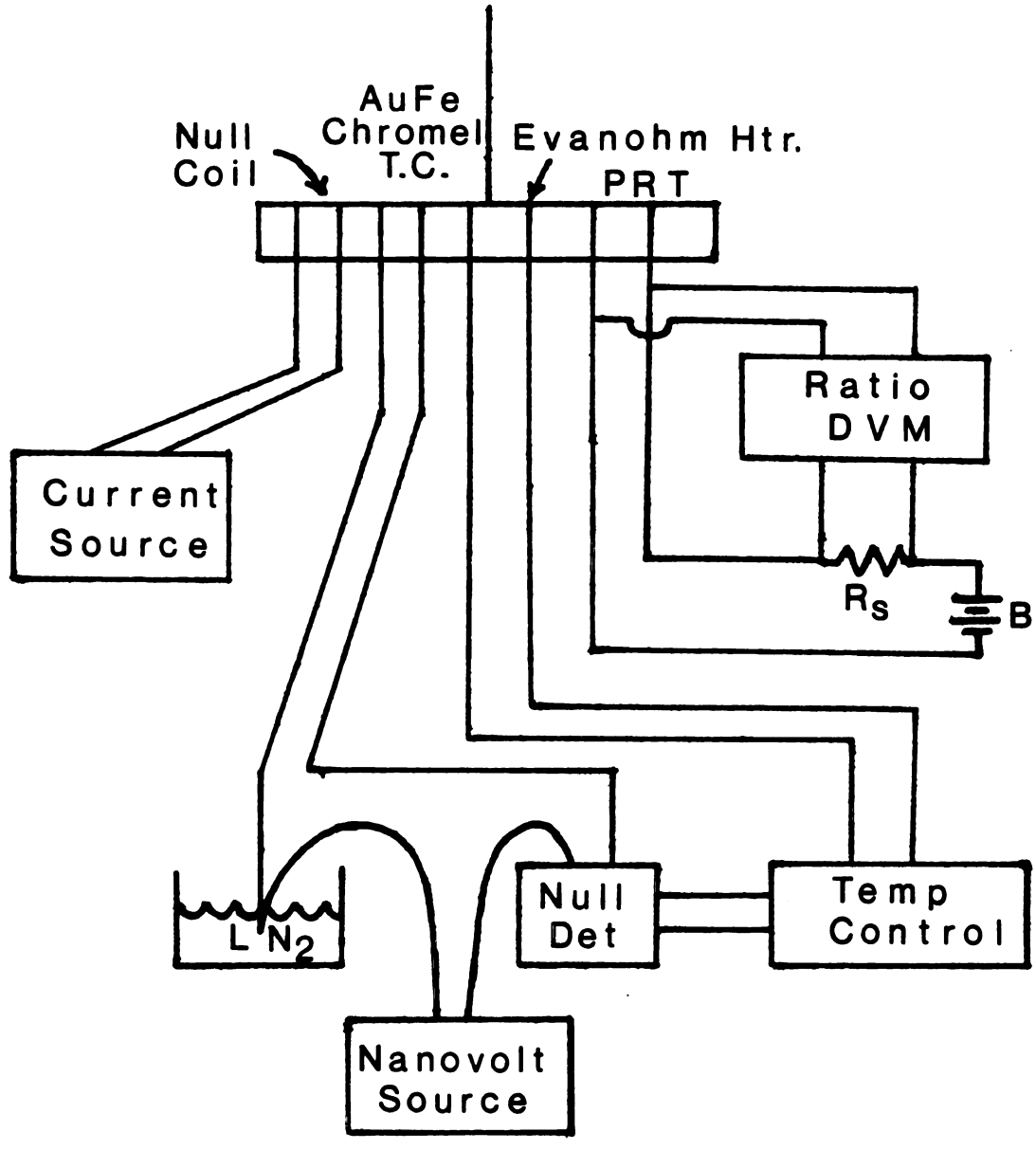

Figure 10. Holder design.

varnishing the coil, and then softening the plastic and removing it. There was no aluminum form. The structural integrity was provided completely by the hardened GE varnish. In addition, there was no heater wire or thermocouple. AuFe (7%) is also a spin-glass and can show hysteretic effects. The thermocouple was left in place and taped higher up on the cryostat so as to still be useful in precooling. All the hysteresis data was taken at 4.2°K so the heater was not necessary. Of course, this restricts you to samples whose spin-glass temperatures are somewhat greater than 4.2°K.

The last holder to be built was basically the same as the first except the platinum resistance thermometer was left off. It was decided that most of the work would be done in the 4.2°K to 77°K temperature range, and that the platinum thermometer would not be required.

The vycor rod which transmitted the speaker vibration was reduced in diameter under heat and given a flat end surface. The holders were then simply varnished onto the end. In addition, previous holders employed a set screw to hold the sample in place. This meant making the holder wall thick enough to support at least several threads of the 0-80 variety. By utilizing silicon grease and eliminating the set screw, the metal form could be made arbitrarily thin.

G. Cryostat Design

The basic mechanical layout of the cryostat is shown in Figure 11. One of the fundamental mechanical concerns in designing a VSM

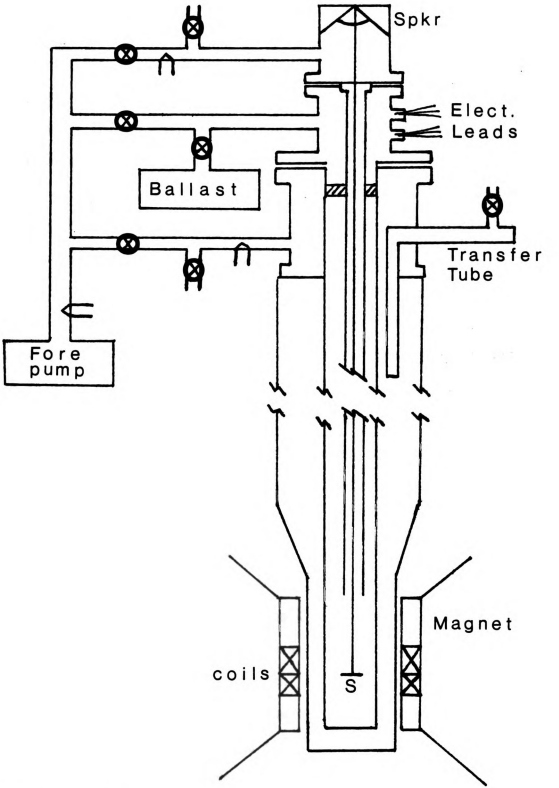

Figure 11. Basic cryostat layout.

is to insure that no mechanical coupling exists between the detection coils and either the cryostat or the pumping system. The vacuum pump was crudely shock mounted and the line going to the magnetometer was at one point firmly anchored to the laboratory wall. All of the final vacuum connections were made with thick walled rubber vacuum hose flexed in such a way as to damp out vibration. Lead bricks were placed on top of the magnetometer to minimize any possible recoil. One should always check to see that the dewar does not contact the magnet pole face.

Another point of general construction interest includes the use of stainless steels in cryostats. Their usefulness stems from their high strength and toughness as well as thermal insulating properties even at 4.2°K. The magnetic properties of stainless steel are probably less well-known. The austenitic phase of the AISI 300 stainless steels is non-ferromagnetic. However, these steels are metastable at temperatures below room temperature and can be transformed to ferromagnetic martensite either by cooling or cold working. A study of the martensite transformation due to cooling alone was done for a wide selection of the AISI 300 stainless steels in Reference 43. They found that of the grades 302, 303, 304, 308, 310, 316, 321, and 347, only the 303 and 304 steels showed any transformation from the austenstic to the martensitic phase after repeated thermal cycling between room temperature and 77°K. Further work was done by Larbaleistur and King.[44] They found ferromagnetic behavior in stainless steep types 321, 347 and 310. The ferromagnetism in the 321 and 347 steels increased in magnitude with

each additional cooling to low temperatures. Both types 321 and 304 were used in the construction of the original magnetometer. It was used to construct the inner dewar and the vibration guide tube. Thus, it became clear these were potential troublespots. Indeed, when samples of these steels were tested in the magnetometer, they were extremely magnetic at low temperatures. Thus, two modifications were made. The lower half of the guide tube was replaced by aluminum tubing and its length was reduced. This allowed the current carrying wires to the holder to be attached to the rod a greater distance from the detection coils. The second modification was to replace the lower half of the inner dewar by pyrex glass using a glass-metal seal. This also allowed visual observation of the sample which is a slight added bonus. Finally, the magnetometer was able to take data above 77°K. One could either transfer liquid nitrogen into the dewar as one did with liquid helium, or one could use a small dewar built by the MSU Scientific Glass Blowing Shop. It was supported by a wooden platform which rested on the NMR coils.

H. Temperature Control and Measurement

The necessity of temperature control is one of the other major differences between this magnetometer and the MF system. The MF system which operated in the 77-300°K range did not employ heaters. Their method involved pouring in the liquid nitrogen and by adjusting the nitrogen gas exchange pressure, control the rate of cooling of the sample. Data points were taken in a quasi-static fashion. As one proceeds to liquid helium temperatures, there are three factors

which make this technique more difficult. The first is that the specific heat of the cryostat is going to be on a steeper part of the Debye curve. Therefore, less energy needs to be removed to cool the sample. This makes the process of cooling much faster. The second point is that the latent heat of ^4He is 2.6 J/ml and is 161 J/ml for N_2. What this means effectively, is that in order for helium liquid to collect, the inner dewar space must be at 4.2°K. Unless the exchange gas pressure is very low, the sample and holder will rapidly approach 4.2°K because of their close proximity to the liquid. Finally, the magnetic susceptibility of most of the materials studied tended to follow a Curie-Law type of behavior. This means that the rate of change of χ with T is much greater at low temperatures than at high temperatures.

The mechanical forepump in our system is incapable of pulling a hard enough vacuum to use the exchange gas technique. Construction of a diffusion pump system to do this was started. Some ideas of how to insert small calibrated amounts of helium gas were also studied, but in the end, it was decided to use electronic temperature control.

This sytem operated on a null basis. The thermocouple output was approximately 1225 μV at 4.2°K and decreased to zero at 77°K (the reference bath was liquid nitrogen) and then switched sign at higher temperatures. The method was to take the thermocouple output and add in series a bucking voltage provided by a Keithley Model 260 Nanovolt source. This sum was fed into a Keithley Model 155 Null detector/microvoltmeter which in turn output a voltage

between 0 and 1 volts, depending on the null imablance. This voltage served as the input to a homemade controller whose job it was to output heater current to the Evanohm heater. Its schematic is included in the Appendix. A brief discussion of the design of temperature controllers can be found in Reference 45. In that article the basis of control theory is presented including the effects of time constants on stability, and how to alter the frequency dependence of $g(\omega)$ (the gain and frequency response of the controller) using proportional, derivative, and integral control. Proportional control is when the control signal is simply proportional to the error signal. Derivative control is a control signal proportional to the time-derivative of the error signal, and integral control is when the control signal is proportional to the integral of the error signal. It is easy to construct such control signals with the aid of operational amplifiers. If one adds to that the unity gain followers and inverters, the design of the controller should be fairly obvious. The overall gain of the loop is controlled by the size of the resistor placed in series with the heater resistance. It's also a good idea to place a DC ammeter in series with the heater to monitor the current being delivered.

I. Typical Run

The following is intended to be a rough guide to operation of the system when taking low temperature data. The details of each step vary according to the taste of the experimentalist.

(1) Periodically, one should check the detection coil balance by

applying a 33 Hz signal to the NMR coils. One should also occasionally check the phase relationship between the reference magnet and the rotating flip coil. The FFC-4 manual describes the sequence of events to minimize the quadrature signal.

(2) The magnet is rolled into position and noted with the plumb bob. The holder is centered in the magnet gap and vertically between the detection coils.

(3) Most of the samples are rolled and cut to size so that mounting of the sample consists of simply covering it with a light layer of silicon grease and inserting it into the holder.

(4) Before the dewars are put into place it is generally worth the time to check lead continuity. This includes checking thermocouple leads, null current leads, and heater current leads.

(5) The inner dewar is fastened into place, usually using some shims to keep it parallel and centered with the magnetometer driving rod.

(6) The outer dewar is added and rotated so that the unsilvered strip exposes the transfer tube. Fine positioning of this dewar can be accomplished by pumping on the outer dewar airspace and gently applying pressure to the inner walls of the dewar near the top. Any contact between the magnetometer drive and the inner dewar should be visible on the oscilloscope. The output from the permanent reference magnet gives a good indication of vibration quality.

(7) Most of the electronics is now turned on. The precooling time is approximately four hours, and this gives the equipment time

to stabilize. Generally the FFC-4 is turned on approximately one hour before the start of data taking, and the main current supply is energized but not delivering current about 15 minutes prior to data taking.

(8) The vacuum jacket of the outer dewar should be pumped out, flushed with nitrogen and pumped out again. Then both dewar spaces are pumped out with a mechanical forepump and filled with gaseous nitrogen.

(9) The precooling is done with liquid nitrogen in the dewar jacket and also in a separate dewar which surrounds the tail.

(10) The sample is given a minimum amount of vibration to prevent the shaft from freezing up.

(11) When the cryostat is sufficiently cold (100°K), the nitrogen gas is evacuated and replaced with helium gas. (The inside dewar space is filled to 1000 microns and the outer dewar space is filled to just above atmospheric pressure.

(12) If the system is to be cooled to 4.2°K in zero field, then one can proceed with the separate dewar in place. If the system is to be cooled in some applied external field, then the external dewar must be removed and the magnet rolled into position and the proper magnetic field maintained.

(13) One can proceed to transfer helium in the normal fashion. Usually it's a good idea to evacuate the vacuum jacket of both halves of the transfer tube prior to transferring helium. If the free half of the split transfer tube should go soft, a flexible transfer tube can be used.

(14) As the helium transfer commences one should monitor both the temperature as indicated by the thermocouple and the end of the transfer tube inside the dewar. A good transfer typically requires approximately 5 liters of helium.

(15) After filling, but before taking data, one should check the exchange gas pressure. A check should also be made that the dewar is not touching either pole face of the magnet. The vibration coupled to the coils will make the data meaningless.

(16) In addition, on humid days, water may condense on the outside of the dewar. Usually a fan will reduce this greatly. I would not recommend taking data unless the exterior of the dewar is dry.

(17) The sample drive amplitude should be increased to approximately 3 VAC and checked for quality with the oscilloscope.

(18) The frequency of vibration should be checked occasionally to see that it is in the center of the narrow band pass of the tuned amplifier. The phase of the sample relative to the lock-in amplifier should now be adjusted using the phase adjust in the reference channel.

(19) The interupt levels of the "Interrupter" should be adjusted according to the ambient magnetic field noise.

(20) If everything checks out, data taking can commence. Generally for data at 4.2°K a relatively large exchange gas pressure is used, because the nulling currents at 4.2°K in reasonable fields can be large enough to cause the sample temperature to rise slightly.

(21) As the temperature is raised, the inner dewar space should be evacuated to about 25 microns so that excessive heater currents are not required. Since the volume of the inner dewar space is small, small changes in the amount of helium gas present cause relatively large changes in the exchange gas pressure. This makes temperature control more difficult. For that reason a ballast tank was added to the system, and should be opened to the inner dewar space at this time. If operating properly, the temperature controller should be able to keep the temperature constant to within $\sim$1 μV on the thermocouple output.

(22) A typical data point involves writing down the null current values required to generate a slightly positive and slightly negative phase-lock voltage. Perhaps a dozen values on each side of zero is reasonable. These values are separately averaged and then one interpolates to find the value of the current that nearly produces zero output voltage.

(23) When the data taking is finished, its important to remember to close the ballast tank valve. It is also a good idea to pump on the inner dewar space. If the pressure within the inner dewar should rise because the gas has warmed up, it could conceivably come out of the quick-disconnect and cause damage.

J. Calibration

The calibration of vibrating sample magnetometers is a very interesting topic. The degree of complexity is a strong funtion of the type of calibration desired. Two approaches will be discussed

The first is an absolute calibration of the instrument based on the dipole approximation. The second is the safer but less flexible comparison method. The dipole approximation is merely a statement that the detection coils are sufficiently far away that the only relevant multipole componet of the field is the dipole component. In that case, the voltage induced in the detection coils due to the changing flux is given by

$$V = \frac{d\psi}{dt} = |\vec{m}|\omega G_S G_C = \chi|\vec{H}|V\omega G_S G_C$$

where χ is the volume susceptibility

H is the applied external magnetic field

V is the sample volume

ω is the frequency of vibration

G_S is some geometrical factor due to the sample geometry

G_C is some geometrical factor due to the coil geometry.

In this way, if one inserts a sufficiently small spherical sample which has a well known moment in a given field (typically the saturation moment of a small sphere of pure nickel), then one can numerically determine $G = G_S G_C$. Then the machine is calibrated as long as any sample measured produces essentially only a dipole field. Complications arise when the samples do not meet this criterion. Foiles and McDaniel[46] investigated the case of right circular cylinders having a diameter to length ratio of ±1 to 5. This involved two basic measurements. One was the effect of fixing the sample length and varying the diameter. The second

was varying the length and holding the diameter fixed. In the first case, they found the voltage output to be directly proportional to the sample area. (The coil diameter was never greater than 1/8 that of any coil dimension. In the second case they found that the dipole approximation was not valid and the voltage output behaved like $V \alpha$ (volume)$\cdot(1 + \beta L)$. Thus, if one is going to use samples in this size and shape regime, more system parameters are going to have to be determined. The easiest way around this is to use the second calibration technique which is just the familiar comparison method. Here the idea is to use a standard sample with exactly the same geometry as the unknown samples. Since the samples studied by the author were essentially of the same geometry as that investigated by Foiles and McDaniel, their results could be employed. In particular, one could use as a reference standard, a sample of palladium which had the same length as the unknown samples, but somewhat smaller diameter. This data will be presented shortly.

There is another approach which can be used if the magnetometer employs a Domenicali coil. In this case, when the axis of the cylinder is parallel to the applied field, the induced dipole moment in the sample can be cancelled by an equivalent current shell produced by the Domenicali coil. Thus, the absolute voltages produced in the former method are replaced by dc nulling currents. In principle one could absolutely calibrate this instrument because presumably one can calculate the magnetic moment of a finite solenoid.

In practice, we also employed the comparison method. The coil to coil distance across the gap is approximately 66 mm in our VSM.

Since the sample length is about 14 mm, we are certainly not in the pure dipole regime. Thus one begins to wonder if the results for varying diameter samples have the same behavior as when they were nulled out electronically. For now one must ask the question; of what form is the field produced by two concentric solenoids of finite length but different diameter? And is the detection coil system such that it only detects dipolar fields and ignores quadrupolar fields? The Foiles-McDaniel study indicates that the coils are detecting more than just simple dipolar fields. My guess is that they are detecting quadrupolar fields also and so if two concentric solenoids produce a quadrupole field we are still OK. The point I'm trying to bring home is that with the nulling current technique one must have some grasp of how the addition of the coil moment changes the effective field of the sample + Domenicali coil. In particular, if different multipole moments become dominant, is the detection coil configuration sensitive to these new components? If it is not, there exists the possibility for error. Figures 12 and 13 show the room temperature palladium calibration runs for the two holders used to take the data shown in this dissertation. The conversion of raw data to useable numbers proceeds as follows:

$$\chi_A^x = \frac{m_s}{m_x} \cdot \frac{I_n^x}{I_n^s} \cdot \frac{A_x}{A_s} \cdot \frac{H^s}{H^x} \cdot \chi_A^s \qquad (3.1)$$

where m_s, m_x are the masses of the standard and unknown, respectively;

I_n^x, I_n^s are the nulling currents;

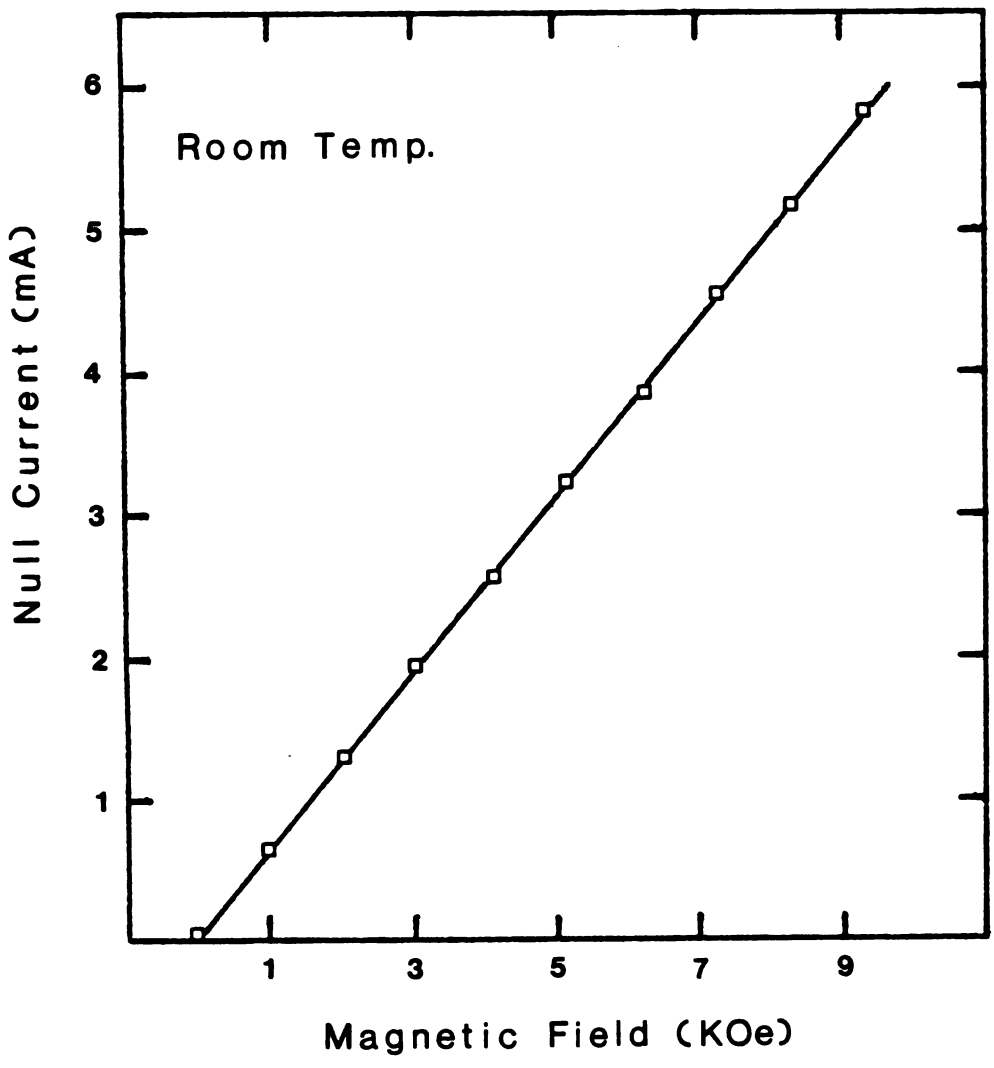

Figure 12. Palladium calibration run.

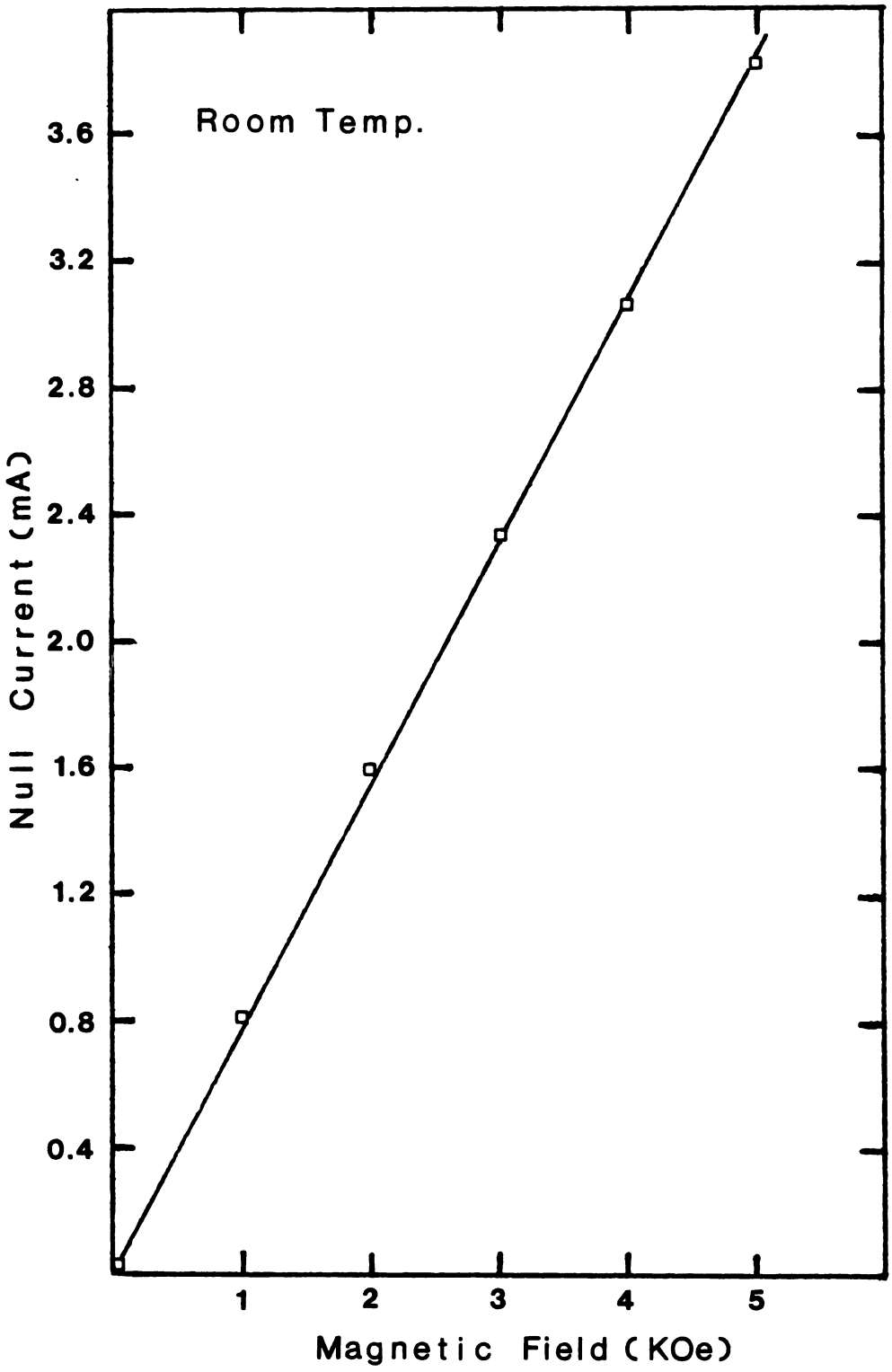

Figure 13. Palladium calibration run.

A_x, A_s are the molecular weights;

H^s, H^x are the applied magnetic fields;

χ_A^s, χ_A^x are the molar susceptibilities.

The host contribution is subtracted out using

$$\chi^{Alloy} = (1 - c)\chi^{host} + c\chi^{impurity}$$

K. Further Improvements

As mentioned previously, the number one problem limiting the sensitivity of the Foner VSM in my case was ambient magnetic field noise. I have previously discussed some of the techniques employed to remedy this situation. Perhaps the most obvious plan of attack was seriously considered, and even begun, but never completed. This involved the simple modification of reducing the pick-up coil size and mounting them inside the dewar very close to the sample (See Figure 14). Since the signal from the sample falls off as $1/r^3$, moving closer to the sample reaps large benefits. Also, shrinking the coil size reduces field noise which tends to go as Nr^2. In addition, a much larger speaker was purchased. A 10 inch guitar speaker with a 7 lb magnet and 2" voice coil capable of using 70 watts RMS was decided upon. Its frequency response was 60-9000 Hz. The plan was to drive this speaker at ≃100 Hz with a Krohn-Hite Model UF-101A ultra low distortion power amplifier. Since the induced emf varies linearly with frequency, one might expect an increase of a factor of three from the frequency change. A sample to detection coil distance reduction of 33 mm to say 19 mm gives a signal

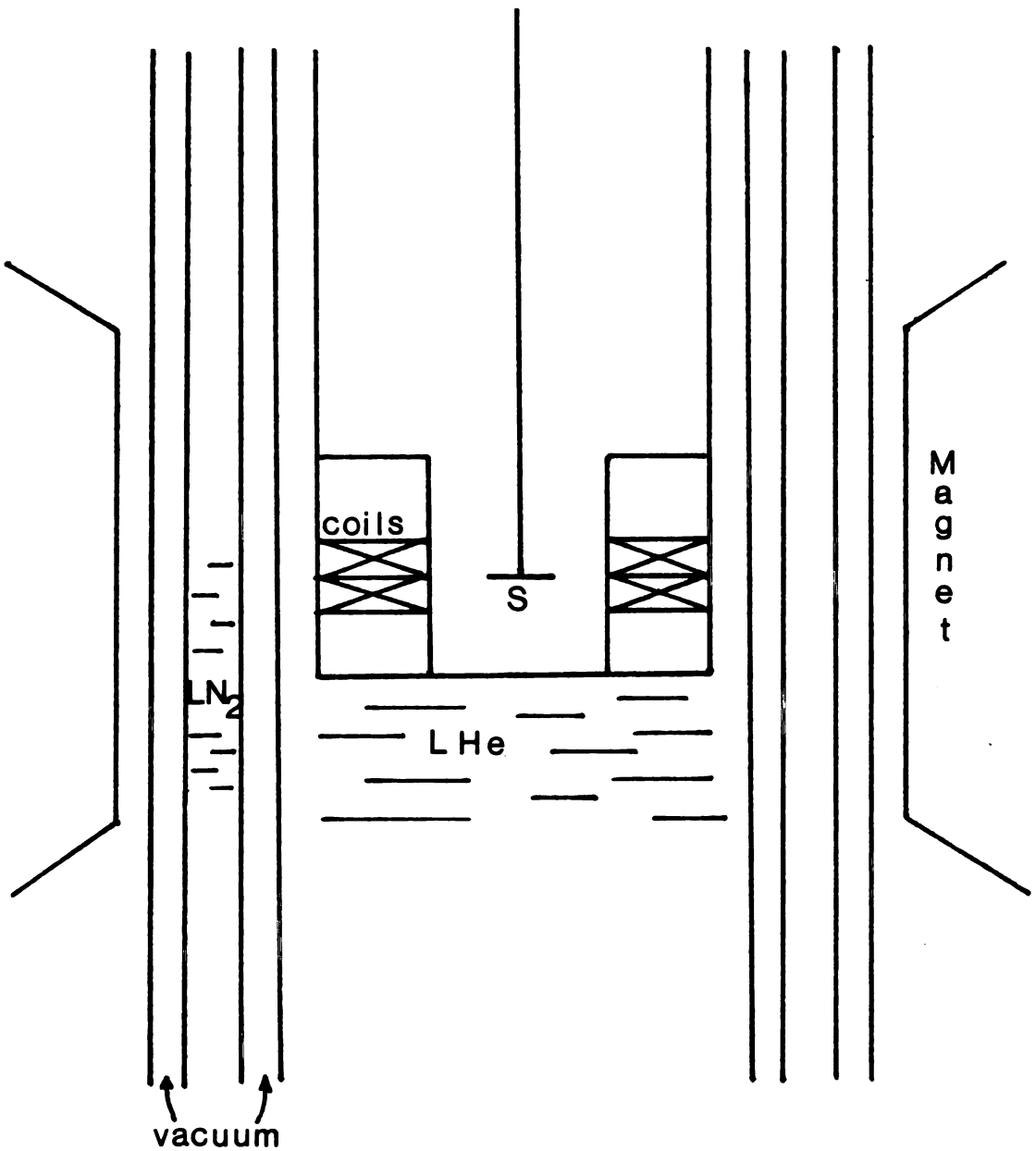

Figure 14. Possible future VSM.

increase of (5.2). A reasonable noise reduction of (3/16)/(11/16) = 0.27 could reasonably be expected. This leads to an overall signal/noise ratio improvement of about 60. There may, however, be a serious problem with this design. A convincing technique for preventing detection coil motion was not available. Indeed, that may be a fatal flaw with this design. Another advantage to this design is the reduction in thermal noise due to the cooling of the detection coils.

It is also worth noting that other attempts to design a VSM which is insensitive to field noise and microphonics have been made. See for example Reference 47.

IV. SAMPLE PREPARATION AND RELIABILITY

A. CuMn

1. Preparation

The preparation of the CuMn samples was accomplished in a straight forward fashion using a Lepel induction furnace. A graphite crucible served as the active heating element. Inside the graphite was an alumina crucible which contained the copper and manganese. Both crucibles were placed inside a vycor glass holder which fit into the induction coil windings. The crucible and glass were baked in an atmosphere of less than 10^{-4} mm Hg.

Prior to melting, the copper was etched in 50% nitric acid and the manganese was etched in acetic acid followed by nitric acid. The appropriate masses were weighed on a Mettler balance. The copper and manganese was induction heated in approximately 1/3 atmosphere of argon to approximately 100°C above the melting temperature of the alloy. After being reasonably certain the mixture was homogeneous, it was swiftly poured into a copper chill cast mold. The copper mold was lightly etched in nitric acid before use. The melt is quenched very quickly due to the sizable mass of the copper mold. The alloy was remelted and repoured usually two more times to insure a good mixture. The resultant alloys are probably quite close to their nominal composition.

The major uncertainty arises from the copper which evaporated and traces were found deposited on the vycor glass holder. Some uncertainty may also be due to not all the contents of the crucible leaving the crucible. Typical numbers for a 5 gram alloy would be a loss of about 0.04 grams. If this is attributed to copper, the deviation of manganese concentration from nominal is probably less than 0.1 at %.

The quenched samples were then rolled into approximate cylinders with diameters of about 3 mm. They were also cut in 14 mm lengths. A final etch was performed before the samples were removed. In addition, some of the samples were annealed in order to ascertain whether or not cold working had any effect, and also to check for possible clustering effects. A typical anneal consisted of first sealing the samples in vapor tubes at approximately 1.5×10^{-4} torr. Then they were baked at approximately 600°C for approximately 30 hours and then cooled at 50°C per hour until the samples reached 450°C. Then they were extracted from the furnace. A check of sample masses before and after annealing showed virtually no change (<0.0005 gm).

2. Magnetization vs. Field

After the CuMn samples were prepared, two basic tests were made to check the quality of the samples. Our principal concerns were whether or not the Mn atoms had gone into solution in a uniformly random fashion, and whether or not the cold working caused by the

rolling process had any effects. Two samples at each concentration were made. One would serve as a control sample and would not be further modified. The second would have its susceptibility measured as a function of temperature, both before and after an anneal. It would also have its magnetization measured as a function of magnetic field at 4.2°K. The magnetization of CuMn (2 at%) and CuMn (3 at%) - annealed samples vs. field are shown in Figure 15. Now the magnetization of weakly coupled moments can be expected to exhibit a magnetization curve based on a Brillouin function: $M = N_g J \mu_B B_J (\frac{g J \mu_B H}{k_B T})$. By going to low temperatures and high magnetic fields, we can best look for evidence of possible cluster formation. At 4°K and 9000 gauss, $\frac{g J \mu_B H}{k_B T} \cong (0.60)$. Figure 16 shows a plot of $B_2(\chi)$. The linear portion of $B_2(\chi)$ extends to just above this value, so we would expect M to be approximately linear in H. The plots in Figure 15 are linear within experimental error. The plots shown, incidentally, are the "worst case" possibilities. One would expect clustering, if it were to occur, to be present in the most concentrated, annealed samples.

3. Annealed vs. Quenched Behavior

The second test was to examine the temperature dependence of χ for annealed and cold worked samples. Figures 17-19 show plots for annealed and cold worked 1%, 2%, 3% Mn samples. The results are summarized in Table 4. The θ-values are essentially independent of heat treatment within experimental error. There may be a slight hint of increasing values of $\Delta\theta$ for increasing concentration.

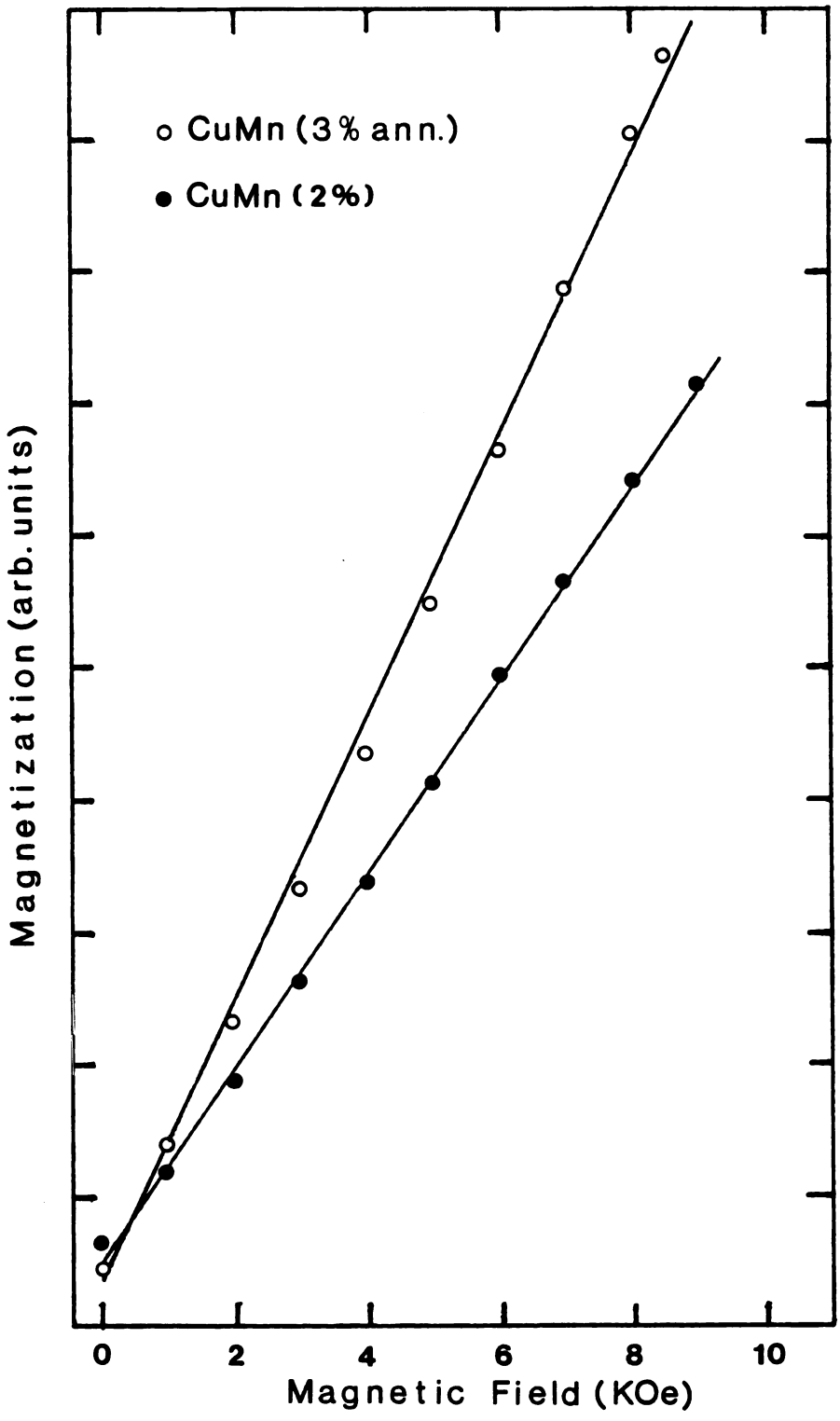

Figure 15. CuMn (3%) - annealed and CuMn (2%) - M vs. H.

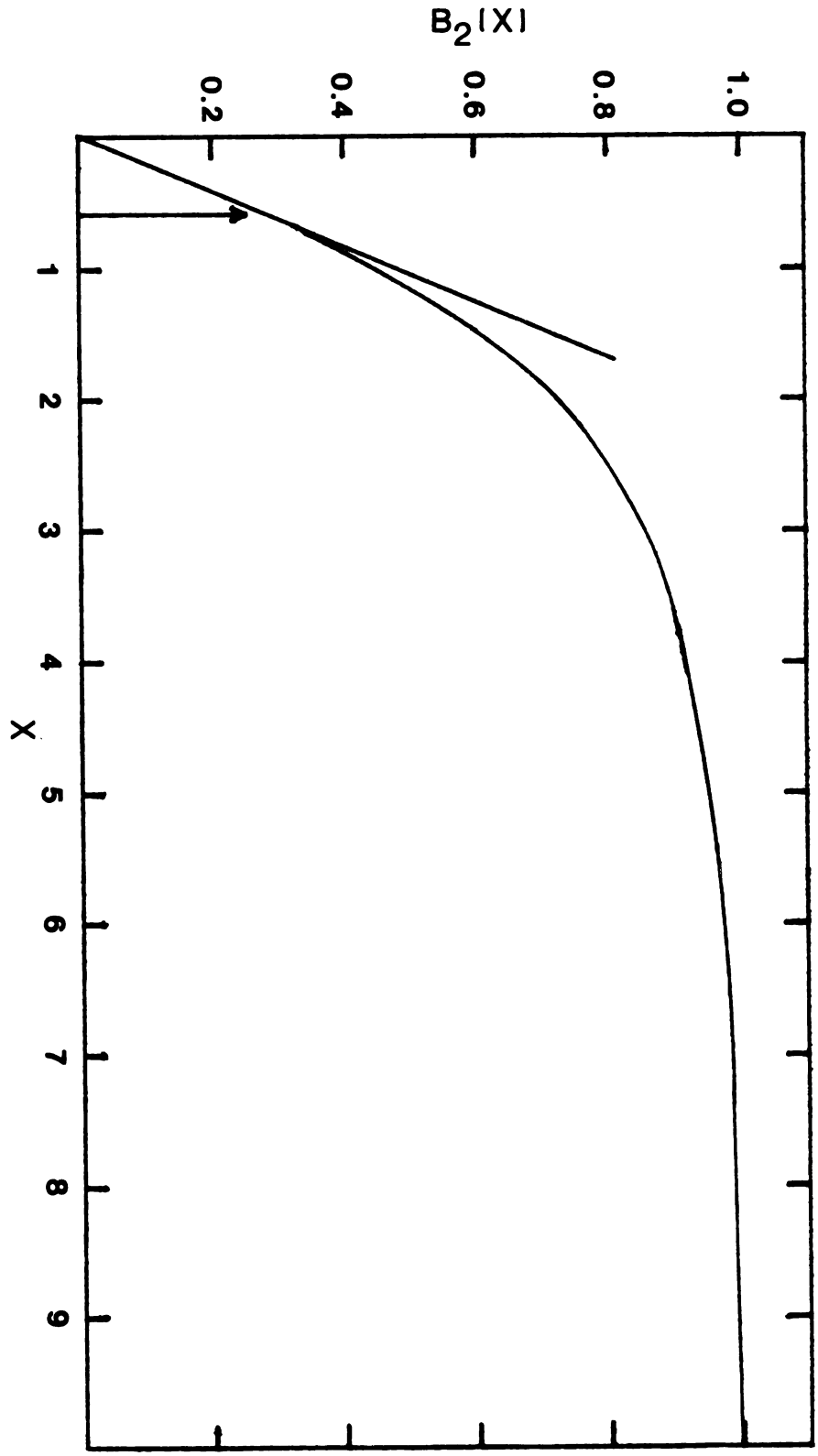

Figure 16. Brillouin function for spin S = 2.

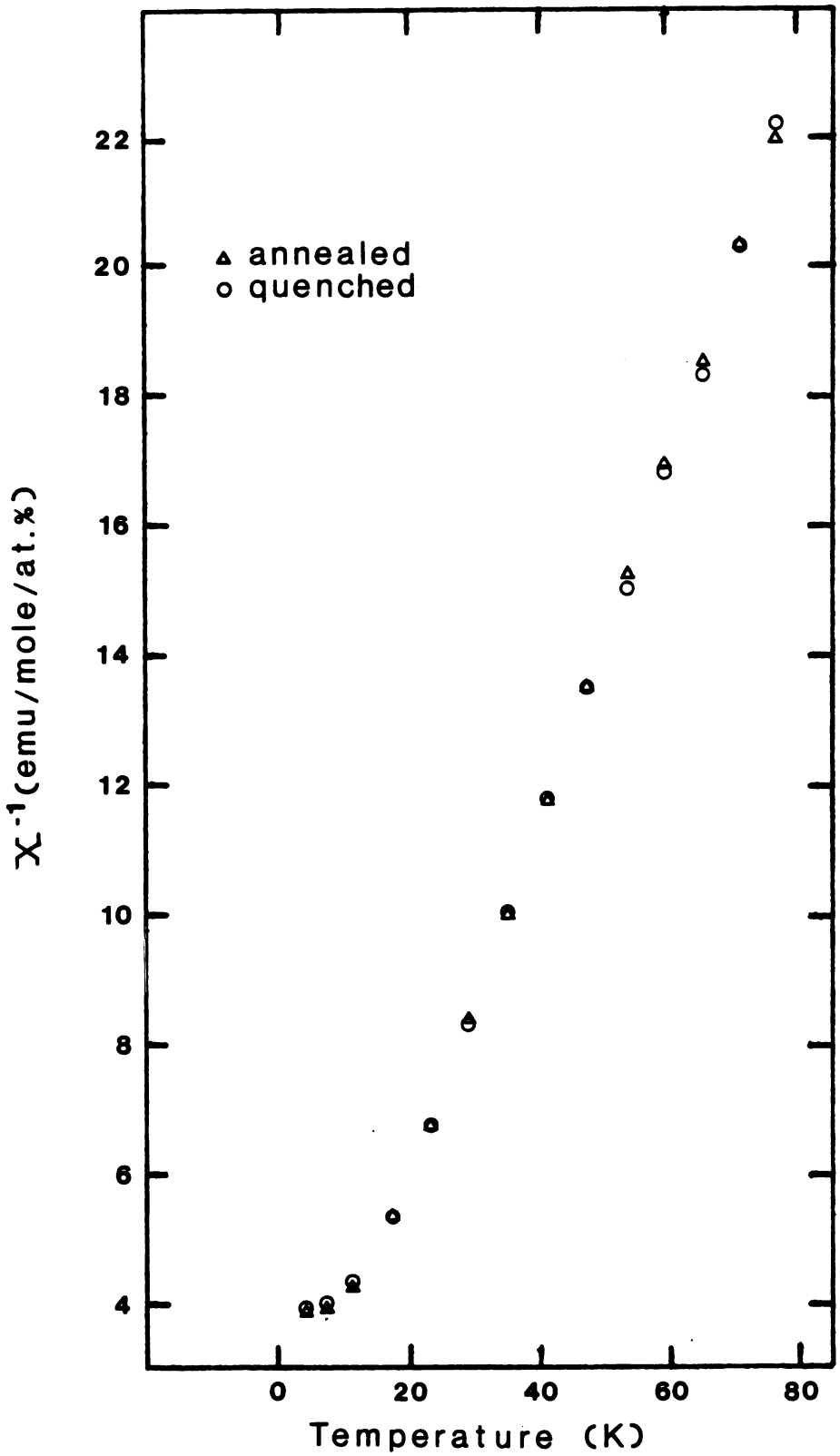

Figure 17. CuMn (1%) quenched vs. annealed behavior.

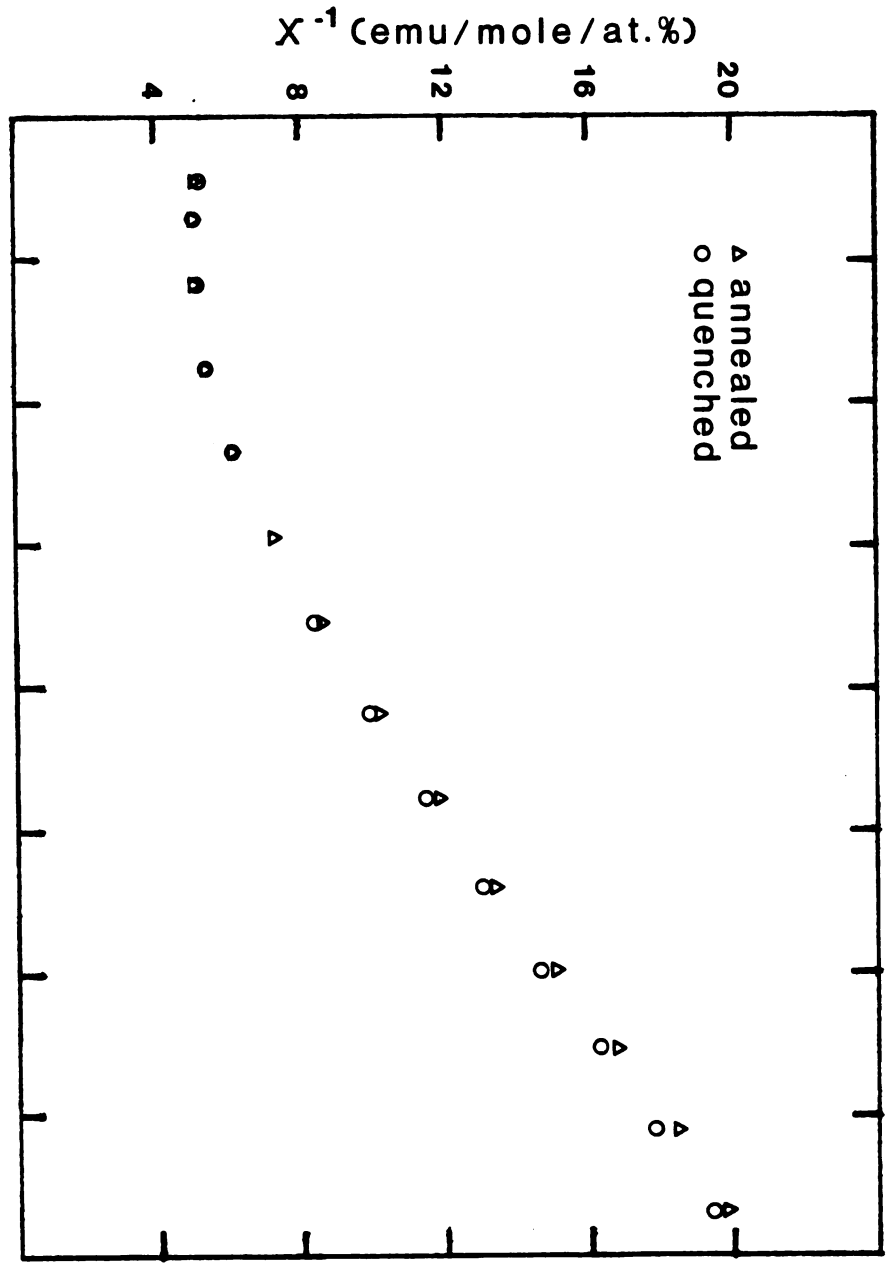

Figure 18. CuMn (2%) quenched vs. annealed behavior.

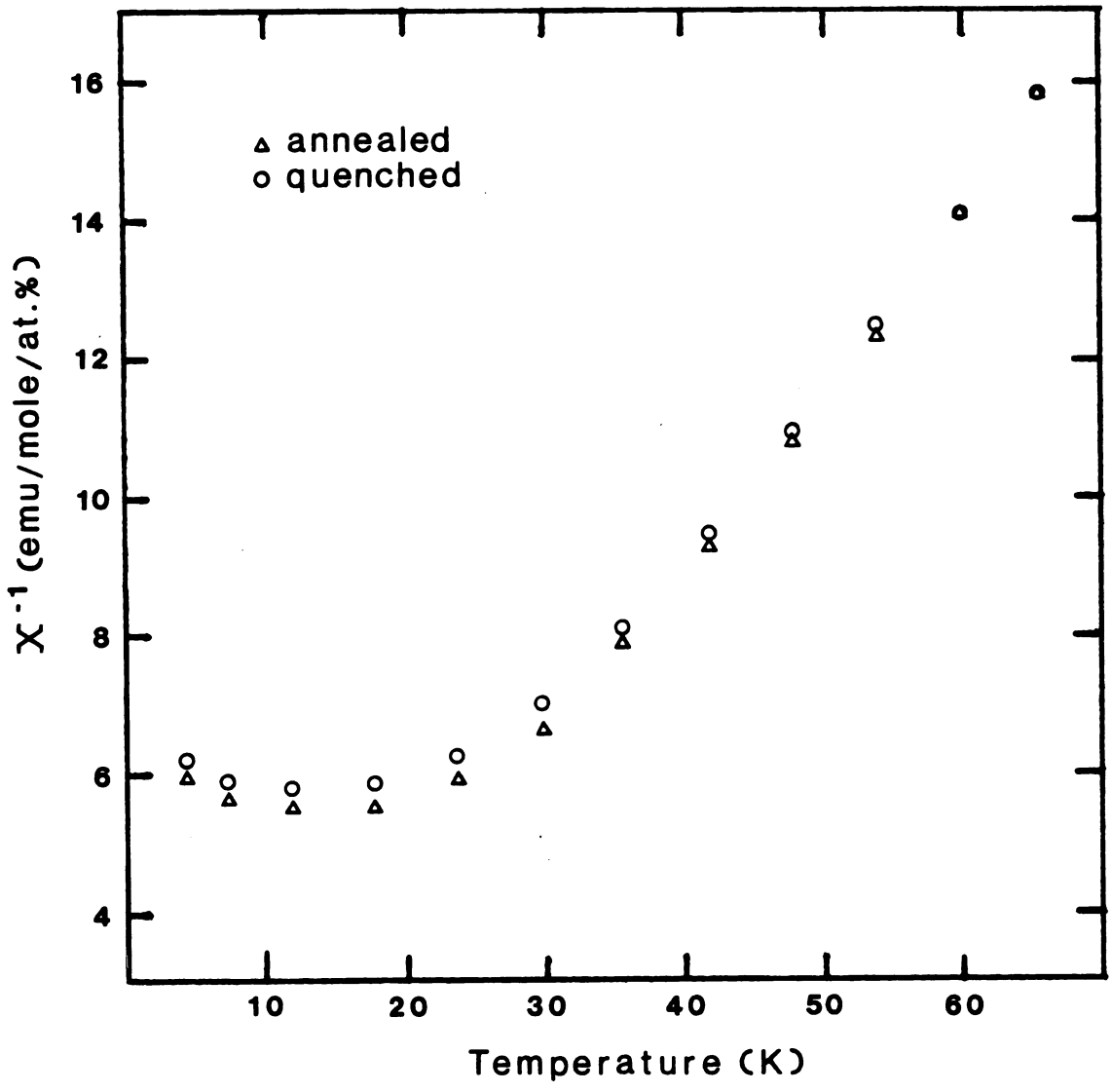

Figure 19. CuMn (3%) - quenched vs. annealed behavior.

Table 4. Comparison of Annealed and Quenched CuMn.

	θ (°K)			P_{eff} (μ_B)	
Alloy	Annealed	Cold Worked	$\Delta\theta$	Annealed	Cold Worked
1% Mn	1.47	2.97	-1.5	5.25	5.19
2% Mn	6.84	7.23	-0.39	5.31	5.37
3% Mn	14.5	13.7	0.80	5.08	5.13

This may be an indication of some short range order effects. But if they are taking place, it is on a small scale and we shall not be concerned with them. The P_{eff} values are a little on the high side, but the agreement between annealed and cold-worked samples is always better than 2%.

B. Ternary Systems

At this stage it would be appropriate to make some comments regarding the homogeneity and overall metallurgical quality of the samples. The Cu_3Pt, CuPd(17) and Cu_3An samples were not prepared by the author, so only a brief description of their character will follow. In general, the ternary alloys also displayed linear magnetization versus field behavior. See Figure 20 for the "worst case" example of Cu_3PtMn (3%) at 4.2°K. On the other hand, the behavior of [θ (annealed) - θ (quenched)] is large and a strong function of manganese concentration for the ternary alloys, which is in marked contrast with the behavior of CuMn. This behavior, in addition to the dependence of P_{eff} and T_{sg} on host condition and concentration, make up the majority of the data to be presented in the next section. However, some prior work on the characterization of these samples was carried out and is worth making reference to.

1. Cu_3PtMn Samples

The best source of information regarding the Cu_3PtMn samples can be found in Reference 48. In particular, x-ray studies to determine

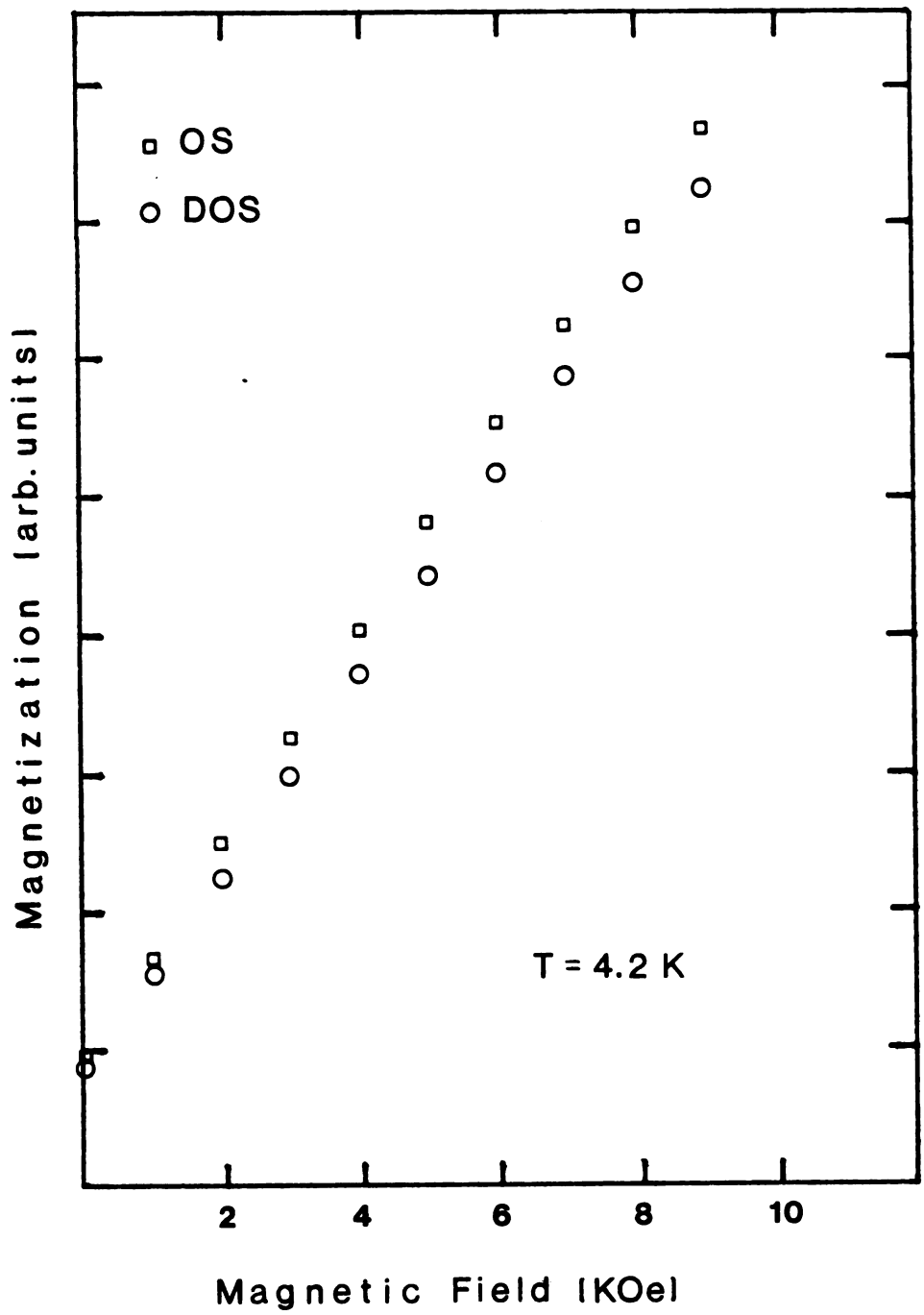

Figure 20. Cu_3PtMn (3%) OS and DOS - M vs H.

the long range order parameter S are described. S was found to increase as the manganese concentration increased. This is strong evidence that there is no long range order among the manganese impurities. For example, were the Mn atoms to preferentially occupy Pt sites only, S would decrease with increasing concentration.

2. CuPd(17)Mn Samples

Reference 9 is the best source of information regarding the preparation of the CuPd(17) samples. It includes magnetization vs. applied field measurements, heat treatment, χ_m vs. C (at %) at constant temperature studies, and electrical resistivity measurements. The major results of most of this work are the following:

(1) Provided the samples were suitably etched to eliminate surface effects, linear M vs. H relationships were found for all the CuPd(17)Mn samples.

(2) The additivity rule for alloy susceptibility [$\chi^A(c) = (1-c)\chi^H + c\chi^I$] works well for the disordered host alloys and also for the ordered state alloys if the concentration dependence of P and θ are taken into account. Two of the nominal concentrations were revised on the basis of the $\chi^A(c)$ plots.

(3) The electrical resistivity is linear in c for both ordered and disordered hosts at both T = 300°K and 78°K and the values strongly suggest atomic ordering was achieved in the heat treatments.

3. Cu_3AuMn Samples

The Cu_3An alloys behave in a very analogous fashion to the Cu_3Pt and CuPd(17) alloys. That is, the phonon contribution to the electrical resistivity increases and the susceptibility becomes more diamagnetic upon ordering. There is little change in the electronic contribution to the specific heat. Earlier work done on these samples showed the presence of superlattice lines,[49] but the quantitative intensity measurements needed to establish the degree of long range order could not be made. Resistivity data from Larch[50] indicates some degree of order. Typically the ordered state data shows a lower residual resistivity, but a larger temperature coefficient of resistivity, and the Cu_3An alloys are no exception. However, one must be very careful when attempting to make quantitative statements about the degree of long range order based solely on resistivity measurements. This is especially true of our binary hosts which all form long period superlattice structures. See Section VI.F. for a more complete discussion.

V. EXPERIMENTAL RESULTS

A. CuMn

The CuMn spin-glass system is certainly one of the archetypical spin-glass systems. It has been extensively studied in the past 25 years or so. So why did we decide to make our own CuMn samples and study them ourselves? There are three basic reasons.

(1) To serve as a "standard" with which to check the operation of the new magnetometer especially as it pertains to dilute magnetic alloys.

(2) To generate our own set of "conventional" spin-glass data with which we can contrast our order-disorder data. In order to be able to make definitive statements about the behavior of Mn impurities in complicated order-disorder binary hosts, one should also examine the behavior of Mn impurities in a simple host.

(3) To attempt to answer an interesting question concerning the concentration dependence of the paramagnetic Curie temperature for low manganese concentrations. In the concentration range, a few hundred ppm $< c <$ 0.05%, the Curie-Weiss constant seems to be large and negative. For $c >$ 0.5 at.%, the Curie-Weiss constant is positive and proportional to c. We would like to have answered the question, does the θ dependence enjoy an interesting and perhaps drastic reversal of sign in the region 0.05 at.% $< c <$ 0.5 at.%?

The data for several CuMn samples is shown in Figure 21. There are several features worth noting about this data. (1) the greater the concentration of Mn impurities, the higher the temperature at which the maximum in χ occurs. Since this curvature is due to the rounding of a spin-glass cusp due to the large magnetic field, this is in accord with other experimental work. Incidentally, other workers report a dependence of the cusp position on the magnitude of the magnetic field. We did not look into this. (2) Some of the data lines are continuously changing smooth curves. The implications here, of course, are that we have not gone to sufficiently high temperatures. Some workers would argue that one should be at best at 5 T_f (T_f is the freezing temperature) before one attempts to use a Curie-Weiss analysis. But work at high temperatures requires an extremely sensitive magnetometer, since the signal falls off as 1/T. It is also advantageous to work at small fields, especially if the spin-glass transition is being examined.

The Curie-Weiss constants and effective moments are shown in Table 5. The parameters θ and P_{eff} are in the realm of expected values, but show clear difficulties. The more or less commonly accepted range of values of P_{eff} for Mn in copper is 4.9 μ_B to 5.1 μ_B. Our observed values are clustered around those values, but the deviation seems a little extreme. The average P_{eff} for the five samples is 5.15 μ_B. The θ-values are also perhaps a bit scattered. A comparison of our data with that of other workers is shown in Figure 22. One should keep in mind, however, that the Mn concentrations are estimates based on the amount of material used in preparing the

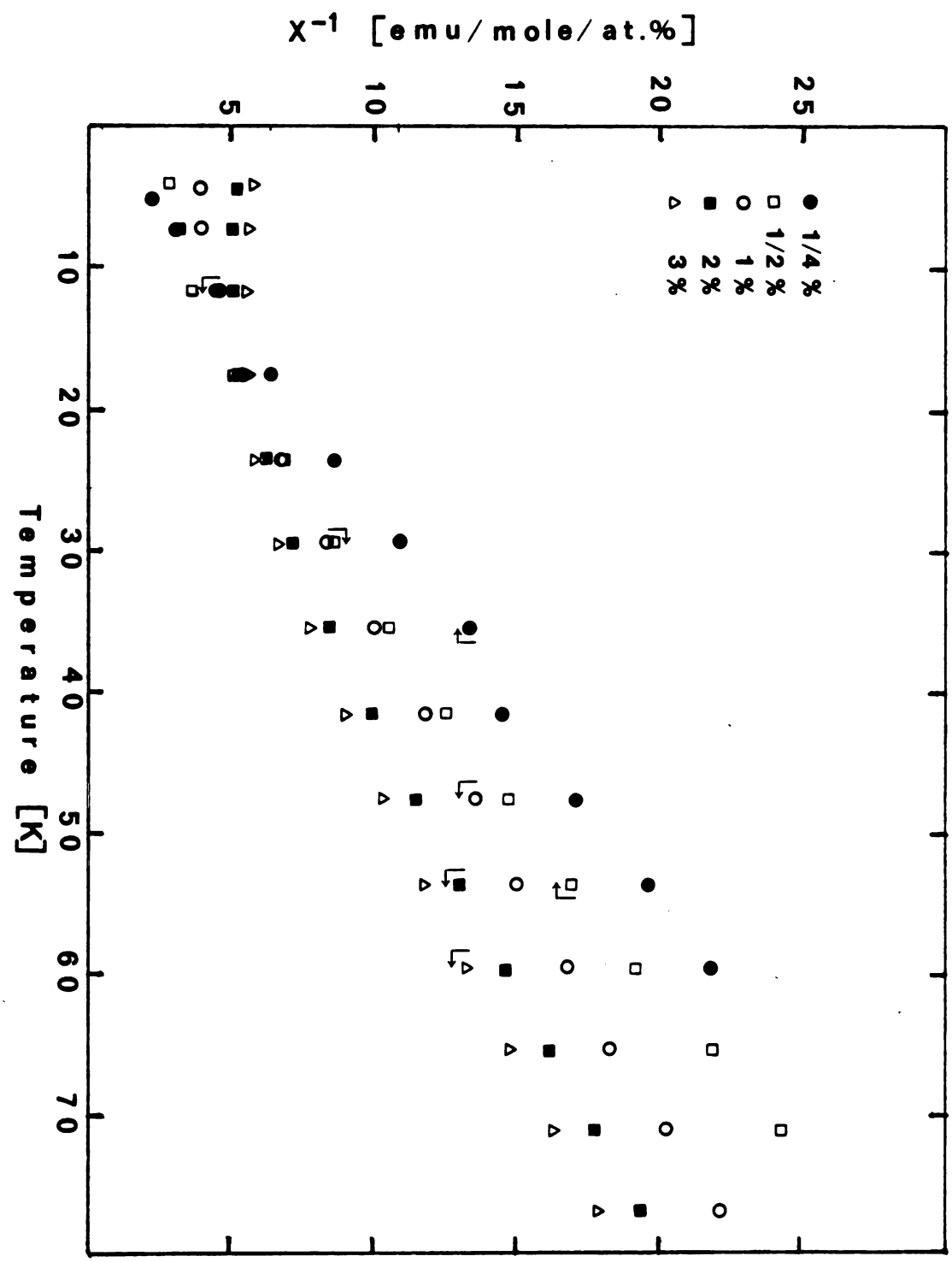

Figure 21. CuMn - inverse susceptibility vs. temperature.

Table 5. Curie-Weiss Parameters for CuMn.

Alloy	θ_c (K)	P_{eff} (μ_B)
1/4% Mn	0.52	4.62
1/2% Mn	4.80	4.84
1% Mn	2.97	5.19
2% Mn	7.23	5.37
3% Mn	10.4	5.45

Figure 22.

1. A. Van Itterbeek, et al., Appl. Sci. Res. B 7, p. 329, (1958).

2. J. Owen, Phys. Rev., 102, p. 1501 (1956).

3. R. W. Schmitt and I. S. Jacobs, J. Phys. Chem. Solids, 3, p. 324, (1957).

4. J. Owen, J. Phys. Chem. Solids, 2, p. 85 (1957).

5. A. F. J. Morgownik and J. A. Mydosh, Phys. Rev. B (1981).

6. C. M. Hurd, J. Phys. Chem. Solids, 30, p. 539 (1969).

7. S. Nagata, Phys. Rev. B, 19, p. 1633 (1979).

8. J. M. Franz and D. J. Sellmyer, Phys. Rev. B, 8, p. 2083 (1973).

9. This thesis.

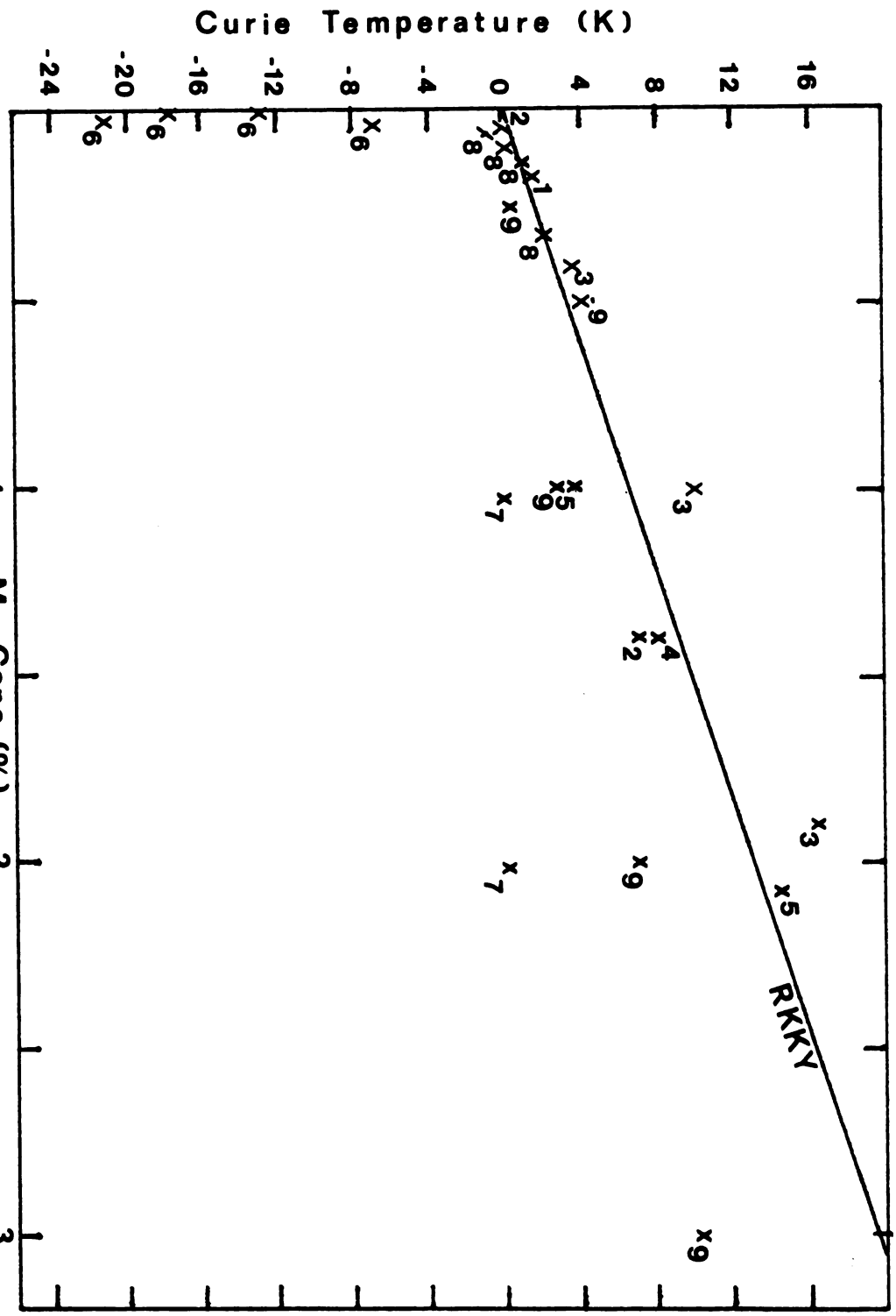

Figure 22. Curie temperature vs. concentration (selected data).

samples. They were not verified after the samples were made, but only slight deviations from the nominal concentrations are expected.

The difficulties in determining θ precisely are evident when the data shows as much curvature as ours does. This would be a good experiment for a squid-based magnetometer where the reduced sample moment at higher temperatures and lower magnetic fields is not a problem. Although the concentration regime of interest was not fully explored a few remarks are in order since this work could easily be finished by future users of the SHE susceptometer.

Recently Morgownik and Mydosh[31] have examined the high temperature magnetic susceptibility of CuMn. They find a small increase in θ when they reduce the atomic short range order by quenching the sample. For CuMn (2%), θ (slow-cooled) $\simeq$ 14.1°K and θ (quenched) $\simeq$ 17.6°K. In addition, the temperature T_d at which the susceptibility deviates from Curie-Weiss behavior is also affected by the heat treatment. For CuMn (2%) T_d (slow-cooled) $\simeq$ 80°K and T_d (quenched) $\simeq$ 96°K. On the other hand, T_f and P_{eff} do not seem to be affected by the heat treatment. They claim their results provide evidence for magnetic interactions far above T_f which they interpret as resulting from the formation of magnetic clusters. Apparently, the magnetic clusters are formed at higher temperatures for the quenched samples.

They also find the effective Mn moments to be nearly independent of concentration and to range from 4.90 to 5.16 Bohr magnetons. They also find θ to exhibit a linear dependence upon concentration; in particular $\theta = -6.9 + (10.4)\ c$.

Since the extrapolation of this linear dependence to zero concentration does not pass through the origin, this may be an indication of short range order effects. The tendency for $|\theta|$ to increase upon annealing may also indicate this. They also claim that $\theta(c)$ increases more strongly with concentration than $T_f(c)$. Our $\underline{Cu_3Pt}Mn$ ordered state data follows this pattern, but the disordered state data does not (recall Figure 5).

Finally, some attempts to understand the peculiar $\theta(c)$ behavior, such as exhibited by dilute $\underline{Cu}Mn$, have been made. See Section VI.G for a brief discussion.

B. $\underline{(Cu_3Pt)}_{1-x}\underline{Mn}_x$

The majority of the experimental time was devoted to the study of $(Cu_3Pt)_{1-x}Mn_x$ alloys because they seem to exhibit the clearest trends, and we have some prior data concerning the actual degree of long range order. The Curie-Weiss temperatures were determined from $1/\chi$ vs T data taken mostly with the VSM at applied fields of 5 KOe and 9 KOe. The ordered state and disordered state data is shown in Figures 23 and 24 respectively. The spin-glass temperatures were measured in either of two ways. The two most dilute samples had their freezing temperatures determined from measurements with the AC susceptibility apparatus. This is shown in Figure 25. The two host dilute samples had their freezing temperatures determined from SQUID measurements. A typical run is shown in Figure 26. This data is summarized in Table 6 and plotted as a function of

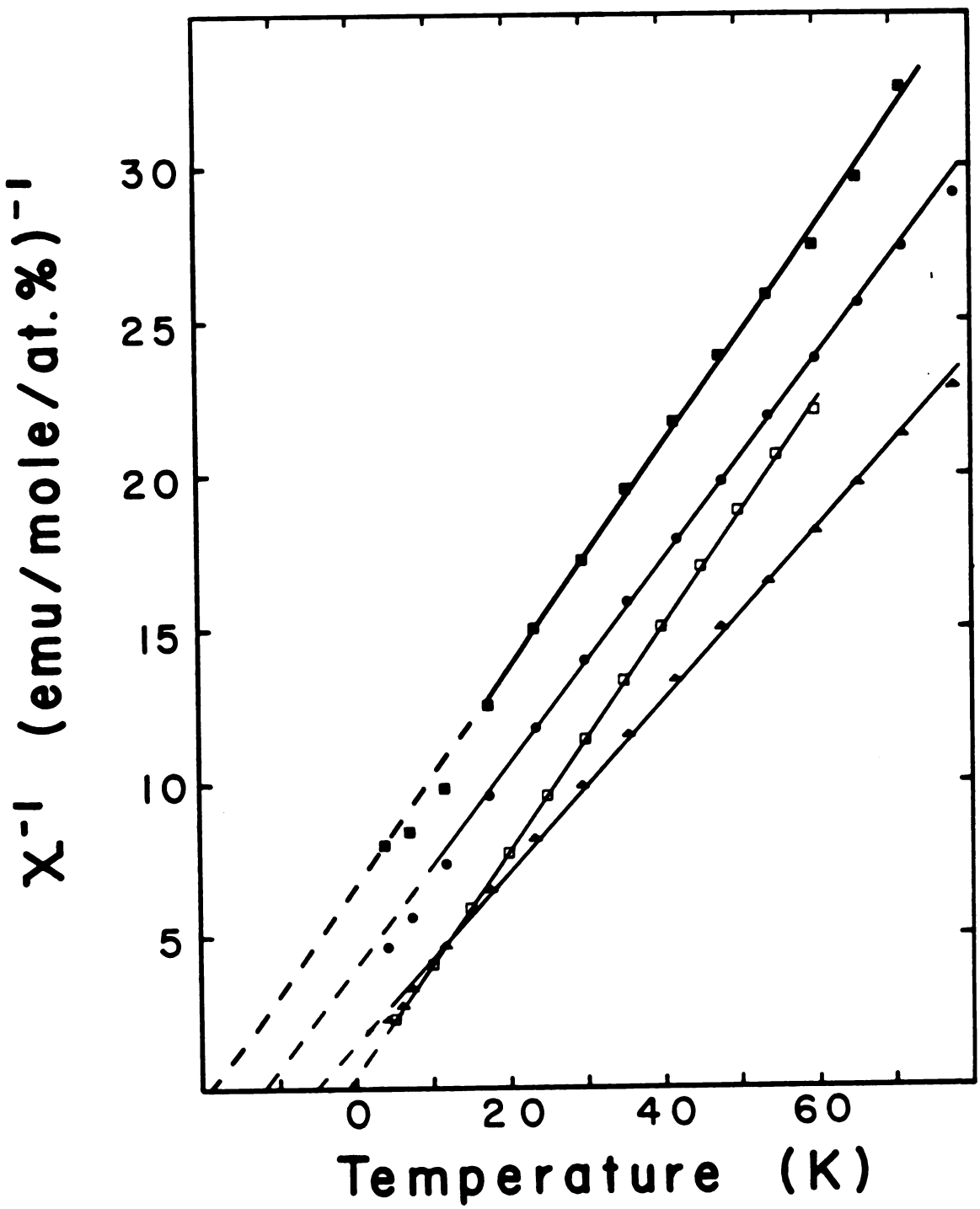

Figure 23. $\underline{Cu_3}\underline{Pt}Mn$ (OS) - inverse susceptibility vs. temperature.

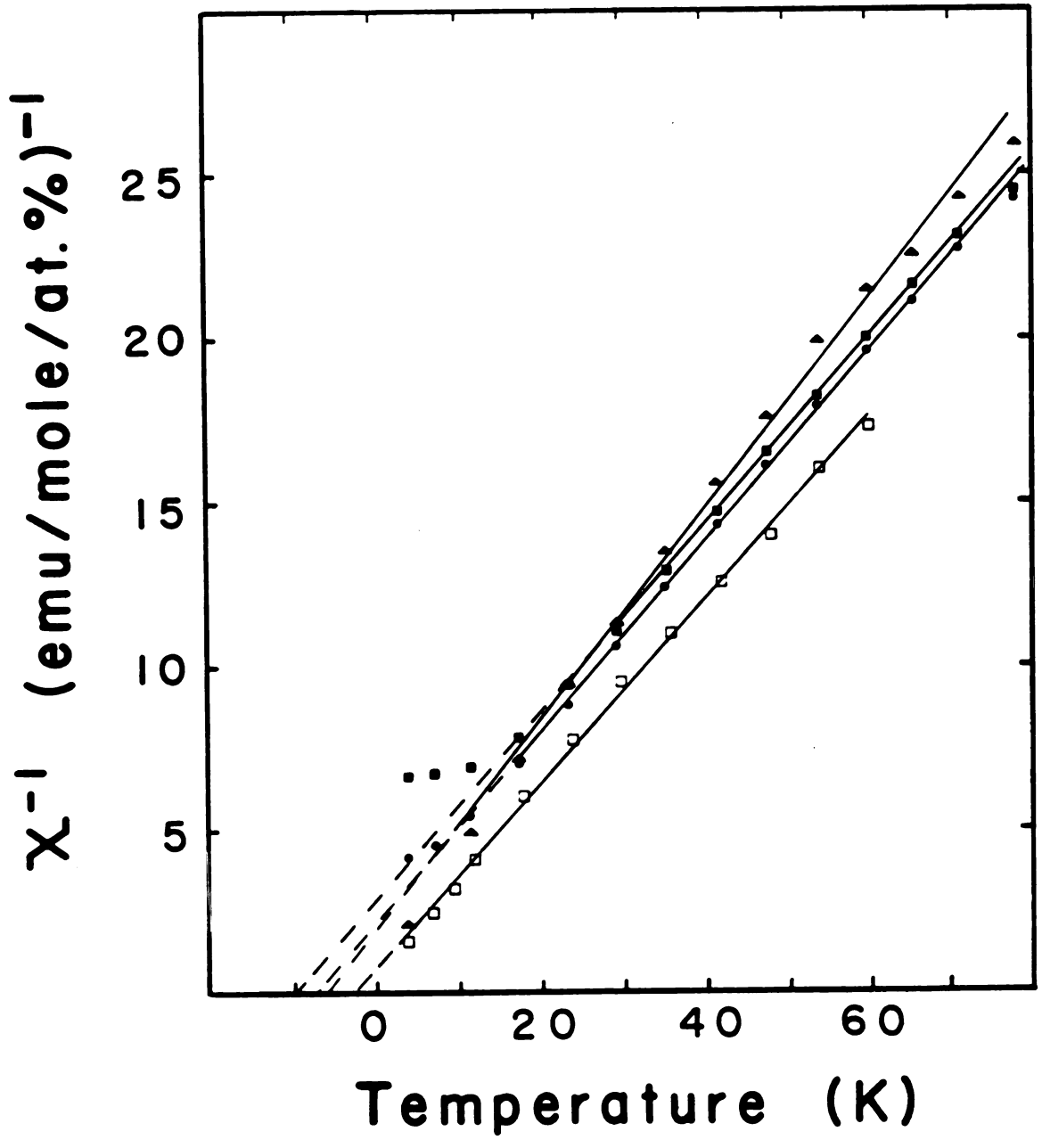

Figure 24. Cu_3PtMn (DOS) - inverse susceptibility vs. temperature.

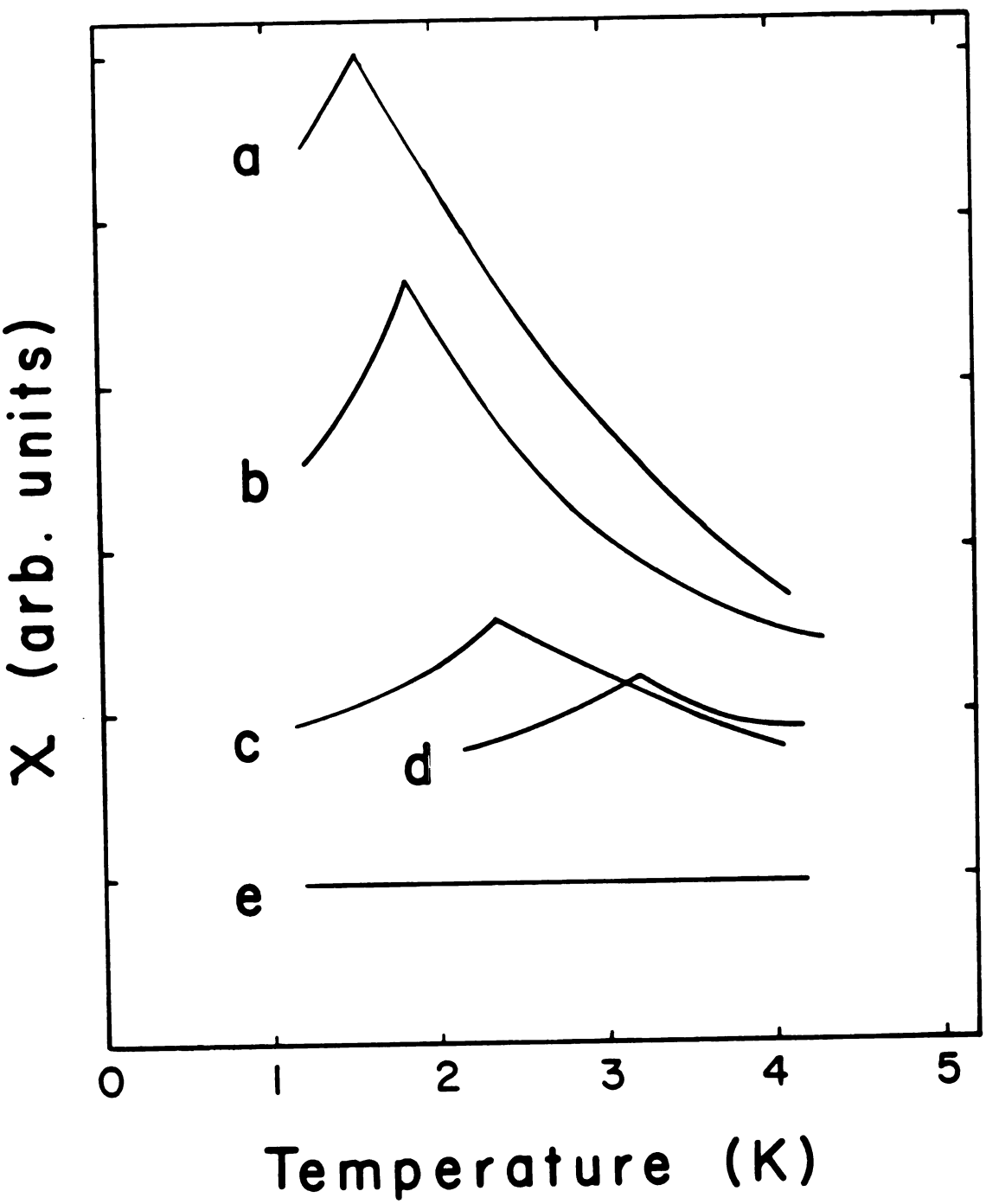

Figure 25. Cu_3PtMn - AC susceptibility vs. temperature.

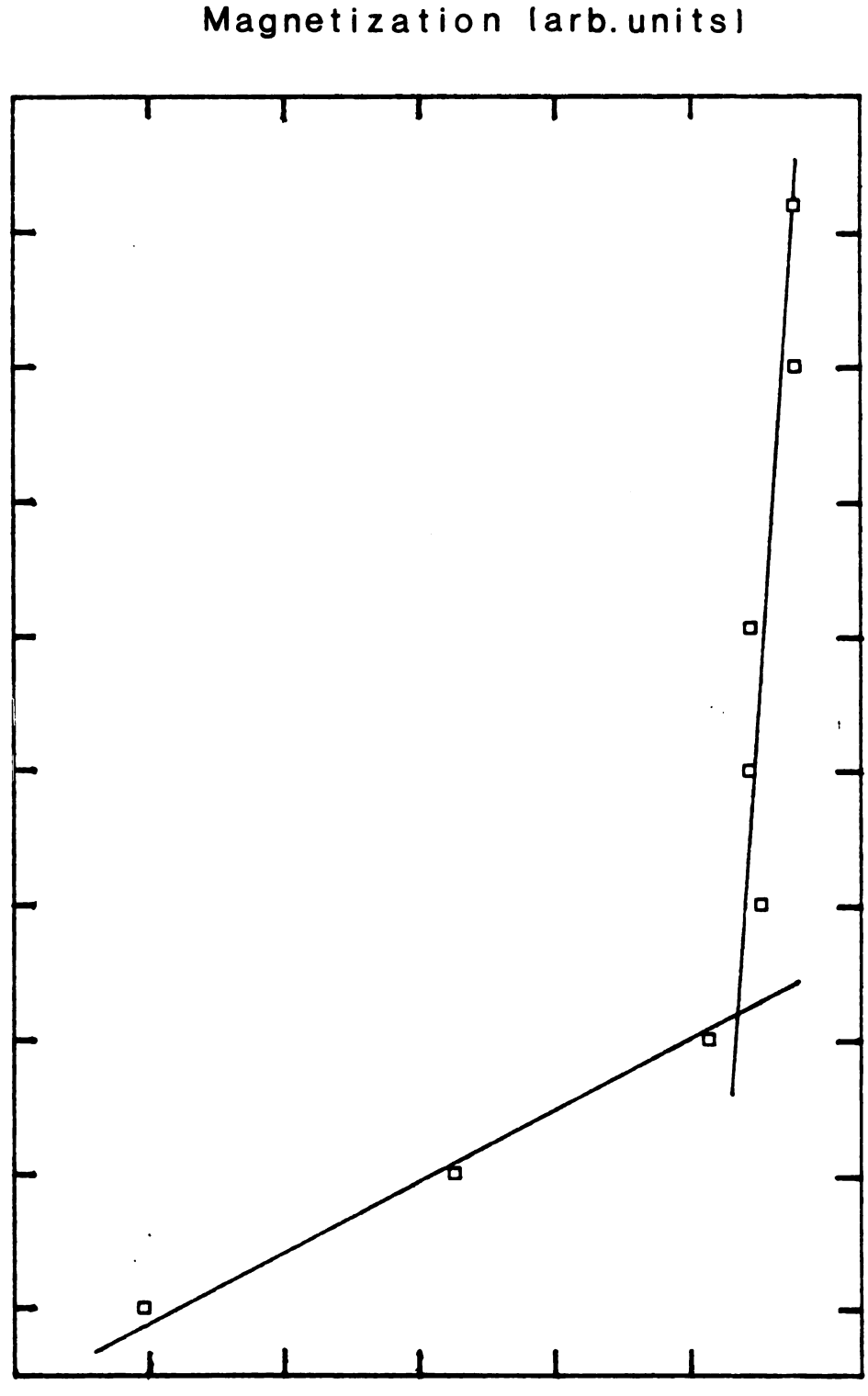

Figure 26. $\underline{Cu_3PtMn}$ (3% DOS) - typical squid T_{sg} data.

Table 6. Experimentally Determined Parameters for Ordered and Disordered Cu_3PtMn Alloys.

Alloy	P_{eff} (μ_B)	θ_c (K)	T_{sg} (K)
Disordered			
0.5% Mn	5.3±0.3	-2.3±0.5	1.85±0.1
0.81% Mn	5.0±0.3	-5.4±0.9	3.3±0.2
1.85% Mn	5.2±0.3	-7.0±0.4	7.5±0.2
3.03% Mn	5.3±0.3	-9.7±0.4	13.6±0.2
Ordered			
0.5% Mn	4.7±0.3	-1.25±0.6	1.55±0.1
0.81% Mn	5.3±0.3	-5.0±0.5	2.3±0.2
1.85% Mn	4.9±0.3	-11.8±0.5	4.3±0.2
3.03% Mn	4.7±0.3	-18.3±0.5	7.8±0.2

concentration in Figure 27. Several trends are obvious. The spin-glass temperatures are essentially proportional to the manganese concentration with the disordered host alloys always having the greater freezing temperature. The Curie-Weiss temperatures are negative possibly linear in concentration. However, this would imply a non-zero $|\theta|$ as $c \to 0$ which is not understood at this time. More likely, the data starts at the origin at $c = 0$ and follows a more complicated concentration dependence.

C. $\underline{(CuPd(17))}_{1-x}Mn_x$

The second dilute metallic spin-glass system to be investigated was the $\underline{(Cu_{0.83}Pd_{0.17})}_{1-x}Mn_x$ system. Many of its properties parallel those of the Cu_3PtMn system, but in general its characteristics are not as well-defined as in the Cu_3PtMn case. Figure 28 shows some temperature dependent susceptibility measurements. Compared to the $\underline{Cu_3Pt}Mn$ data two contrasts are rather striking. There is less rounding off of the data at low temperatures which indicates the spin-glass transition is occurring at lower temperatures. Secondly, there seems to be some evidence for the curve to become concave down relative to the temperature axis. This is especially true for the ordered state samples 0.7% and 1.1%. Some might argue that this is possible evidence for Kondo-like behavior. We have not addressed that question. Figure 29 shows some similar data taken with the SHE Squid susceptometer. The argument with the previous VSM data is rather good. The paramagnetic Curie temperatures agree within error bars of ±1.5°K and the P_{eff} agree to within

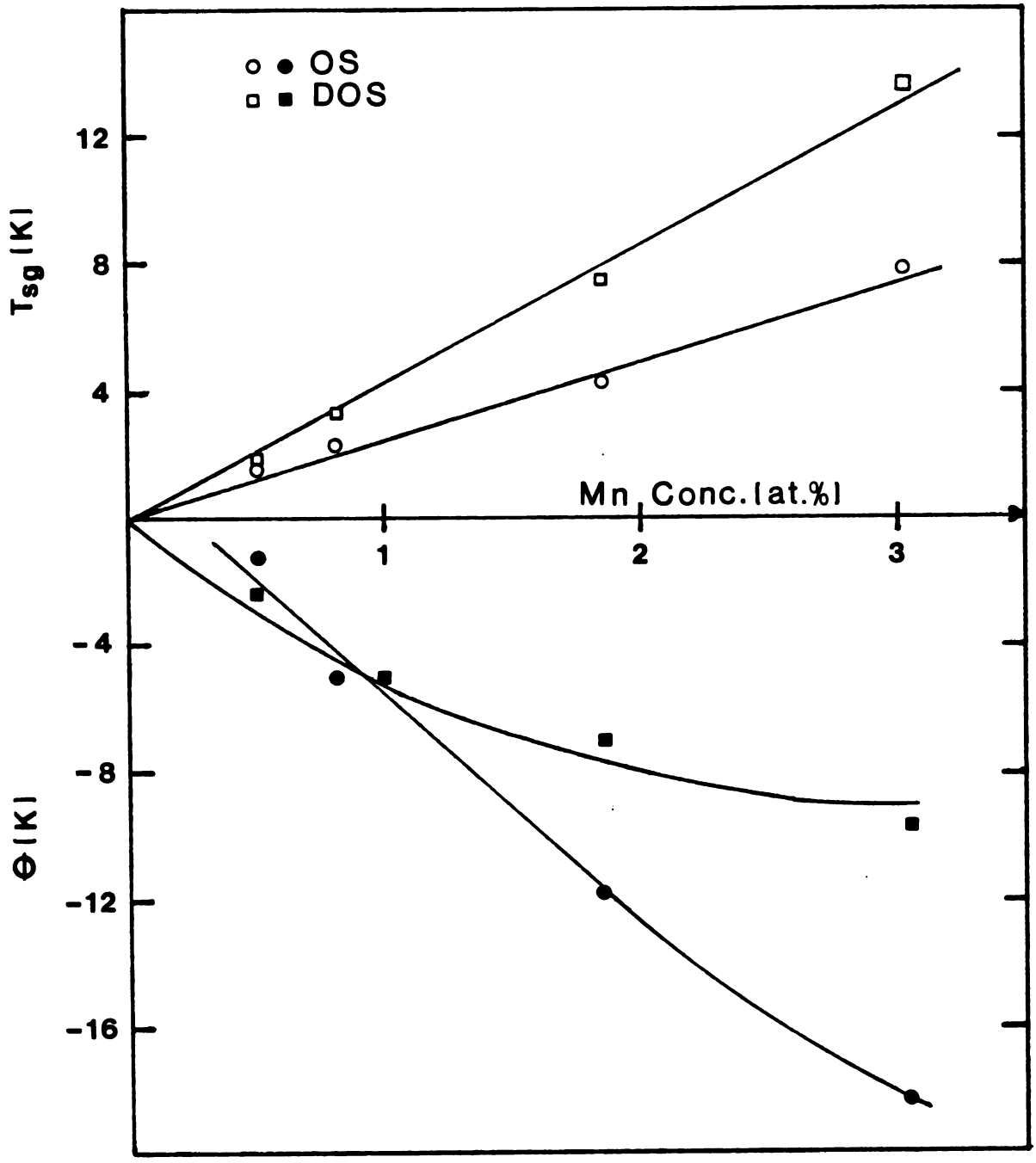

Figure 27. T_{sg} (c) and θ (c) for $\underline{Cu_3PtMn}$.

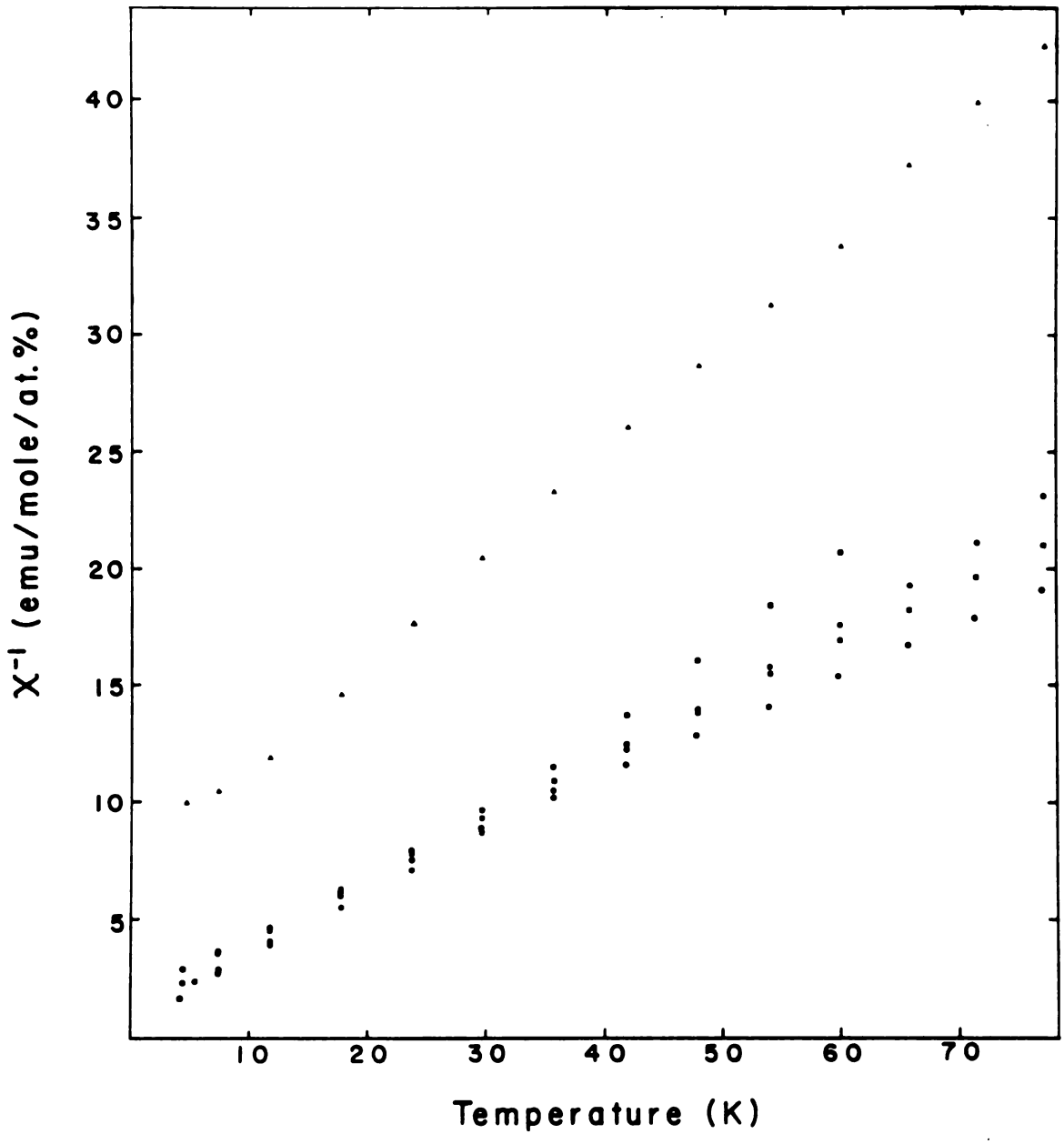

Figure 28. CuPd(17)Mn - inverse susceptibility vs. temperature - VSM.

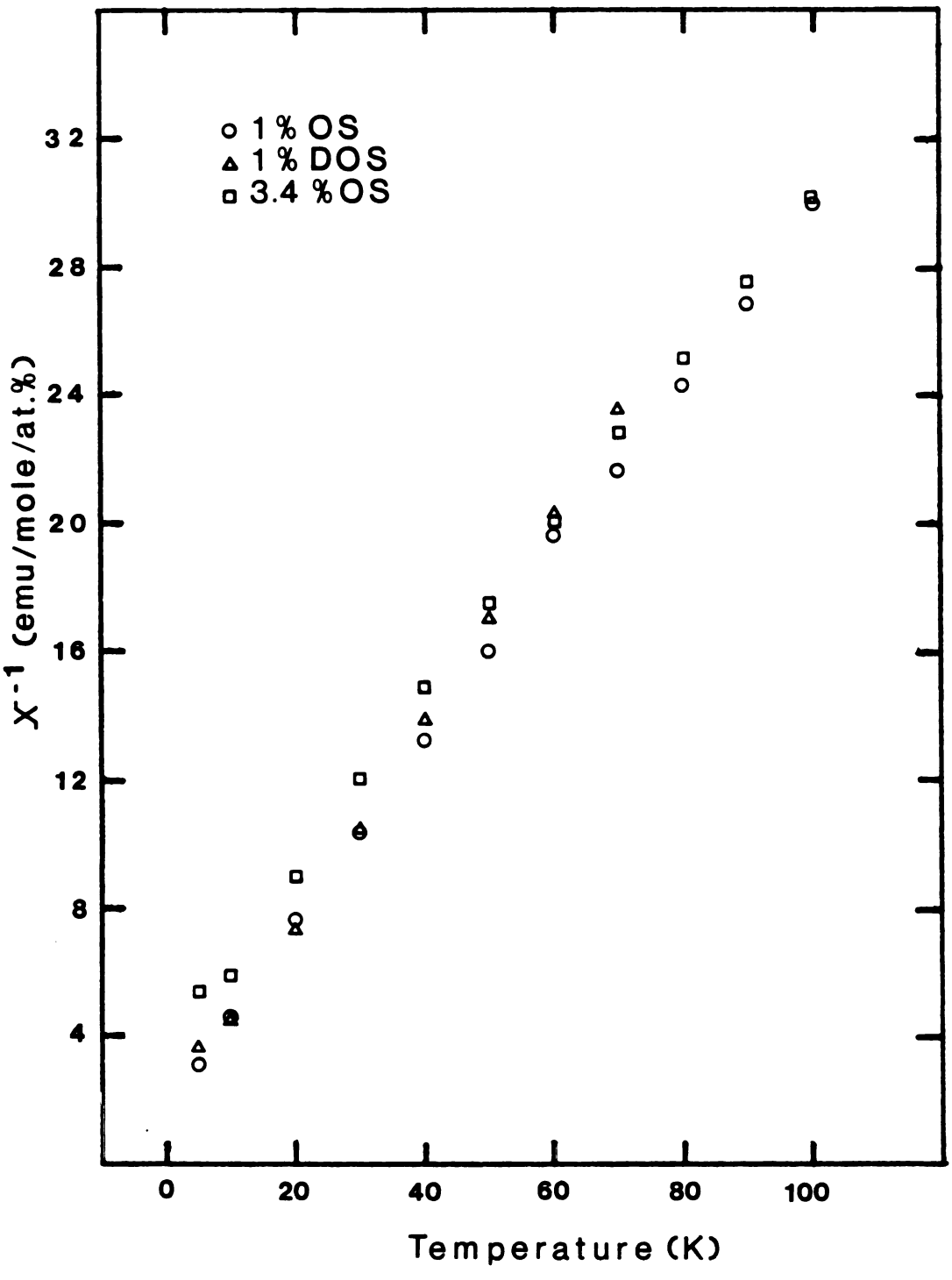

Figure 29. CuPd(17)Mn - inverse susceptibility vs. temperature - Squid.

$\pm 0.3\ \mu_B$ (for CuPdMn (1% OS and 3.4% OS)) (see Table 7). Figure 30 shows some typical low field χ vs T Squid data that was used to determine some of the freezing temperatures. The actual concentration dependence of T_{sg} and θ for the CuPd(17)Mn alloys is shown in Figure 31. As one can see, the concentration dependencies are not so clearly established as in the Cu_3PtMn case, but the two basic trends seem to reappear. That is, all θ's are negative with $|\theta|_{OS} > |\theta|_{DOS}$ and $(T_{sg})_{DOS} > (T_{sg})_{OS}$. These are the same trends displayed by the Cu_3PtMn samples.

D. Hysteresis Study

Only a very slight beginning into the study of the hysteresis behavior of our alloys was made, but the results are quite interesting. As a first check of our ability to make reliable low field hysteresis measurements, we examined one of our CuMn (2 at %) samples. The hysteresis curve for a sample cooled in -4 kilogauss is shown in Figure 32. It agrees quite well with the general sort of behavior other investigators have found. It has a width of approximately 320 gauss and a displacement of about 195 gauss. The magnetization reversal at approximately 350 gauss is quite sharp. Similar measurements for Cu_3PtMn (3%) OS and DOS are shown in Figures 33 and 34 respectively. The ordered state data exhibits no sharp changes in magnetization and very little hysteresis. The width of the hysteresis loop is only about 40 gauss with a displacement of only 20 gauss. This is in many ways very similar to what one would see for CuMn if the hysteresis loop was measured at a relatively

Table 7. Experimentally Determined Parameters for Ordered and Disordered CuPd(17)Mn alloys.

Alloy	P_{eff} (μ_B)	θ_c (K)	T_{sg} (K)
Disordered			
0.22% Mn		0[1]	≃1.25
0.7% Mn	5.23	-0.59	
1.0% Mn	4.99[2]	-3.03	5.5
Ordered			
0.22% Mn	4.88	-0.065	<1.25
0.7% Mn	5.65	-7.5	3.3
1% Mn	6.02	-10.3	3.5
	5.36[2]	-7.3[2]	
3.4% Mn	4.15	-14.3	8.7
	5.52[2]	-15.9[2]	

[1] T. W. McDaniel - Reference 9.

[2] Squid Data.

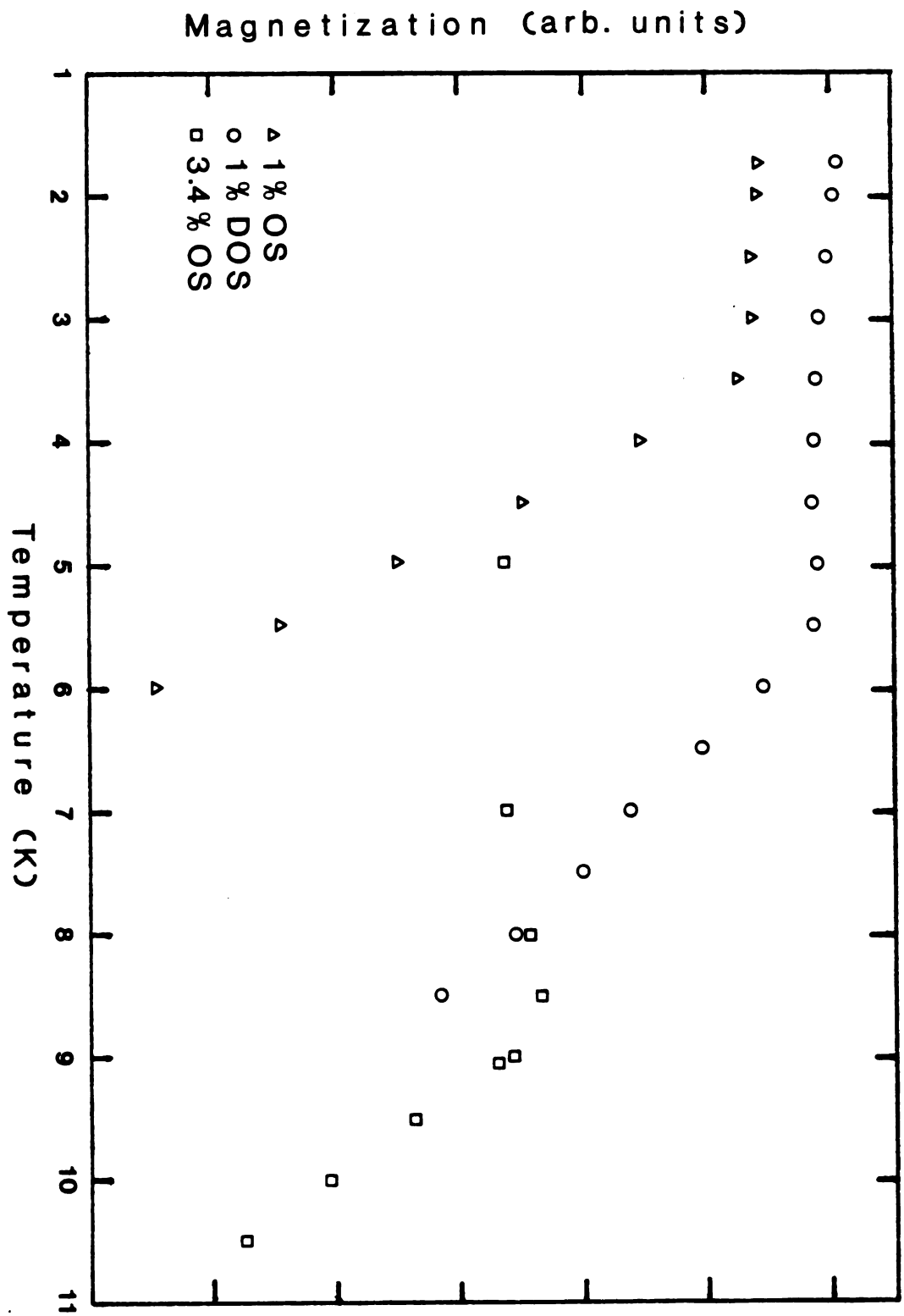

Figure 30. CuPd(17)Mn - susceptibility vs. temperature - Squid.

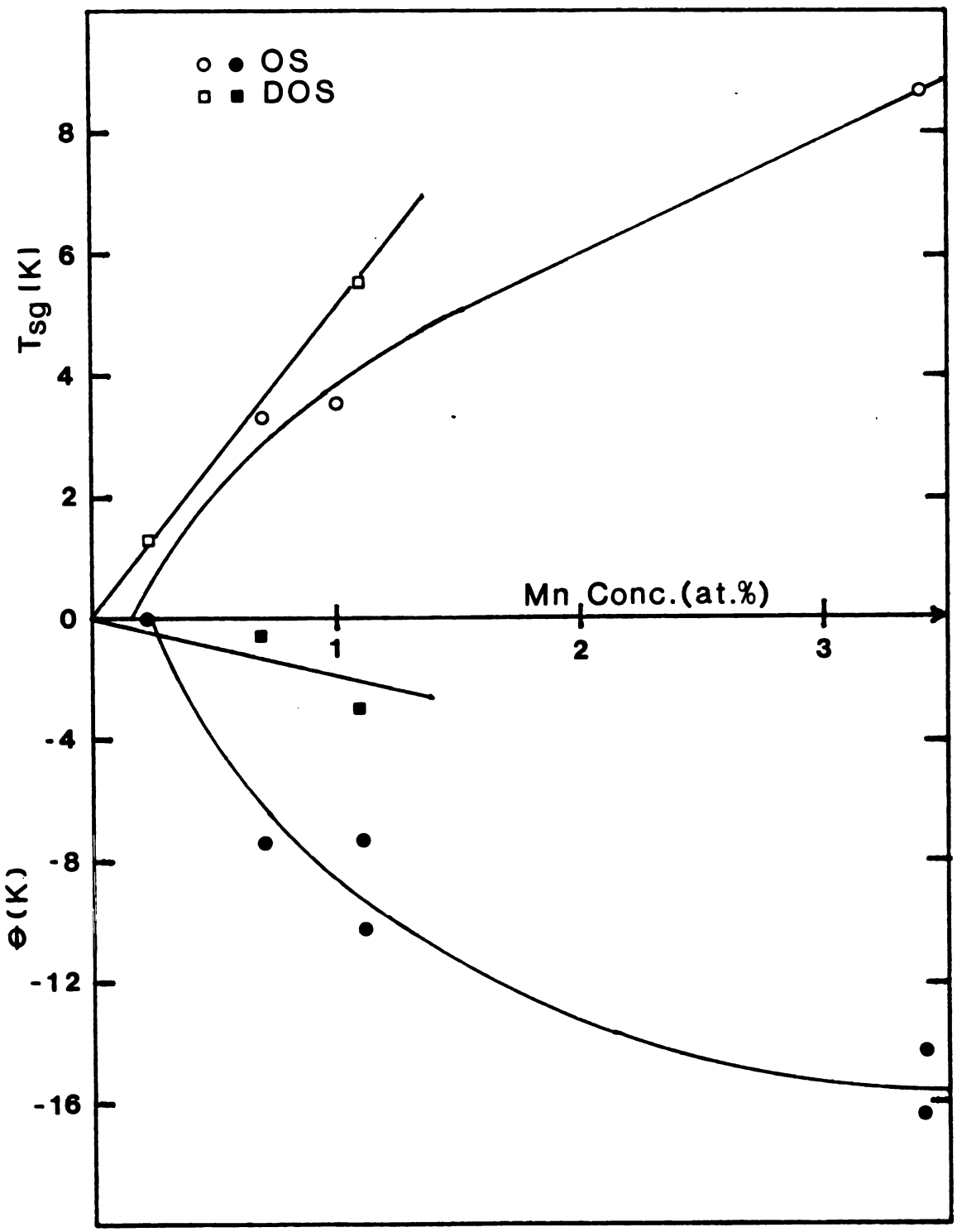

Figure 31. T_{sg} (c) and θ (c) for CuPd(17)Mn.

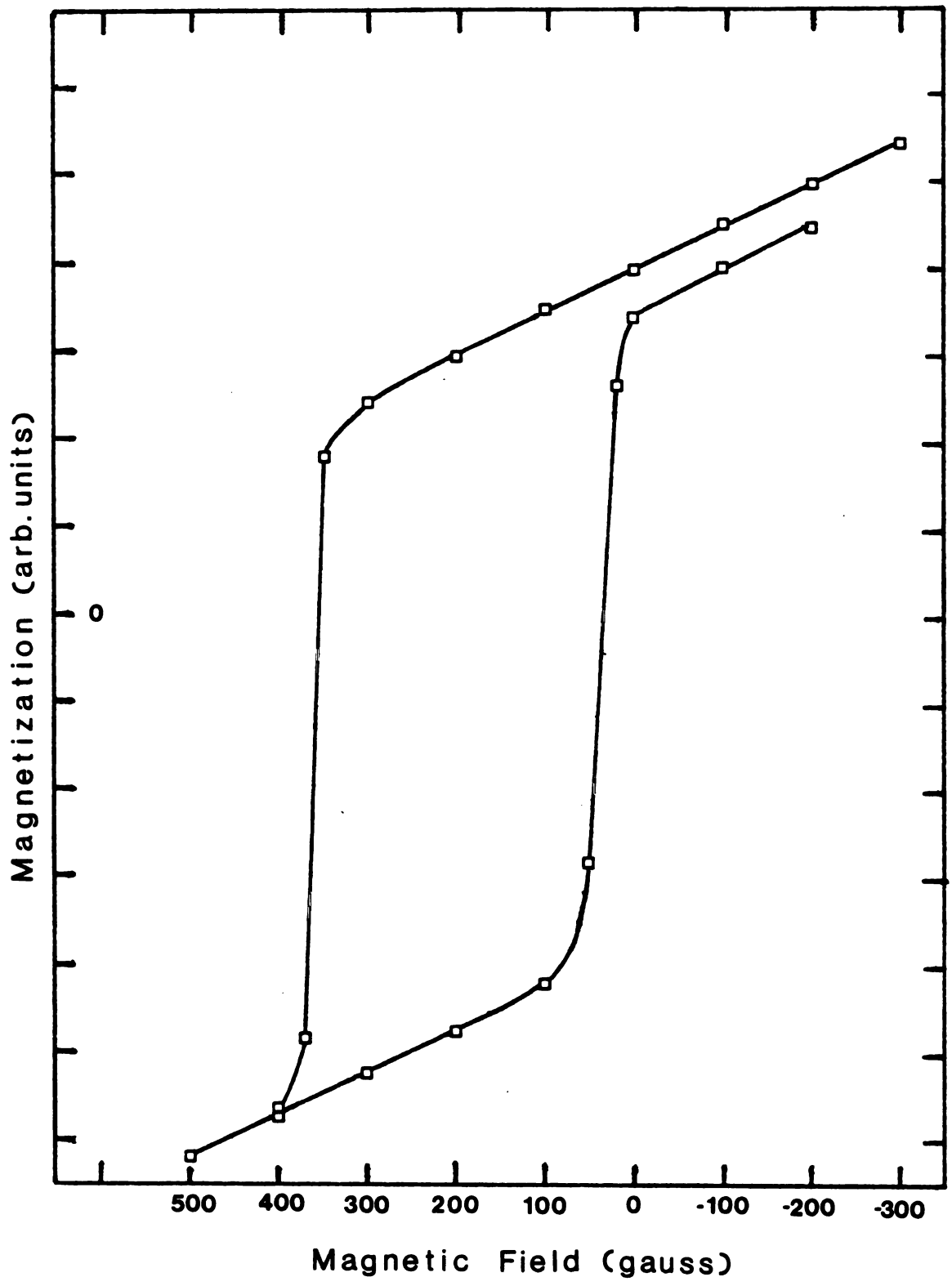

Figure 32. CuMn (2%) - Hysteresis curve.

Figure 33. Cu_3PtMn (3% OS - hysteresis curve.

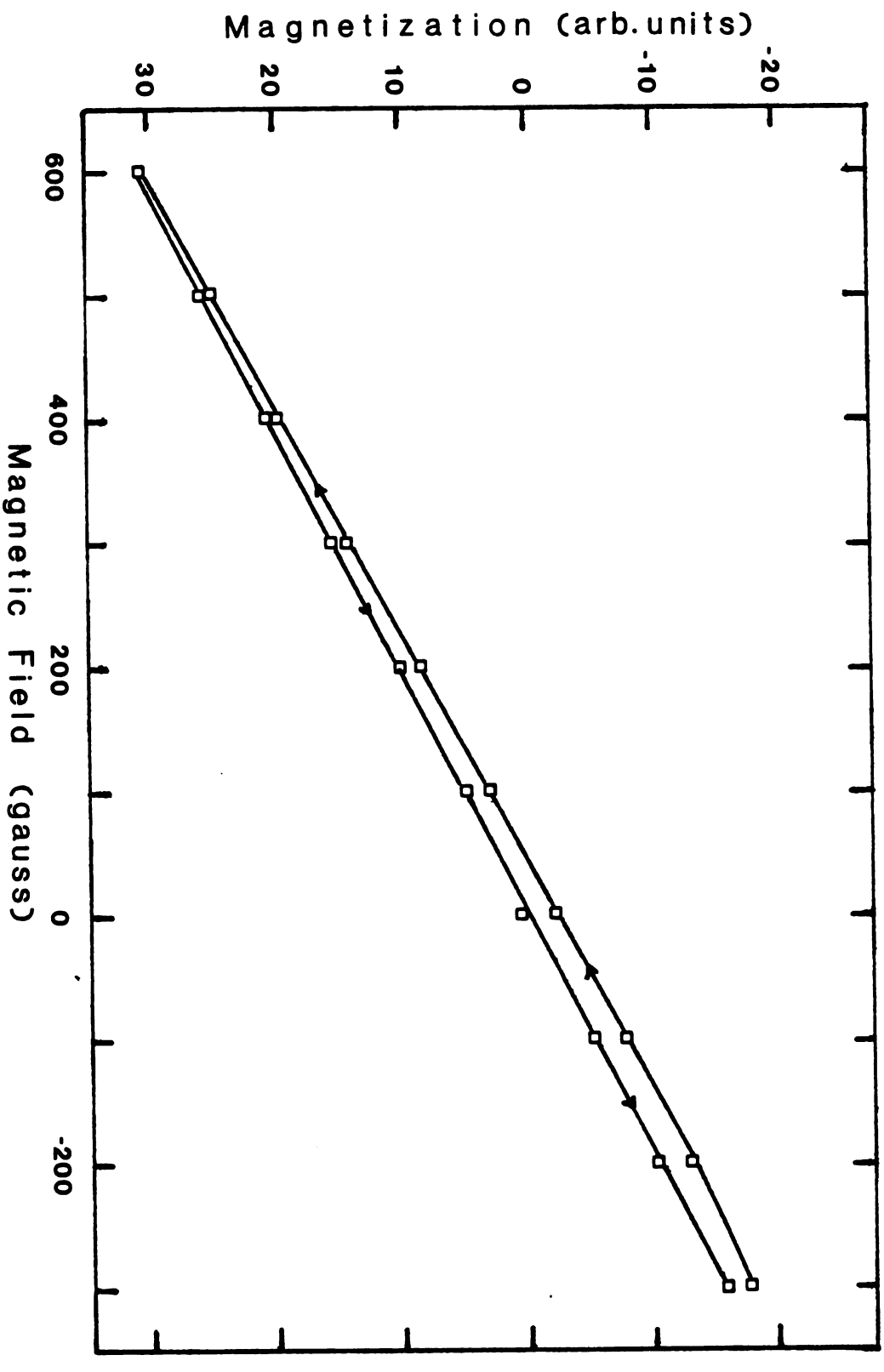

Figure 33. Cu_3PtMn (3% OS - hysteresis curve.

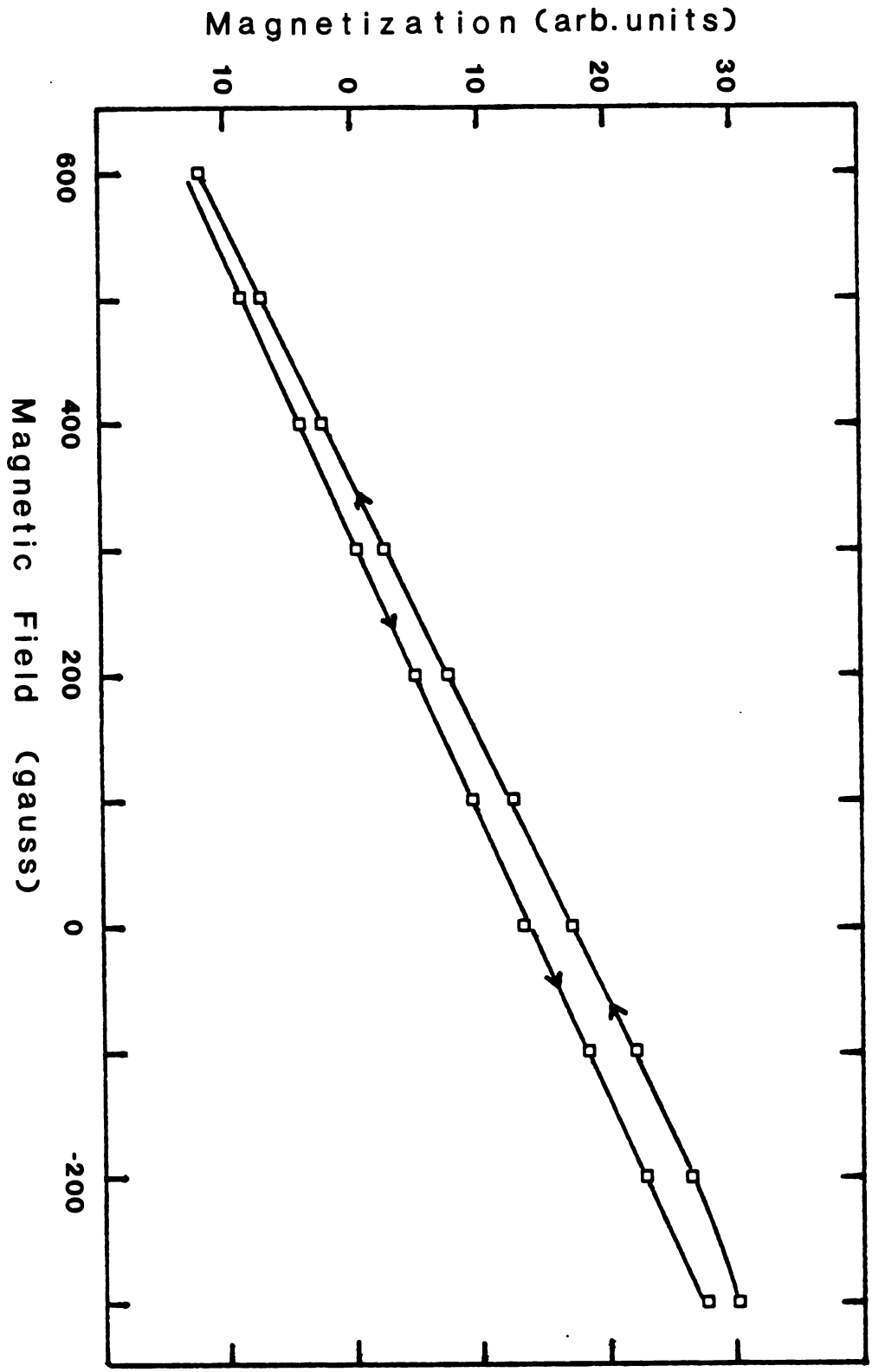

Figure 34. Cu_3PtMn (3% DOS - hysteresis curve.

high temperature, say 0.5 T_{sg}. Generally speaking, as one raises the temperature the hysteresis loop widens and the sharp features round out and the displacement field decreases. For our $\underline{Cu_3Pt}Mn$ (3% OS) the data was taken at 4.2°K = (0.54) T_{sg}. However, when one examines the DOS data one finds a similar curve (width ≃ 45 gauss) but the displacement field is 325 gauss. From the results of Prejean et al.[83] one expect the reversal field to get very large as one adds Pt to the Cu, but for dilute amounts of Pt the width and displacement field have the same linear Pt concentration dependence as Hr. This is clearly not the case for 25% Pt. Analysis of these hysteresis cycles in terms of anisotropy fields, etc. is very difficult because there is no squareness to the cycle. As one adds more and more Pt, the magnetization reversal amplitude corresponds to a smaller and smaller fraction of the remenant magnetization. One would like to be careful not to include that part of the hysteresis cycle in large positive field where the magnetization processes are of the IRM type rather than large scale remanent magnetization reversal. There is presently no way to distinguish between these mechanisms when their effects are comparable. Even the disordered alloy data was taken at relatively high temperature, 4.2°K = (0.31) T_{sg}. Another crucial idea to keep in mind regarding the different behavior is concerned with the symmetry of the Pt atoms in the lattice. Because of the antisymmetric nature of the D-M interaction, we would expect spin-orbit effects to be stronger in the disordered state alloys. Experimentally being able to control the amount of order in a binary host which contains

Pt, Pd, or Au may be very useful in determining the importance of anisotropy in spin-glass phenomenon. Several investigators claim it is essential. Walker and Walstedt[51] made a Monte Carlo study of classical spin systems with RKKY coupling. They found no evidence of spin-freezing unless a small amount of anisotropic interaction is introduced. Likewise, Harris and Zobin[52] require some amount of anisotropy for the existence of a spin-glass phase when their spins were S = 1. This may be related to speculations by P. W. Anderson[53] that the Heisenberg model (which has L.C.D. = 3) has no spin-glass transition unless a small anisotropy causes a phase transition as one gets crossover to Ising behavior. Thus the key role is played by the weak anisotropy forces and not the strong exchange forces.

VI. INTERPRETATION

A. Binary Host Alloys

The alloy systems $\underline{(Cu_3Pt)_{1-x}}Mn_x$, $\underline{(CuPd(17))_{1-x}}Mn_x$, and $\underline{(Cu_3An)_{1-x}}Mn_x$ have many properties which parallel those of the archetypical spin-glass CuMn. A quick examination of Table 8[54] should convince the reader that the binary hosts are comparable to copper in many ways. The phonon contribution to the electrical resistivity for the disordered state alloys is within 16% of the value for pure copper. Upon ordering, the phonon contribution to the electrical resistivity increases substantially with little change in the Debye temperature θ_D. This may suggest the introduction of new band gaps which reduces the number of carriers. The similarity in the number of valence electrons per unit volume and the electronic contributions to the specific heat for all these alloys suggests that there are no major d-band effects. Finally, the fact that all the alloys are diamagnetic lends further support to the notion that the d-bands do not play an important role. This is not to imply that everything about these alloys is well-understood. For example, it is not clear to the author why the atomically ordered hosts are twice as diamagnetic as the disordered hosts (for the Cu_3Pt and CuPd(17) alloys).

In addition to the previously mentioned physical properties,

Table 8. Selected Properties of Binary Hosts and Pure Copper.

Material	10^{-6} emu/mole χ	Crystal Structure	R.T. ($\mu\Omega$ ρth cm)	(°K) θ_D	10^{22} cm^3 n	mJ mole°K γ
Cu	-4.2	FCC	1.55	320	8.46	0.69
Cu_3Pt (DOS)	-4.6	FCC	1.8		5.93 to 7.91	
Cu_3Pt (OS)	-8	SC	2.7	7.9		
CuPd(17) DOS	-6.6		1.4	327	6.70 to 8.08	0.74
CuPd(17) OS	-13.1					
Cu_3Au (DOS)	-12.5	FCC	1.8	269	7.62	0.68
Cu_3Au (OS)	-15	SC	2.9	285		0.65

the geometrical (lattice) properties of all the hosts are similar, although there are a few subtle differences. All the hosts (Cu_3Pt, CuPd(17), Cu_3An) are A_3B-type face-centered cubic alloys. The disordered state alloys are all FCC with the well known truncated octahedron forming the Brillouin zone (see Figure 35). The volume of this Brillouin zone is $4/a^3$. It can accommodate two electrons per atom. The Cu_3Pt and CuPd(17) hosts have approximately 0.75 electrons/atom and copper and Cu_3Au has approximately one electron/atom. Since the volume of an inscribed sphere is 0.681 times the volume of the zone, the sphere can contain 1.362 electrons/atom. Thus one would expect a very nearly free electron type Fermi surface for these hosts. However, since we know that the copper Fermi surface actually touches the zone faces in a few locations, it is also possible for the Cu_3Au host and somewhat less likely for the Cu_3Pt and CuPd(17) hosts. When the alloys become ordered, the crystal structure is simple cubic with a basis of four atoms. This causes the Brillouin zone to split, and indeed the first zone is bounded by {100} planes (See Figure 35). Its volume is $1/a^3$ and it can accommodate 0.5 electrons per atom. This zone should be completely filled. The second Brillouin zone is bounded by {110} planes and forms a rhombic dodecahedron. This zone can accommodate one electron per atom and should play an active role in determining alloy properties. It is interesting to note that the choice of $Cu_{0.83}Pd_{0.17}$ was made so as to produce A_3B-type structure. Johansson and Linde[55] found the maximum intensity of the superlattice lines at 17 atomic percent palladium instead of the expected 25 atomic

Figure 35.

(a) Billouin Zone for FCC A_3B type disordered alloy is a truncated octahedron bounded by the planes {111} and {200}.

(b) Brillouin Zone for FCC A_3B type ordered alloy in the K_x-K_y plane.

(c) Second Brillouin Zone for FCC A_3B type ordered alloy is a rhombic dodecahedron formed by 12 (110) planes.

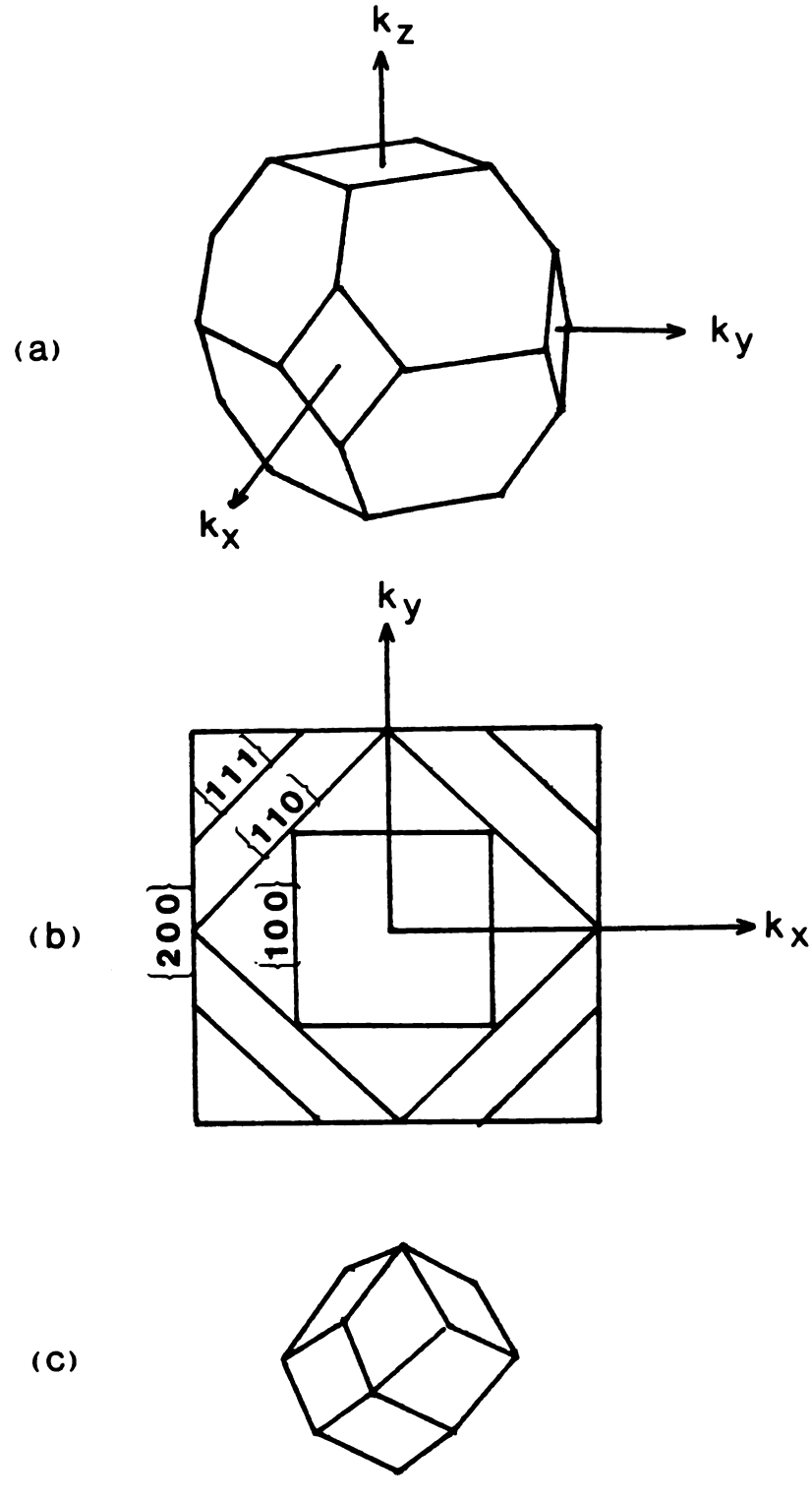

Figure 35. Brillouin zone structure for our binary alloys.

percent palladium. Resistivity measurements also indicate the possible existence of anti-phase domains, as found in Cu_3Au for alloys containing up to 18 atomic percent palladium. Later work by Sato and Toth provide evidence for long-period superlattices for Pd contents ranging from 20-30 at.%. Both one and two dimensional superlattices are found in this alloy. It may be worth mentioning that the generation of long-period superlattice structures is qualitatively different for the Cu_3Pt, CuPd(17) structures as compared with the Cu_3Au structure. The relationship between the domain size M and the electron/atom ratio is given by $\frac{e}{a} = \frac{\pi}{12t^3}\{2 \pm 2\chi + \chi^2\}^{3/2}$ where t is the truncation factor and $\chi = 1/2M$. The plus sign applies to alloys with $e/a \gtrsim 0.85$ and the negative sign to alloys with $e/a \lesssim 0.85$. (See Figure 36.) The theory developed by Sato and Toth explains the former case as arising from stabilization by the outer Brillouin zone and the latter case arising from stabilization due to the inner zone boundary. Cu_3Pt and CuPd(17) lies in the first class, and Cu_3Au lies in the second class.

We will see in the next section that the Mn moments are similar in all the hosts considered. Therefore, we would conclude that the effects discussed previously may affect the interactions between the moments, but have relatively little effect on the moments themselves.

B. Effective Mn Moments

Perhaps the most direct way of addressing the host suitability question is to introduce small amounts of Mn impurities and examine

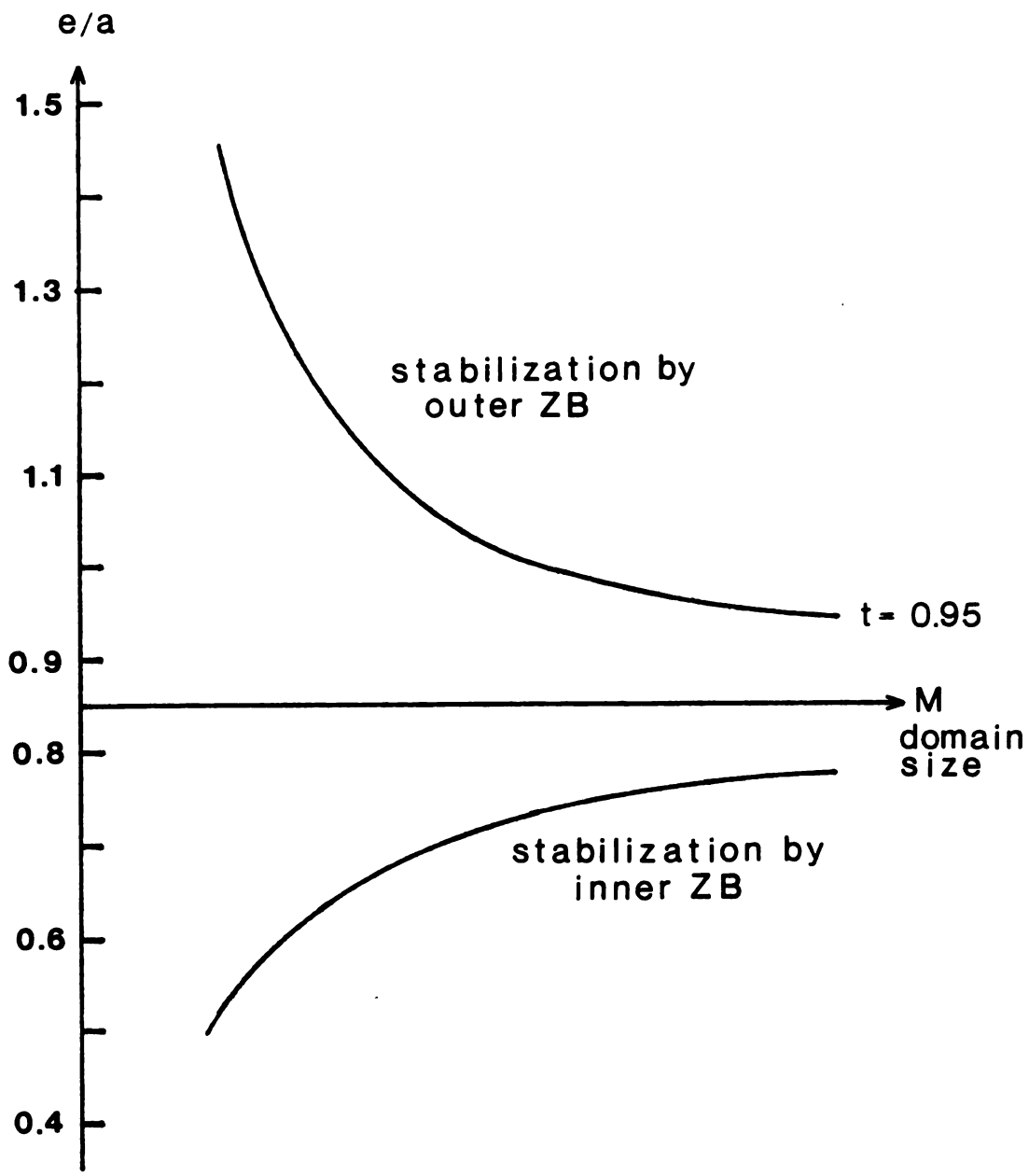

Figure 36. Electron/atom ratio vs. domain size.

the effective moments. The results are summarized in Table 9. The similarity in values for P_{eff} suggests no unusual behavior. However, if one looks into the matter a bit more closely, the situation is not entirely clear. The classical interpretation of CuMn involves Friedel resonant bound states. An effective moment of 4.9 μ_B implies $\vec{\mu} = 4\mu_B$ and spin S = 2. Myers and Westin[56] would argue this implies an electronic configuration 3d'4s', for a valency of 1. The resonant bound states are spin-split ($\sim$5 eV) with the bottom band completely filled and effectively 4 holes in the upper band. Since the manganese is monovalent, replacing copper with manganese should not change the electron content of the conduction band. There is evidence that this is true until a manganese concentration of about 20%. On the other hand, there exists evidence disputing Myers and Westin. Owen et al.[57] observed no Mn^{55} hfs even in the most dilute alloys. This suggests the Mn electronic configuration does not contain appreciable unpaired S-electrons. Optical and photoemission experiments on CuMn imply 5 spin states lie totally above the Fermi level. Also, the relative positions of the resonant impurity d states and the Fermi level show little dependence on composition. Thus, one would expect a magnetic moment of roughly 5.9 μ_B (g = 2). The observed moment is roughly 4.9 μ_B. Conduction electron polarization effects do not help much in removing the discrepancy.[58] The standard approach is to assume the resonant states are sufficiently wide that they overlap the Fermi level and one can adjust the number of unbalanced species.

Experimental studies of effective manganese moments in CuPd

Table 9. Effective Manganese Moments.

Material		Mn Moment (μ_B)
CuMn		4.9
Cu_3PtMn	(0.5)	5.3
	(0.81)	5.0
(DOS)	(1.85)	5.2
	(3.03)	5.3
Cu_3PtMn	(0.5)	4.7
	(0.81)	5.3
(OS)	(1.85)	4.9
	(3.03)	4.7
CuPd(17)Mn	(0.7)	5.2
(DOS)	(1.0)	5.0
CuPd(17)Mn	(0.22)	4.88
	(0.70)	5.65
(OS)	(1.0)	5.7
	(3.4)	4.8
Cu_3AuMn	(1% OS)	5.0
	(1% DOS)	5.0

tend to support the energy spectrum with 5 states above and below the Fermi level, provided the system exhibits some Kondo behavior. Anderson would argue that as the electron content of the alloy is reduced by the addition of palladium, the density of states at the Fermi level will increase due to Brillouin zone boundary effects.

Finally, the Mn moments in Cu_3Pt are also scattered around 5 μ_B. The average moment in the ordered samples is 4.9 μ_B. The average moment in the disordered samples is slightly higher ($\simeq$ 5.2 μ_B). It is not clear why this is so.

C. Mean Field Interpretation

1. SK Phase Diagram

The development of a random molecular field model based on a novel type of order parameter was previously discussed when referring to the work of Edwards and Anderson. Since conventional mean field theories can often be solved in the limit of infinite ranged interactions, Sherrington and Kirkpatrick attempted to do so for a system described by an infinite-ranged random Hamiltonian. They use classical spins on a periodic lattice and a standard Heisenburg Hamiltonian where the J_{ij} are independently distributed with a Gaussian probability distribution. Most of the thermodynamics of these systems have been well examined. Extensions to exchange distributions offset from zero to allow for competition between spin-glass and ferromagnetism or antiferromagnetism followed almost immediately. For exchange distributions centered upon a positive

mean, ferromagnetism can occur and this is well documented both theoretically and experimentally. However, the case for a negative mean is uncertain. Theoretical statements range from the initial implications that an antiferromagnetic structure analogous to the ferromagnetic structure occurs if the appropriate sublattice is chosen[59] to claims that a spin-glass phase occurs at low temperature whenever the mean is negative. Some even doubt that spin-glass behavior occurs when the mean is negative.[60] It is with regards to this controversy that our data is most interesting. We claim spin-glass behavior in dilute magnetic alloys when $\theta_c/T_{sg} \simeq (-2.5)$.

In order to make a connection with the SK model, some discussion concerning the relationship between the average and variance of the Gaussian distribution of interactions and the experimentally observed spin-glass freezing temperature and Curie temperature is necessary. Probably the most straight forward way to see the connection is to examine some work by B. Southern.[61] Using simple molecular field theory and assuming no site-to-site correlation for J_{ij} he derives a spin-glass ordering temperature to be $kT_{sg} = \hbar^2\{S(S+1)/3\}(\overline{\sum_{ij} J_{ij}^2})^{1/2} = \hbar^2[S(S+1)/3]\tilde{J}$.

He also predicts the high temperature susceptibility will have a Curie-Weiss behavior with $k\theta = \frac{1}{3}\hbar^2 S(S+1)\overline{J(0)} = \hbar^2[S(S+1)/3]\tilde{J}_0$. Using these ideas, $\tilde{J}_0/\tilde{J} = (\theta/T_{sg})$.

In another paper Sherrington and Southern[62] consider general quantum spins with a Gaussian exchange distribution and non-zero mean. They find for the spin-glass ordering temperature

$$T_{sg} \simeq (\frac{\hbar^2\tilde{J}}{3k})\{(S(S+1))^2 + (S(S+1))/2\}^{1/2}$$

which for Mn spins (S = 2) can be written as

$$k_B T_{sg} = \frac{\hbar^2}{3} S(S+1)\tilde{J}(1.041)$$

The Curie-Temperature for the onset of ferromagnetism is predicted to be

$$k_B T_c = [S(S+1)/3]\hbar^2\tilde{J}_0(\tfrac{1}{2})\{1 + [1-(\tilde{J}^2/\tilde{J}_0^2)(3/S(S+1))]^{1/2}\}$$

which for Mn spins (S = 2) can be written as

$$k_B T_c = \hbar^2[S(S+1)/3]\tilde{J}_0(\tfrac{1}{2})\{1 + [1-(\tilde{J}/\tilde{J}_0)^2(\tfrac{1}{2})]^{1/2}\}$$

$$= \hbar^2[S(S+1)/3]\tilde{J}_0\{\tfrac{1}{2} + (\tfrac{1}{4} - (\tilde{J}/\tilde{J}_0)^2\,\tfrac{1}{8})^{1/2}\}$$

for

$$|\tilde{J}/\tilde{J}_0| = 1, \quad k_B T_c = \hbar^2(S+1)S/3\ \tilde{J}_0\ (0.854)$$

for

$$|\tilde{J}/\tilde{J}_0| = \tfrac{1}{2}, \quad k_B T_c = \hbar^2(S+1)S/3\ \tilde{J}_0\ (0.968)$$

So at the multicritical point, for example,

$$\frac{k_B T_c}{k_B T_{sg}} = \frac{\hbar^2 (S+1) S/3 \; \tilde{J}_0 \; (0.854)}{(\hbar^2/3) S(S+1) \tilde{J} \; (1.041)}$$

or

$$\frac{\tilde{J}_0}{\tilde{J}} = 1.22 \; (\frac{T_c}{T_{sg}}).$$

Therefore, considering the approximations made by Sherrington and Souther[1] and the above demonstration of only a 22% difference, we feel we can safely employ $\tilde{J}_0/\tilde{J} = \theta/T_{sg}$.

Using this result, we can plot the results of our $\underline{Cu_3PtMn}$ data (See Figure 37) and our $\underline{CuPd(17)Mn}$ data (see Figure 38) on an SK diagram. Our data extends the antiferromagnetic portion of the phase diagram to $\tilde{J}_0/\tilde{J}$ nearly equal to -3.0. For a more complete discussion of the applicability of the Sherrington-Kirkpatrick model to real spin systems, see Appendix H.

2. Mean Random Field

One final attempt to learn something from the high temperature data will now be presented using Klein's random molecular field model. (A more complete discussion can be found in Appendix I) His principle result, is the high temperature magnetic susceptibility given by

$$\chi(T) = \frac{N_0 c P_{eff}^2 \mu_B^2}{3k_B (T-\theta)} \; [1 - (\frac{2}{\pi})^3 \frac{\Delta(T)}{k_B T}] \qquad (6.1)$$

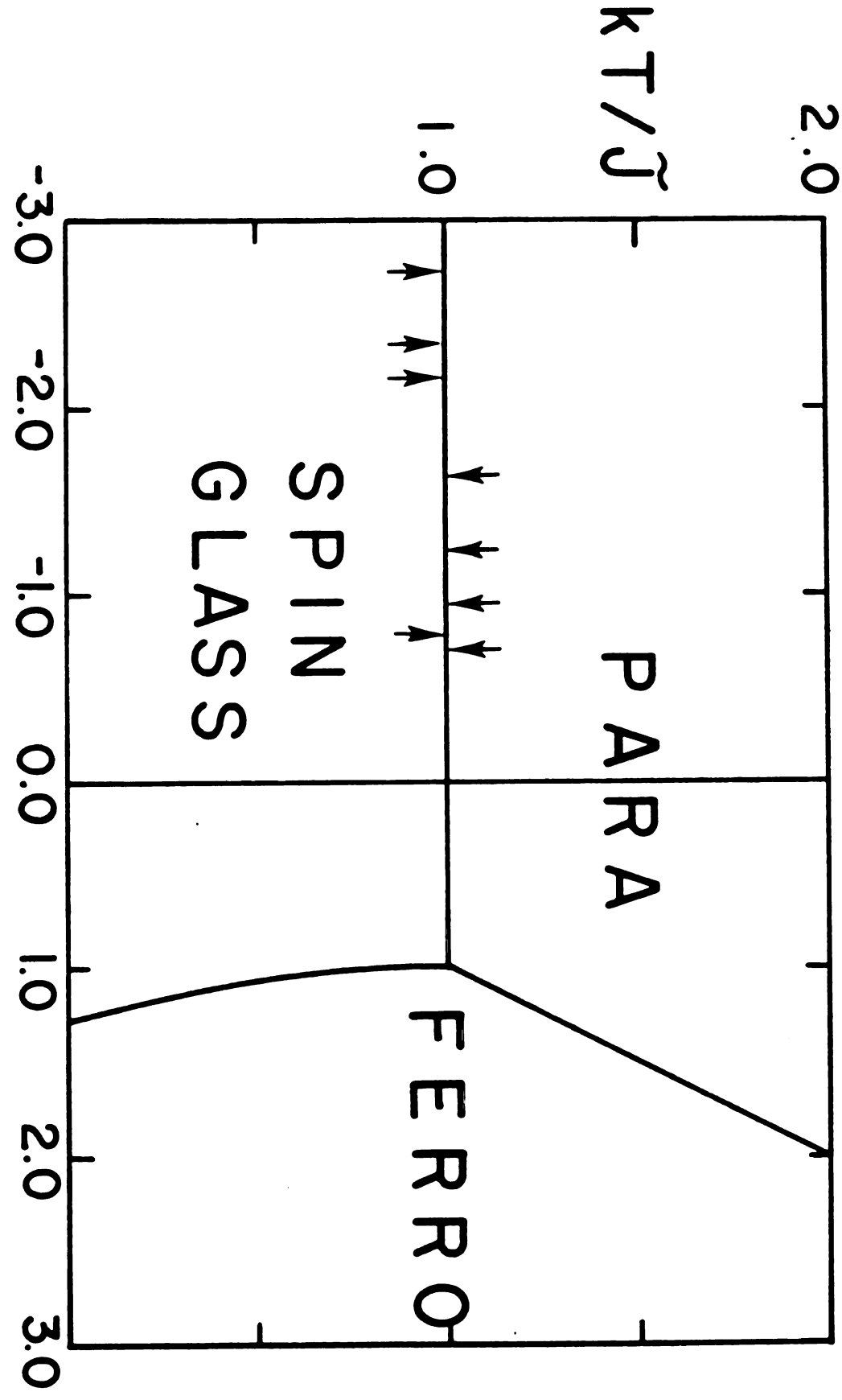

Figure 37. Cu_3PtMn-SK phase diagram.

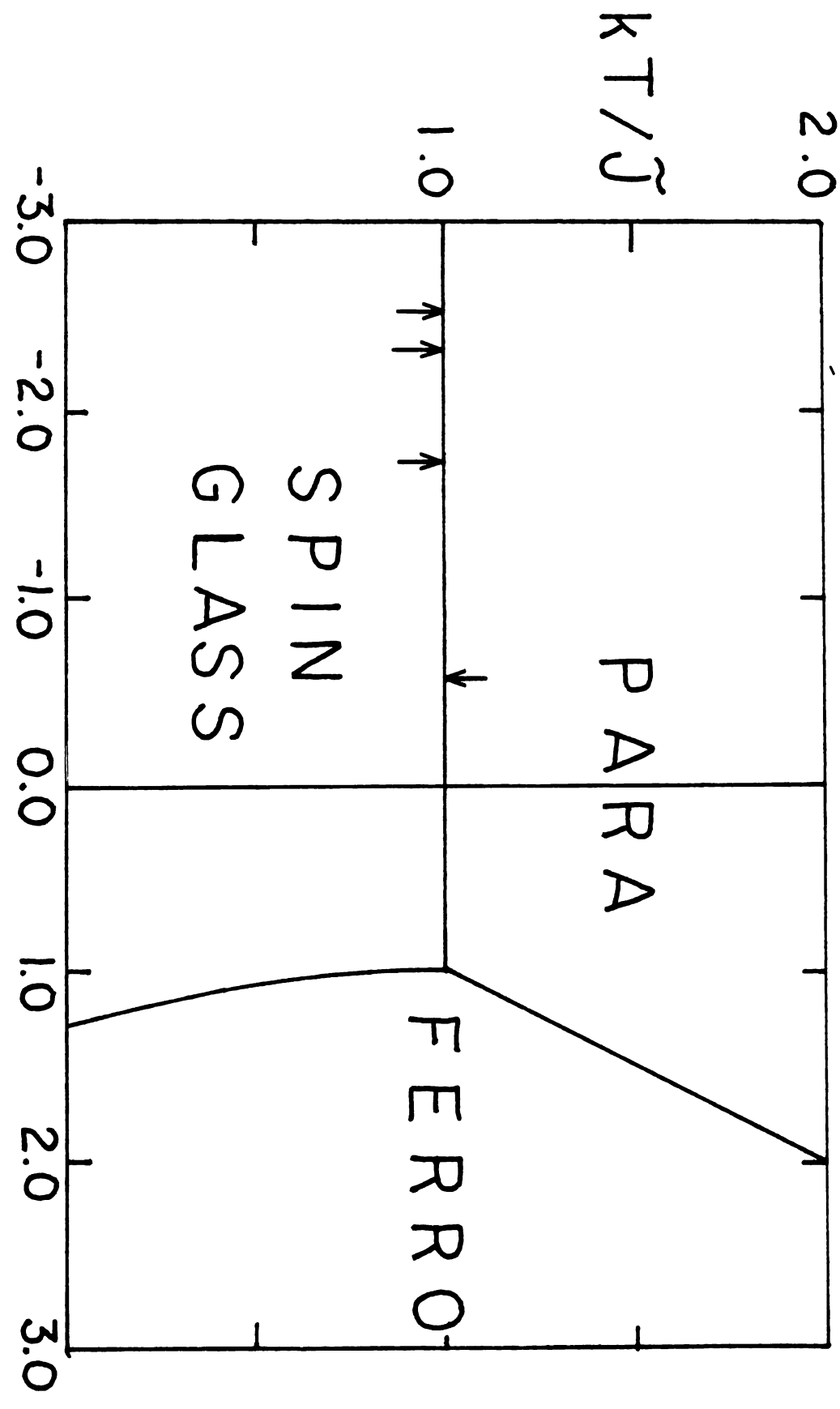

Figure 38. CuPd(17)Mn-SK phase diagram.

In the temperature range $T_{max} < T < 2T_{max}$, Δ is only weakly temperature dependent and a plot of $\frac{(T-\theta)\chi(T)}{c}$ vs. $\frac{1}{T}$ should yield a straight line with a slope proportional to $\Delta(T \simeq 0)$. At sufficiently high temperature Δ approaches zero and therefore $\frac{(T-\theta)\chi}{c}$ should become a constant. When the figures are made for the Cu_3PtMn system, several interesting features result. The 2% DOS and 3% DOS do appear to follow the predicted behavior with the intersection of the linear portion and constant portion in the interval $(T_{sg}, 2T_{sg})$ (see Figure 39). The 2% OS and 3% OS do not show this behavior at all. Rather than having a linear portion with a negative slope, there is a sloping curve with a positive slope. This behavior certainly seems contrary to MRF expectations since

$$\frac{\chi(T-\theta)}{c} = \frac{N_0 P^2 \mu_B^2}{3k_B} \left(1 - \left(\frac{2}{\pi}\right)^3 \frac{\Delta(T)}{k_B T}\right)$$

can never exhibit a positive slope. The 1% DOS and 1/2% DOS data are even more pathological. The slope in the temperature regime $(2T_{sg}, T_{sg})$ is positive and quite large and at temperatures less than T_{sg} the curves become concave down. (See Figure 40.) The reasons for this unusual behavior are not known, but one possibility certainly exists. The early MRF calculations (including the one on which the data is analyzed) predict a probability distribution

$$P(H,T) = \frac{1}{\pi} \left\{\frac{\Delta(T)}{\Delta(T)^2 + H^2}\right\}$$

which is non-zero as $H \to 0$. More recent calculations by Held and

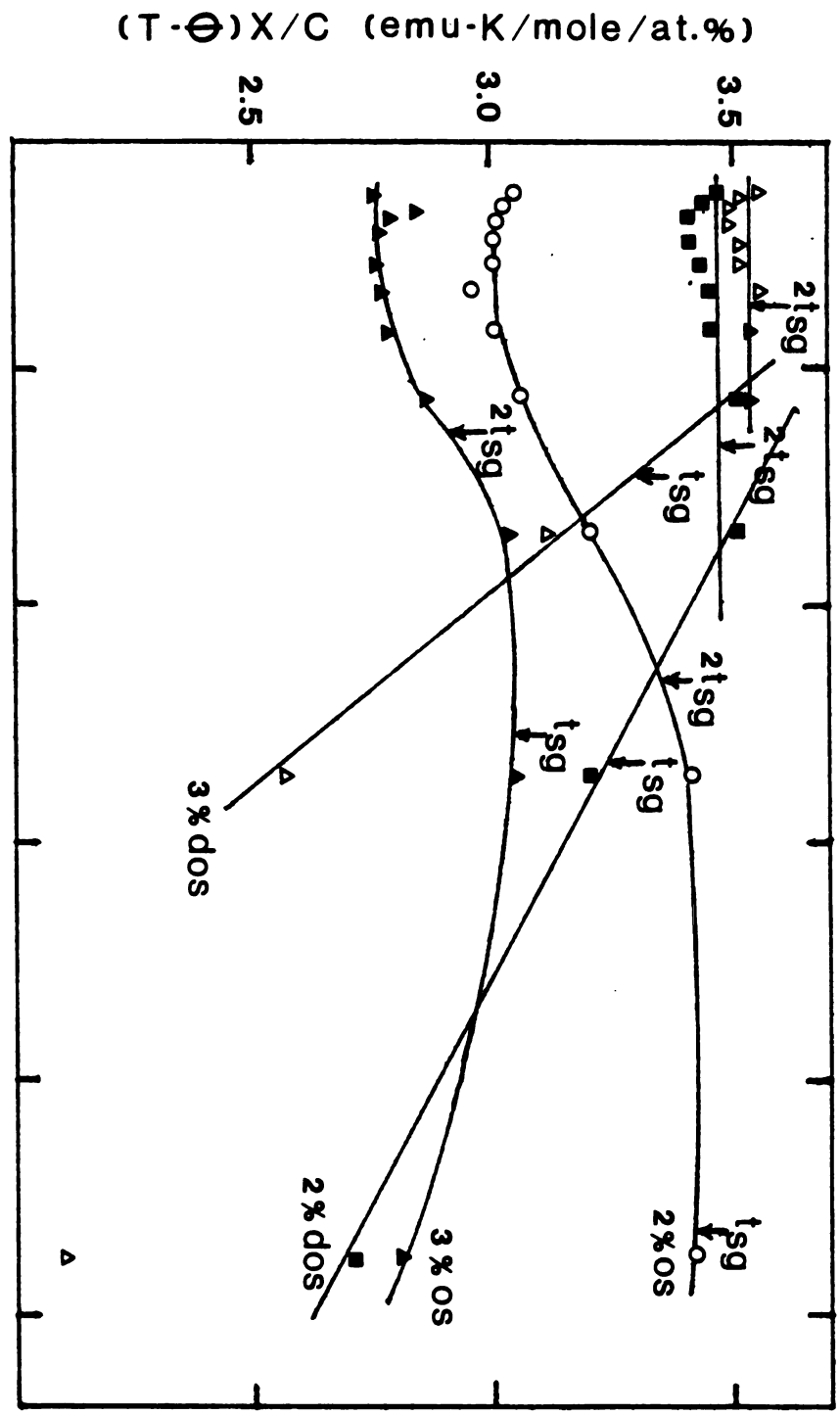

Figure 39. Cu_3PtMn (2%, 3%) - Klein diagram.

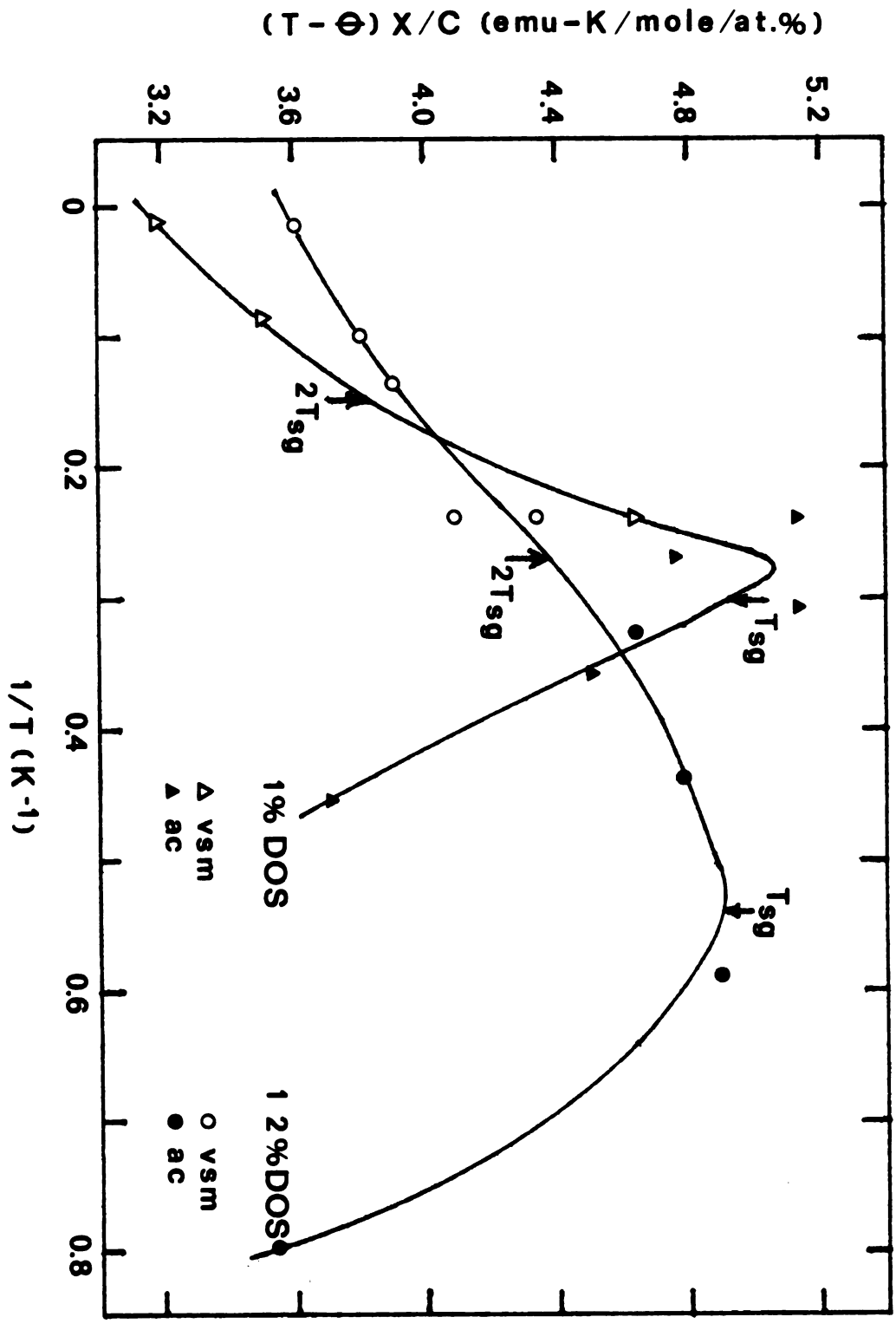

Figure 40. Cu_3PtMn (1%, 1/2% DOS) - Klein diagram.

Klein[63] predict

$$P(|\vec{H}|) = \frac{4}{\pi} \frac{\Delta H^2}{\{\Delta^2 + H^2\}^2}$$

which approaches zero has $H \to 0$. Therefore the neglect of the part of $\chi(T)$ which arises from the term involving $\frac{\partial P(H,T)}{\partial H_{ext}}$ is no longer a good assumption. $P(H)$ is not so slowly varying with H_{ext} near $H_{ext} \to 0$. There are several other assumptions that went into the theory which may prove fatal. They include:

(1) Since each $\bar{H}_j$ and $\bar{\mu}_j$ was assumed to be independent of all other $\bar{H}$'s, the spin-spin correlation between the impurities have been neglected.

(2) In principle, each random field may have a different probability distribution. They were assumed identical.

(3) The model gives too large a probability for obtaining high fields because there is no cut-off on the minimum nearest-neighbor distance between the impurities.

However, why the expected behavior occurs for the concentrated disordered samples but not for the other samples remains a mystery.

D. Free Electron RKKY Coupling

One of the most satisfying of tasks would be to explain the general trends of the data shown in Figure 27. For example, one would like to understand the following:

(1) Why are all the concentration dependencies approximately linear?

(2) Why is $|d\theta/dc|_{OS} > |d\theta/dc|_{DOS}$?

(3) Why is $(dT_{sg}/dc)_{DOS} > (dT_{sg}/dc)_{OS}$?

It would be nice if one could find some common ground on which to analyze all the different kinds of behavior. The first to come to mind is the use of a free electron RKKY coupling between impurities. Simple explanations based on RKKY coupling are probably not possible. Either a more sophisticated RKKY treatment is needed, or additional interactions are required. Nevertheless, some general thoughts may be worthwhile.

For example, the dependence of θ on host condition may have some explanation in the work of Kok and Anderson.[13] They were able to explain the experimental observations that $\theta \simeq 0$ for amorphous and liquid alloys, but is not zero for the same alloys in crystalline form. Their analysis is based in part on the performance of a lattice sum. It is generally accepted that $\theta \propto \sum_{ij} J_{ij}$ and $T_{sg} \propto (\sum_{ij} J_{ij}^2)^{1/2}$. Kok and Anderson argue that in an amorphous or liquid matrix, the lattice sum for θ averages nearly to zero. However, the lattices for ordered and disordered hosts are quite similar, so application of Kok-Anderson ideas is not quite straightforward.

Mattis[64] has tabulated FCC lattice sums as a function of the Fermi momentum. If one could predict the change in Fermi momentum upon ordering, one could make a definite prediction about the behavior of θ. A similar study has been carried out by A. Freudenhammer[65]

for the spin-glass freezing temperature. He calculates the dependence of T_{sg} on the Fermi momentum and also finds a strong quasi-periodic dependence. Such an approach is nice conceptually, but runs into trouble when looked at in detail. First of all, CuMn also has an FCC lattice sum. Since e/a $\simeq$ 1 for both CuMn and Cu_3PtMn the change in sign of $d\theta/dc$ is puzzling. Secondly, the strong quasi-periodic dependence of T_{sg} on k_f is only true if the nearest neighbor interaction is assumed to be zero and RKKY otherwise. The oscillations are all but wiped out if one assumes a nearest neighbor direct exchange D and RKKY for larger distances (where $D/J_0 = 1$). The original calculation was probably based on the idea that the direct Mn-Mn interaction would be anti-ferromagnetic and might essentially cancel the ferromagnetic RKKY nearest neighbor exchange. One must certainly worry about suppression of the oscillations for a non-zero nearest neighbor interaction. Finally, some electron-positron annihilation studies done by I. Y. Dekhtyar et al. have indicated that the Fermi momentum doesn't change upon ordering for the Cu_3Au alloys.[66] Cu_3Pt may very likely exhibit similar behavior. It was originally thought that if the Brillouin zone splits in half due to ordering of the alloy, and the zone was originally half filled, the energy of the electrons (and Fermi energy) may decrease due to the compression of the energy levels near the zone boundary. It's more likely that the ordering transition takes place because a binary alloy can lower its energy by surrounding all A atoms by B atoms and vice versa. The greater the size difference in A and B, the stronger the tendency to order.

E. Mean Free Path Effects

Another approach to the understanding of experimental results might be to focus on the role of the Pt, Pd, or An and their influence in the copper matrix. One could argue that the role of the transition metal is that of an impurity scatterer which reduces the range of the RKKY interaction. This may be true, but a comparison of (CuAl)Mn, (CuZn)Mn, and (CuPd)Mn alloys suggests there is more to the story. In addition, although the θ-values decrease with increasing electron concentration, they never go negative except in Pd and Pt systems. It appears as though the Mn ions behave quite differently in host matrices with electron concentration > 1 (CuAl, CuGc, CuZn) compared to their behavior in host matrices with electron concentration less than 1 (Cu_3Pt, CuPd). This implies that changes in Fermi wavevector and density of states at the Fermi level may be important in addition to impurity scattering processes. Both aspects of this will be touched upon briefly.

The binary host spin-glass alloys, which are the concern of this dissertation, are all of the form $(A_yB_{1-y})_{1-x}M_x$, when A and B constitute the binary alloy and M is the magnetic impurity. The concentration parameter y is held fixed and only the concentration of magnetic impurities χ is allowed to vary. Since the disorder in the matrix is large, $0.17 \leq (1-y) \leq 0.25$, there is considerable change in resistivity depending on whether the host is ordered or disordered. As one would expect, the total resistivity is smaller for the ordered host alloy, but perhaps surprisingly, the phonon

contribution can be larger for the ordered alloy (ex., Cu_3Pt) (See Table 10 for some typical resistivities of our $\underline{Cu_3Pt}Mn$ alloys). Several items should be noted. (1) There is little change in the resistivity of the Cu_3Pt (DOS) upon addition of 1 atomic percent manganese ($\sim$1% change). (2) This is not the case for the ordered state alloys ($\sim$43%). This is a good indication that the ordered state alloys are indeed ordered, but also raises one subtle possibility. Any attempts to understand changes in behavior of $\underline{Cu_3Pt}Mn$ (1%) based solely on mean free path effects, should bear in mind that the ordered state resistivities have a large contribution from the magnetic impurities, whilst the disordered state alloys do not. In the discussion to follow, we will distinguish between these sources of disorder. As derived by Ruderman and Kittel, the response of an electron gas to a magnetic impurity consists of spin density oscillations. One can think of these as arising from the interference of the scattered outgoing spherical wave with the incident Bloch wave. If the translational symmetry of the lattice is disturbed by the addition of non-magnetic scattering centers, (i.e., Pt, Pd, Au), the exact states of the free electrons are no longer simple Bloch waves, but linear combinations of many such waves with different k values. This leads to a damping of the interference oscillations such that the RKKY spin density oscillations are of the form $\sigma(r) \sim \frac{\cos 2k_f r}{r^3} e^{-r/\lambda}$ when λ is the mean free path. DeGennes looked at this problem in somewhat more detail[14] and found the magnitude was damped in approximately the expected manner, but in addition, there was also a shift in the phase of the oscillations.

Table 10. Resistivity of Cu_3PtMn (0.81%) and CuPd(17)Mn (1%).

Alloy	(77°K) μΩ-cm	Δρ(77°K) μΩ-cm
Disordered		
Cu_3Pt	40.58	0.42
Cu_3PtMn (0.81%	41.0	
CuPd(17)	11.5	2.1
CuPd(17)Mn (1%)	13.6	
Ordered		
Cu_3Pt	7.81	3.35
Cu_3PtMn (0.81%)	11.16	
CuPd(17)	6.5	1.3
CuPd(17)Mn (1%)	7.8	

It should also be noted, that there are arguments which contend that the concept of a mean free path does not really enter into these discussions. P. F. deChatel[67] argues that in disordered systems the non-local susceptibility of a homogeneous, isotropic conduction electron system $\chi(R_i,R_j) = \chi(|R_i-R_j|)$ must be replaced by a susceptibility that depends on the particular distribution of atoms in the region between sites i and j.

$$\chi(R_i.R_j) = \sum_{n,n'} \frac{f(\varepsilon_n)-f(\varepsilon_{n'})}{\varepsilon_{n'}-\varepsilon_n} \psi_n(R_i)\psi_n^*(R_j)\psi_{n'}^*(R_i)\psi_{n'}(R_j)$$

If one chooses

$$\psi_n(R_i)\psi_n^*(R_j) = e^{ik_n\cdot(R_i-R_j)} \quad \text{and} \quad \varepsilon_n = \frac{h^2k_n^2}{2m}$$

one gets back the free electron RKKY interaction.) The point here is that the non-local susceptibility is determined by the energy eigenfunctions, whether they are wavelike or not. One does not need an undisturbed propagation of Bloch waves. DeChatel argues that $\chi(R_i,R_j)$ will not be drastically cut off even if the eigenfunctions are far from Bloch waves. Even though he does argue that the mean free path cannot play the role of a damping length, he advocates its use as such since it is the best one can do when working within certain approximations, although these approximations may be fatal. In that spirit, we will briefly discuss a model developed by U. Larsen[95] to examine the effects of damping and fluctuations in nearest neighbor distance on the spin-glass temperature of RKKY

coupled alloys. In particular, the evidence to be presented will suggest that the changes in T_{sg} due to the order-disorder transformation cannot be attributed solely to mean free path effects.

The formalism developed by Larsen is an RKKY version of the Sherrington and Southern model.[62] They obtain a freezing temperature $kT_{sg} = b_S\{\Sigma_j \Delta_{ij}^2\}^{1/2}$ where $\Delta_{ij} = \Delta(R_{ij})$ is the width of a Gaussian distribution of the exchange coupling $J_{ij} = J(R_{ij})$. Larsen assumes that J(R) is the RKKY interaction and $\Delta(R)$ is its envelope, so that

$$\Delta(R) = \frac{9\pi J^2 (2\ell+1)^2}{2E_F\ (2k_F R)^3}\ e^{-R/\lambda}.$$

If one temporarily omits the damping (assume pure RKKY) and sets all nearest neighbor distances equal to the average, then one finds

$$kT_{sg} = \frac{9\pi A}{4k_F^3}\left\{\frac{16\pi c}{a_0^3}\int_{<\zeta>}^{\infty}\frac{dR}{R^4}\right\}^{1/2}. \qquad (4.1)$$

where

$$A = \frac{b_S J^2 (2\ell+1)}{4E_F}, \qquad b_S = \frac{[(2S+1)^4-1]^{1/2}}{12},$$

and $<\zeta> = a_0\ (\frac{3}{16\pi c})^{1/3}$ is the radius of a sphere containing one spin.

In the case of finite λ, spins beyond the distance λ are excluded and kT_{sg} is reduced below the value given by (4.1). When the dominant scattering is due to magnetic impurities and not defects or phonons, this is called self-damping and $\lambda \sim \frac{1}{c}$. Thus the number of shells of width $<\zeta>$ which contribute in the sum for kT_{sg} behaves

as

$$\lambda/\langle\zeta\rangle = \frac{1}{c}/\frac{1}{c^{1/3}} = c^{-2/3} \ .$$

Thus self-damping is increasingly important at high concentrations.

If λ is due to a fixed number of non-magnetic impurities (such as Pd, Pt, or Au), the number of shells within λ is $\lambda/\langle\zeta\rangle \sim c^{1/3}$, and is important at low concentrations. Larsen's final result, including fluctuation and self-damping effects is given by

$$kT_{sg} = Ac\{\frac{3}{c}\int_1^\infty \frac{dx}{x^4} e^{-rcx} [1 - e^{c'(1-x^3)}]\}^{1/2} \qquad (4.2)$$

where $r = \frac{4\beta e^2 \rho}{a_0 hc}$. Here ρ is assumed to be the total resistivity.

One can see already that there are major problems between theory and experiment. Larsen's theory would predict that the disordered state alloys have a lower spin-glass temperature than the ordered state alloys because their total resistivity is higher. In fact just the opposite is true. (The calculated spin-glass temperatures are shown in Table 11 based on the resistivities shown in Table 10.) If one assumes that for some reason the magnetic resistivity is dominant in these alloys (for the purposes of determining T_{sg}) then the trend is in the correct direction for the $\underline{Cu_3PtMn}$ (0.81%) sample but still in the wrong direction for the $\underline{CuPd(17)Mn}$ (1%) sample. In addition, the calculated difference in T_{sg} between ordered and disordered hosts is generally considerably smaller than observed experimentally.

Table 11. Calculated Spin-Glass Freezing Temperatures for Cu_3PtMn (0.81%) and CuPd(17)Mn (1%).

Material	Spin-Glass Temperature (K) Calculated[3]	Calculated[4]	Experimental
[1] Cu_3PtMn (0.81%) OS	3.33	3.10	2.3
[1] Cu_3PtMn (0.81%) DOS	3.59	1.79	3.3
[2] CuPd(17)Mn (1%) OS	4.89	4.18	3.5
[2] CuPd(17)Mn (1%) DOS	4.79	3.7	5.5

[1] $J = 0.1$ eV, $E_F = 7$ eV, $S = 2$, $d = 3.70$ Å, $\beta = 3.5$.

[2] $J = 0.1$ eV, $E_F = 7$ eV, $S = 2.3$, $d = 3.70$ Å, $\beta = 3.5$.

[3] T_{sg} calculated using magnetic resistivity.

[4] T_{sg} calculated using total resistivity.

However, the Larsen theory is not at a complete loss. The general behavior of T_{sg} as one adds Pt to the copper is to decrease the spin-glass temperature. This is in accord with Larsen's theory. In addition, resistivity studies have been done[68] to check the mean free path dependence of the RKKY coupling in $(Au_{1-x}Cu_x)Mn_y$ alloys and reasonable agreement was found. His theory also seems to work well for dilute spin-glasses where the host is a single noble metal. This suggests to the author that changes occur during the order-disorder transformation that are not accounted for by λ. It is quite possible that J_{sd} or E_F change as a result of the transformation. The effects could be sizeable since $kT_{sg} \sim J^2/E_F$. This possibility will be discussed briefly in the next section.

F. Brillouin Zone and Fermi Momentum Effects

By way of introducing the suggestion that Fermi momentum dependencies may be a useful approach to sorting out T_{sg} and θ behavior in our spin-glass alloys, I would like to briefly discuss the possibility of Brillouin zone effects. Admittedly, these arguments are handwaving, but in the mind of the author, they are strongly suggestive. First of all, if one examines the magnetic susceptibility of Cu_3Au and Cu_3Pt, the ordered state is considerably more diamagnetic than the disordered state. See Table 8. Forgetting about the ion core contribution (since it doesn't involve conduction elections, it is not susceptible to Brillouin zone effects) one can write $\chi = \chi_s + \chi_d$, where χ_s and χ_d are the Pauli paramagnetic and orbital diamagnetic contributions. Now, the spin paramagnetic contribution, even if significant in magnitude, is considered to be insensitive to the order-disorder transformation since electronic specific heat measurements show only a few percent change. This follows because the Pauli susceptibility and the electronic specific heat are both strongly dependent on the density of states at the Fermi surface. Therefore, one's attention turns to the orbital diamagnetic term given by

$$\chi_d = -\frac{2}{3}\frac{e}{4\pi ch}\iint \frac{1}{|\text{grad}E|}\left\{\frac{\partial^2 E}{\partial k_x^2}\frac{\partial^2 E}{\partial k_y^2} - \left(\frac{\partial^2 E}{\partial k_x \partial k_y}\right)^2\right\} ds$$

when the integral is over the Fermi surface. Such a term is therefore highly dependent on the curvature of the energy surfaces. Therefore,

changes in Fermi surface geometry caused by Brillouin zones could have a significant effect on χ_d. To explain such strong diamagnetic effects, one might be tempted to adopt ideas out forward by Mott and Jones.[69] They examine the case of small overlap between the Brillouin zone and the Fermi surface (See Figure 41). Here the surfaces of constant energy form approximately a family of ellipsoids.

$$E = \frac{h^2}{2m} \{\alpha_1 k_x^2 + \alpha_2 k_y^2 + \alpha_3 k_z^3\}$$

Electrons near states A and B may have an α_1 which is 30 times the value of α_2 or α_3 and makes large contributions to the diamagnetism in the y-axis direction.

Now, one might ask if there is any reason to believe the BZ-Fermi surface overlap to be small. Generally speaking the answer is yes because we know from the Hume-Rothery rules that other things being equal, that structure is preferred in which the overlap out of the first Brillouin zone is as small as possible. To be more specific, one need only examine studies of the long-period superlattice alloy phase of Cu_3Pt.[70] This phase has been well documented by x-ray studies. These systems are superlattices with stable antiphase domains of definite size. A detailed study of the origin of the long-period superlattice has been carried out by Sato and Toth.[71] They find a definite relation between the electron-atom ratio and the domain size M. They develop a model based upon the stabilization of alloy phases using the Brillion zone theory which fits the experimental data very well. In addition, they study A_3B type alloys

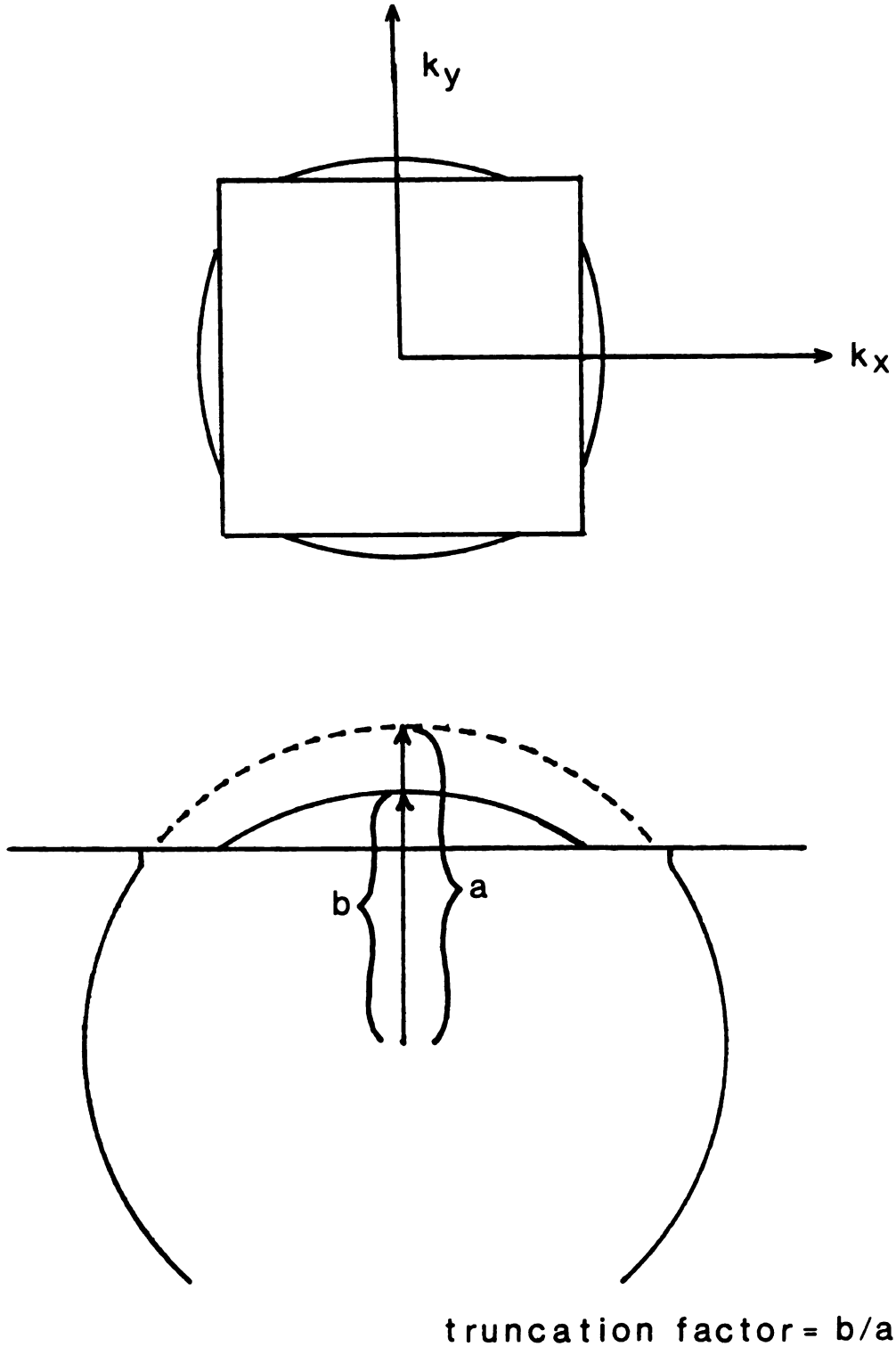

Figure 41. Brillouin zone effects on the Fermi surface.

including the Cu-Pt system and find they can fit the experimental data (M vs e/a) very well if they use a truncation factor t = 0.958, (See Figure 41) which seems to agree with the general ideas of Mott and Jones. Furthermore arguments by J. C. Slater[72] and J. F. Nicholas[73] claim that the order-disorder transformation in CuPt, CuAu, and Ag_3Mg are driven by Brillouin zone effects and do not simply follow from lattice strain relief. Because the local environment of Cu and Pt in Cu_3Pt (ordered vs. disordered) is considerably different than that for CuPt (ordered vs. disordered) a straightforward generalization is not possible, but only suggestive. Finally, it should be remarked that determining changes in the Fermi surface due to an order-disorder transformation based on non-equilibrium (transport) properties is difficult at best. The principle difficulty is that the Boltzmann transport equation can be solved in a simple way only for the unrealistic case of a spherical Fermi surface and for scattering elements that depend only on $|\vec{q}|$ where $\vec{q}$ is the scattering vector. Changes in resistivity are difficult to sort out because of dependencies on periodicity, and number and kind of carriers. In the case of thermopower,[49] individual contributions do show systematic changes with atomic ordering, but they can be opposite in presumably similar alloys.

G. Quantum Effects

It has been suggested (see Reference 75) that subtle effects, such as the change in sign of θ with concentration are due to quantum

mechanical effects. Matho argues that the distribution of exchange energies $D(w) = \Sigma\delta(w-w(R))$ summed over all lattice positions $R \neq 0$ can be represented by a continuous function with high energy cut-offs. In fact, if $D(w) = w_1/w^2$ and the high energy cut-offs are chosen according to $T_{1f} + T_{1a} = \frac{D^{(2)}(w)}{w_1}$ and

$$(T_{1f} - T_{1a})/(T_{1f} + T_{1a}) = \tanh\left(\frac{D^{(1)}(w)}{2w_1}\right)$$

then the continuous distribution reproduces the moments $D^{(1)}$ and $D^{(2)}$. This leads to asymmetric saturation values for the spin-spin correlation function:

$$\text{That is,} \quad \langle \vec{S}_1 \cdot \vec{S}_2 \rangle = \begin{cases} +S^2 & \beta w \gg 1 \\ -S(S+1) & -\beta w \gg 1 \end{cases}$$

This appears to manifest itself as a distribution in favor of antiferromagnetic couplings. A real asymmetry toward ferromagnetism can cancel this effect and lead to the speculated sign change of θ. This brings up the point that most of the work dealing with spin-glasses to date has employed classical spins. Recent work by Klemm[98] indicates that there may not exist an Edwards-Anderson spin glass phase for S = 1/2 Heisenberg spins. More quantum mechanical calculations are needed.

VII. GENERAL CONCLUSIONS AND THE FUTURE

The principle experimental claim of this thesis is that spin-glass behavior does occur in dilute magnetic alloys when the average interaction is antiferromagnetic. More specifically, unlike the ferromagnetic case, the condition $|\theta_c| = T_{sg}$ need not be associated with the onset of magnetic order. Present data for two different alloys systems ($\underline{Cu_3Pt}Mn$ and CuPd(17)Mn) suggest that $|\theta_c|$ nearly equal to $3T_{sg}$ does not cause the loss of spin-glass behavior.

The majority of the experimental results presented are an attempt to systematically explore the effect on the magnetic properties of host atomic order-disorder transitions. It is the author's view that this novel approach to the study of spin-glass behavior will enjoy a bright future. This approach is similar to the crystalline versus amorphous host studies commonly performed, but may be superior because the alteration in host structure is not so drastic. It's one of the few methods available to alter the impurity-impurity interaction without changing the concentration. In addition, because the basic lattice structure is always present, the more powerful, conventional solid state theory techniques can be brought to bear on this problem.

The basic experimental trends which have been established by this research include:

(1) The paramagnetic Curie temperature is a strong function of host order with $|\theta|_{ord} > |\theta|_{DOS}$. The concentration dependence is approximately linear with some possible interesting subtleties at low concentration.

(2) The spin-glass temperatures are also a strong function of host order with $(T_{sg})_{DOS} > (T_{sg})_{OS}$. The spin-glass temperatures are nearly proportional to the concentration.

(3) The spin-glass temperature T_{sg} appears to be a stronger function of concentration than the Curie temperature for the disordered host samples. The opposite seems to be true for the ordered state alloys.

(4) The beginnings of some very interesting hysteresis work have been presented. Earlier studies by other workers with dilute amounts of Pt find the width and the displacement field to have the same linear Pt concentration dependence as the reversal field. Our concentrated (25%) Pt samples are certainly not an extension of this behavior. The value of the reversal field is difficult to ascertain, the width is quite small ($\sim$40 gauss) and the displacement field is non-negligible only for the disordered host data.

(5) Finally, some preliminary results for $\underline{Cu_3Au}Mn$ (1%) indicate that this is an alloy system where the spin-glass temperatures are greater for the ordered host samples than for the disordered host samples.

The reader also found presented in this thesis a few possible approaches one might take to try and understand the experimental trends in a qualitative fashion. An attempt to use the Mean Random

Field approximation to learn something from the high temperature susceptibility proved essentially impossible. Nevertheless, the fact that the Cu_3PtMn (2% DOS and 3% DOS) followed the expected behavior but the other Cu_3PtMn samples did not may help clarify weaknesses in the MRF approximation. Conversely, it may indicate that there exists a fundamental difference between ordered and disordered host spin-glasses. Experimental trend #3 above already hints at this.

Attempts to understand the data using a naive free electron RKKY interaction and involving Fermi momentum changes upon ordering look promising on the surface but fade somewhat when examined in detail. The periodic and quasi-periodic dependence of θ and T_{sg} on k_F respectively looks hopeful at first, but is probably too simple-minded. One must keep in mind that even drastic changes in sign probably occur for θ as a function of concentration in simple noble metal hosts. The situation is not likely to be any simpler for the binary hosts. Along these lines, considerable discussion was also given to the possible importance of Brillouin zone effects. The diamagnetism of the hosts, the formation of long-period superlattice structures, and studies of CuPt, CuAu, and Ag_3Mg all suggest Brillouin zone effects may be important. However, there does not exist, to the best of the author's knowledge, any theories relating changes in Fermi surface geometry to spin-glass properties. They will probably be needed. Finally, attempts to understand the spin-glass freezing temperature on the basis of mean free path effects also failed dismally. The qualitative behavior was not even correct. However, it's quite possible that the effect on mean free path due to ordering

at a fixed concentration of non-magnetic scatterers is qualitatively different from the addition or removal of further scatterers. In short, none of the theoretical attempts to understand the data were effective in the short run, but it is the author's view that new insights into the physics of spin-glasses will be achieved through the analysis of spin-glass behavior in order-disorder alloys.

In closing, I would like to briefly discuss where one goes from here. Some future experiments which immediately come to mind include:

(i) diffuse x-ray scattering to establish the nature of the chemical short range order,

(ii) extend the maganese concentration in the $(\underline{Cu_3Pt})_{1-x}Mn_x$ and $(\underline{CuPd(17)})_{1-x}Mn_x$ alloys to see how far one can extend the SK phase diagram;

(iii) initiate similar studies in alloys with different lattice structures. For example $(\underline{CuPt})_{1-x}Mn_x$ has a layered structure (alternating planes of Cu and Pt). $(\underline{CuPd})_{1-x}Mn_x$ has a body-centered cubic structure;

(iv) the placement of Mn impurities on specific chemical sites. For example, $Cu_{3-x}PtMn_x$, where the Mn resides only on the copper sites or $Cu_3Pt_{1-x}Mn_x$ where the Mn resides only on the Pt sites;

(v) Continue studies of FCC order-disorder hosts like $(\underline{Cu_3Au})_{1-x}Mn_x$ which was already begun;

(vi) continue to study the hysteresis properties of these ternary alloys. A systematic study of $(Cu_{1-x}Pt_x)Mn_y$ for fixed y with variable x may lead to new physical insight.

APPENDICES

A. SIGNAL DETECTION COIL CONSIDERATIONS

Probably the most complex and yet most crucial design aspect of VSM's is the size, shape, and relative position of the signal detection coils. For a good discussion of this subject see References 76-78. I would like to discuss briefly the work of Mallinson[79] since a set of coils based on his calculations were made but never used to take actual measurements. His derivation is based on the principle of reciprocity which states that the mutual flux threading two coils is independent of which one carries a current I. His final working result is

$$\dot{\Phi} = \mu\left(\frac{dhx}{dy}\right)v_y \qquad \text{(A1)}$$

where he assumes the sample is magnetized in the x-direction and vibrates in the y-direction. A more general derivation of Mallinson's result is given by R. Reeves and J. Reeves.[80] They consider the induced EMF in a filamentary circuit due to a magnetic dipole. Let $\vec{d\ell}$ be an infinitesimal element of the loop, $\vec{m}$ be the dipole moment of the sample, and $\vec{r}$ the vector from $\vec{d\ell}$ to $\vec{m}$.
Then the vector potential at $\vec{d\ell}$ due to $\vec{m}$ is

$$\vec{A} = -\frac{\mu_o}{4\pi}\frac{\vec{m} \times \vec{r}}{r^3}$$

using $\vec{E} = -\frac{\partial \vec{A}}{\partial t}$ the electric field produced at $d\vec{\ell}$ due to $\vec{m}$ is given by

$$\vec{E} = \frac{\mu_o}{4\pi} \frac{\partial}{\partial t} \left(\frac{\vec{m} \times \vec{r}}{r^3}\right)$$

Therefore, the EMF generated around the loop is given by

$$V = \frac{\mu_o}{4\pi} \oint \frac{\partial}{\partial t} \frac{\vec{m} \times \vec{r}}{r^3} \cdot d\vec{\ell}$$

Interchanging dot and cross and integration and differentiation leads to

$$V = -\frac{\mu_o}{4\pi} \frac{\partial}{\partial t} \oint \vec{m} \cdot \frac{d\vec{\ell} \times \vec{r}}{r^3}$$

$$= -\frac{\mu_o}{4\pi} \frac{\partial}{\partial t} \vec{m} \cdot \oint \frac{d\vec{\ell} \times \vec{r}}{r^3}$$

where $\vec{N} = \oint \frac{d\vec{\ell} \times \vec{r}}{r^3}$ is a purely geometric function defined by the coil configuration. (One can see reciprocity entering here since $\vec{N}$ is really the magnetic field per unit current which would be produced at $\vec{r}$ due to a unit current flowing in the coil). Thus,

$$V = -\frac{\mu_o}{4\pi} \frac{\partial}{\partial t} \vec{m} \cdot \vec{N} \qquad \text{(A2)}$$

Now equation A2 is a very general result. For example, if the dipole is stationary then N is constant and $V = -\frac{\mu_o}{4\pi} \vec{N} \cdot \frac{d\vec{m}}{dt}$. If $|\vec{m}|$ is constant but its orientation changes with angular velocity $\vec{\omega}$

then $V = -\frac{\mu_o}{4\pi\pi} \cdot (\vec{m} \times \vec{N})$. If the dipole does not move or rotate but changes in magnitude, then $V = -\frac{\mu_o}{4\pi} \vec{N} \cdot \hat{m} \frac{dm}{dt}$.

Finally, if the dipole moves with velocity $\vec{v}$ without otherwise changing then

$$V = -\frac{\mu_o}{4\pi} \vec{m} \cdot \frac{d\vec{N}}{dt} \tag{A3}$$

This is the equation which applies to the VSM. Equation A3 can be rewritten as

$$V = -\frac{\mu_o}{4\pi} \vec{m} \cdot \{\frac{\partial \vec{N}}{\partial x} v_x + \frac{\partial \vec{N}}{\partial y} v_y + \frac{\partial \vec{N}}{\partial z} v_z$$

or

$$V = -\frac{\mu_o}{4\pi} \{m_x (\frac{\partial N_x}{\partial x} v_x + \frac{\partial N_x}{\partial y} v_y + \frac{\partial N_x}{\partial z} v_z)$$

$$+ m_y (\frac{\partial N_y}{\partial x} v_x + \frac{\partial N_y}{\partial y} v_y + \frac{\partial N_y}{\partial z} v_z)$$

$$+ m_z (\frac{\partial N_z}{\partial x} v_x + \frac{\partial N_z}{\partial y} v_y + \frac{\partial N_z}{\partial z} v_z)\} \tag{A4}$$

This is the principle result of this appendix. If our sample vibrates only in the y-direction then equation A4 reduces to

$$V = -\frac{\mu_o}{4\pi} \{m_x \frac{\partial N_x}{\partial y} + m_y \frac{\partial N_y}{\partial y} + m_z \frac{\partial N_z}{\partial z}\} v_y .$$

If the magnetic field is in the $\hat{x}$ direction, so that $\vec{m}$ is essentially a vector in the $\hat{x}$ direction, then

$$V = - \frac{\mu_o}{4\pi} m_x \left(\frac{\partial N_x}{\partial y}\right) v_y.$$

But N_x can be identified with Mallinson's h_x using the Biot-Savat Law.

Now the idea is to maximize $\dot{\Phi}$ by maximizing $\frac{dh_x}{dy}$. So let's consider the situation shown in Figure 43 where the sample is located at the origin, the distance of closest approach is x_o, and the sample vibrates in the y-direction. The output voltage from this loop is

$$\dot{\Phi} = \mu \dot{y} \left[\left(\frac{dh_x}{dy}\right)_A - \left(\frac{dh_x}{dy}\right)_B\right]$$

where

$$\left(\frac{dh_x}{dy}\right) = \frac{2(x^2-y^2)}{(x^2-y^2)^2}$$

This implies that maximum output is achieved if conductor A is placed at the coordinates $(x_o,0)$ and conductor B is placed anywhere along $(x_o, \sqrt{3}\, x_o)$. Thus Mallinson preducts the optimum coil configuration to be that shown in Figure 42. Here four identical N turn coils were used. By connecting them properly in series opposition the signal output was increased and some immunity to magnetic field fluctuations was achieved. Such a set of coils was constructed by the author. They were approximately 2.55 inches in diameter and consisted of 1700 turns of #36 HVY polythermaleze copper wire per coil. Each coil had a dc resistance of approximately 460 ohms. Their self-resonant frequency was measured to be close to 1400 Hz. Their

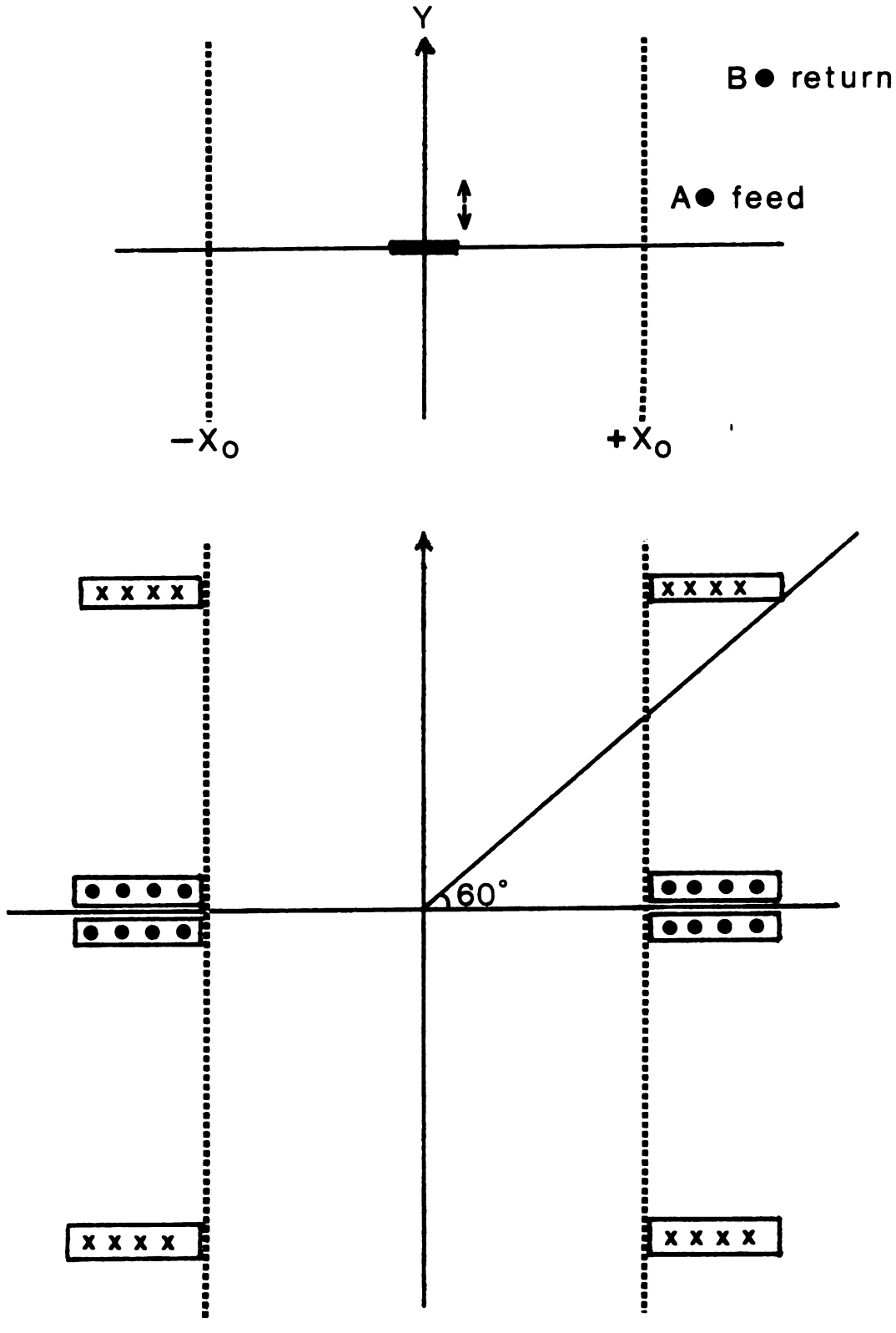

Figure 42. Optimum pick-up coil geometry.

inductance was 1.14 Henries. These coils were constructed in an attempt to increase the signal-to-noise ratio. The previous set of coils were #986 Miller air core RF chokes. Their mean diameter is approximately 11/16 inches and they have approximately 1300 turns of wire with a DC resistance of 95 ohms each. The signal was expected to increase by a factor of (2.3) $(\frac{1700}{1300}) \simeq 3.0$. The actual measured increase in signal was of the order of 2. However, the increase in noise due to magnetic field fluctuation was greater than 2 and the overall signal-to-noise ratio decreased. The sensitivity to applied field noise goes as Nr^2. Therefore

$$\frac{(Nr^2)^{new}}{(Nr^2)^{old}} = \frac{(1700)(1.63)}{(1300)(0.12)} = 17.8 \qquad (2.16)$$

In fact, the only way to really increase the signal-to-noise ratio is to make the detection coils smaller and move them closer to the sample.

One final attempt to reduce field noise effects was made by attempting to externally balance the Miller coils. By sweeping the magnetic field linearly, the output from the four pick-up coils was measured to be 10 μV/4000 gauss/min. This implies a total turn imbalance of approximately 15 turns. Coil turns were added and subtracted systematically in an attempt to balance the coils. Once the coils were reasonably well balanced with these quasi-static fields, an attempt was made to match reactive components at 33 Hz. This was done by driving the NMR coils at approximately 33 Hz and adjusting

the values of trimming capacitors. This seemed to meet with some success, but the reactive components were never completely balanced out. Overall, these measures probably increased the signal/noise ratio, but a quantitative estimate was never made.

B. SCHEMATIC DIAGRAMS

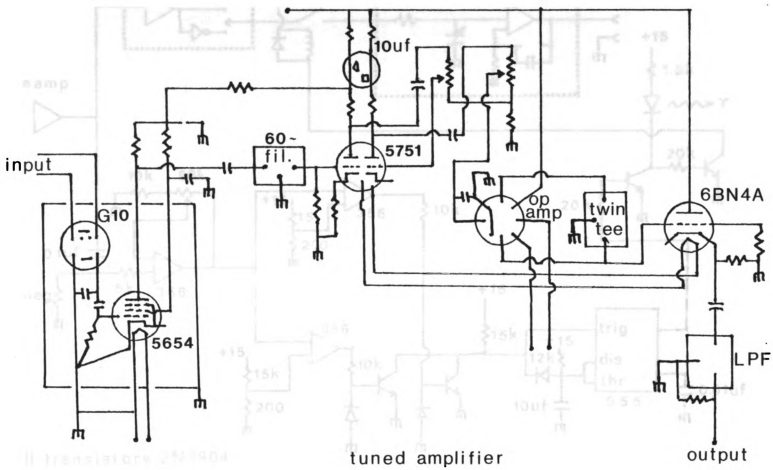

Figure 43. Tuned amplifier.

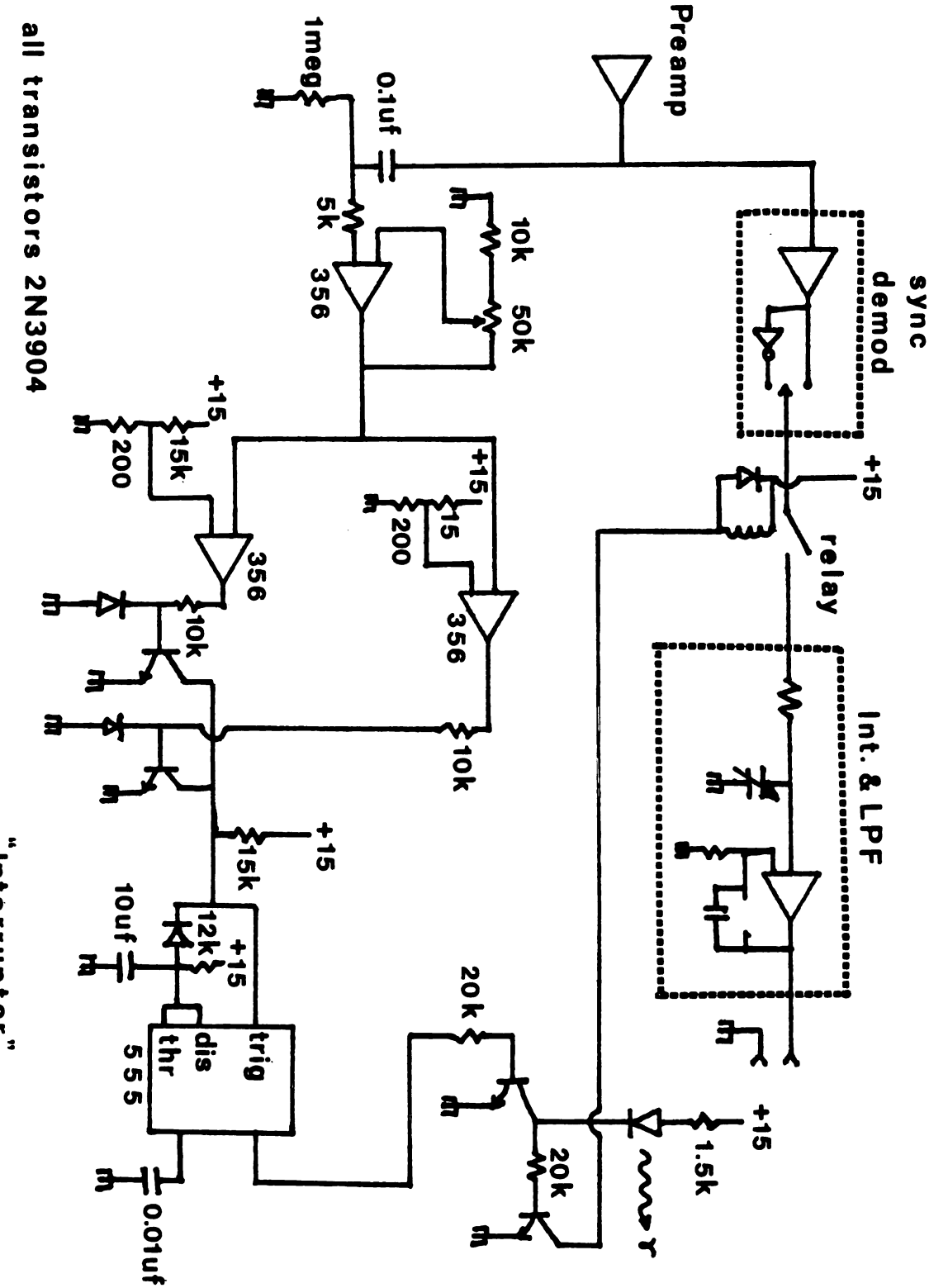

Figure 44. "Interrupter".

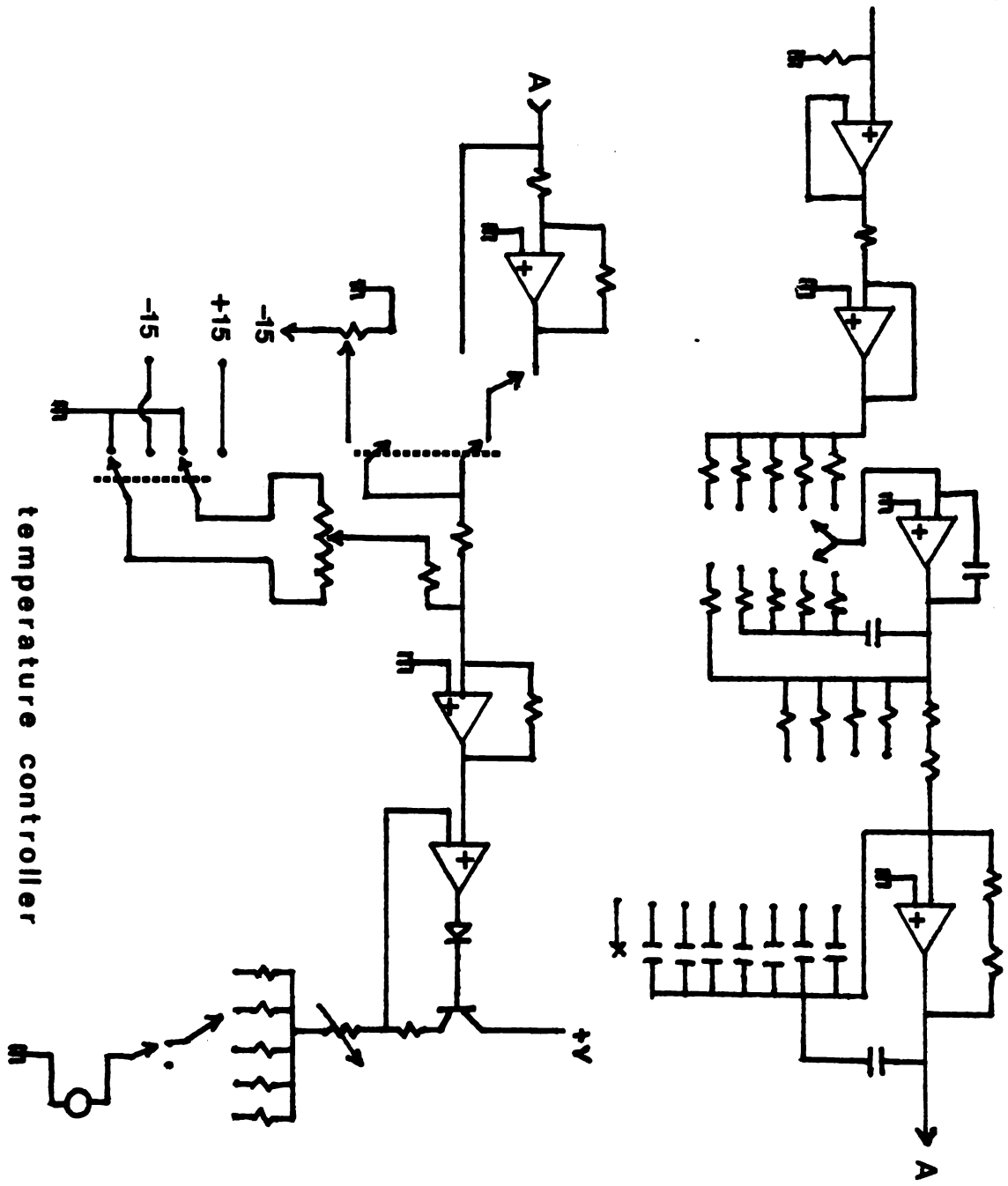

Figure 45. Temperature controller.

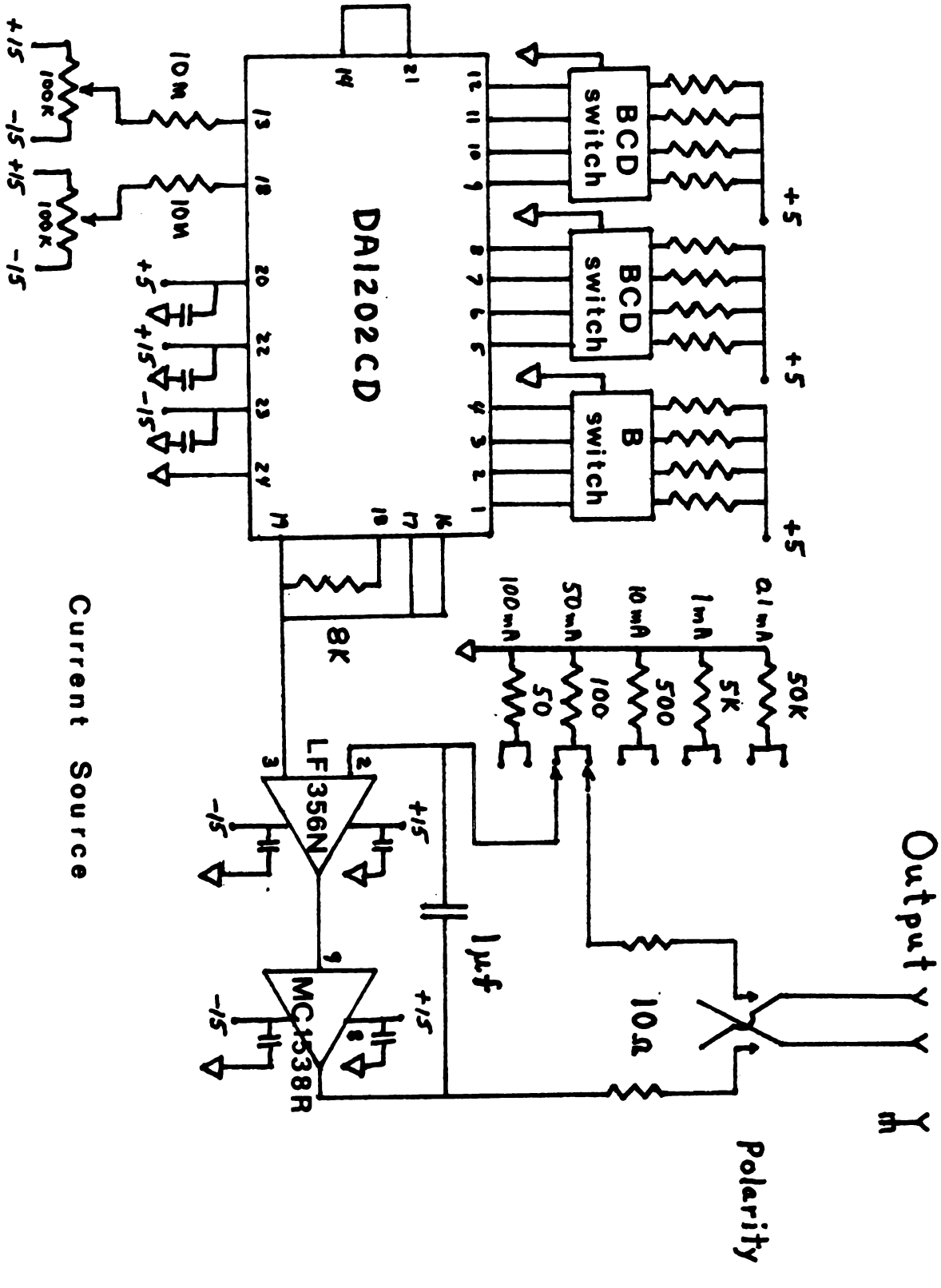

Figure 46. Current source.

C. MAGNET AND POWER SUPPLIES

Some discussion of low noise amplifiers and the like was presented, but the major factor limiting the sensitivity of the system was ambient magnetic field fluctuations. For this reason I should like to briefly discuss the magnet and associated power supplies. The magnet is a Magnion 12-inch diameter electromagnet with a 3-inch gap. It has an H-frame cast magnetic yoke, is indirectly water-cooled, and utilizes low impedence foil wound copper coils capable of continuous operation in excess of 65 amperes. The power supply is a model HS-1365/FFC-4 8.5 kilowatt magnetic field regulated power supply. It has a maximum output of 65 amperes at 130 VDC. The FFC-4 field regulator utilizes a rotating flip coil to sense the strength of the magnetic field directly. A permanent magnet in a controlled environment is mounted on the same shaft as the flip coil and provides a standard voltage output. A ratio transformer selects some fraction of the reference generator signal and this is compared with the flip coil output (which is about 50 mV/kilograms). The probe coil is turned at 1800 RPM by a synchronous motor and generates a 30 Hz signal. The difference between the flip coil and the precisely attenuated signal from the reference generator is amplified by a tuned amplifier. A demodulator selects that portion of the signal which is at the correct phase and converts it into a DC signal. This in-phase error signal is used in the field set or regulate

modes for control of the magnetic field. The regulator also employs a stationary field rate sensing coil mounted around one pole cap. It develops a voltage proportional to the ratio of change of the field. The in-phase error signal is combined with the signal from the rate coil and sent to an integrating amplifier. This causes the power supply to act as a current amplifier in controlling the current to the magnet. The power supply consists of basically 2 servo loops. The coarse or secondary loop consists of a motor-driven variac which is designed to control the amount of DC voltage supplied to the precision regulator. Its job is to maintain approximately 3 volts between the collector and emitter of the series bank transistors. The precision servo loop is essentially the FFC-4 field regulator. The integrating amplifier receives the demodulated chopper signal and the AC signal from the rate coil. It raises the power level sufficiently to drive the power transistor bank. The advertised stability of one part in 10^5 means ±0.09 gauss at 9000 gauss. In fact, the field stability was often times more like ±1 gauss. Sudden changes in the magnetic field would cause voltage surges which were large enough to overload the tuned amplifier and cause it to ring at ≈33 Hz. The phase-lock amplifier was only partially successful in discriminating against these unwanted signals. Attempts to deal with this problem began with an investigation of the magnet power supply itself. The most puzzling discovery was the presence of a 500 KHz signal at the output of the tuned amplifier, even when the input of the amplifier was grounded. It appeared as though some part of the system had begun to oscillate. Additional work suggested

problems with the Twin-T network. If certain capacitors were slightly increased in value the high frequency noise could be eliminated. Other games were played including an in situ tuning of the Twin-T. This was done by observing the field deviation meter which sees the dc output from the demodulator. By adjusting certain trimming resistors so that one acquired minimum oscillation of the field deviation meter around its correct value (as specified by the ratio transformer) a slight improvement of the field stabilization was effected. It is also possible that due to the age of the supply (approximately 14 years) and the germanium semiconductor technology employed, field stabilities of one part in 10^5 are unlikely to be regained. Some further testing yielded no new clues, it was decided to try and treat the symptons rather than the cause. More on this later. For those days when the ambient field noise was just too great to take data, we often switched power supplies. Most of the data at 5 kilograms utilized an Alpha Scientific Laboratories Model 3002 current-regulated power supply. It had output current and voltage capabilities of -0.3 to 30 amperes and -0.35 to 50 volts, respectively. Since the dc impedance of the magnet coils is approximately 2 ohms, supply currents as great as 25 amps were available. It was found necessary to plug this unit into the 235 volt single phase line to obtain 25 amps. In general, the field produced by this supply was quieter. Since this is a current regulated supply, the strength of the magnetic field had to be independently measured. This was generally done with an LDJ Model 101B Gaussmeter which utilizes a Hall probe. Finally, when the hysteresis measurements were being taken

in relatively low field, it was found that the Heathkit IP-2710 power supply was the quietest of them all. It was capable of delivering 30 V at 3 amps.

D. GROUNDING AND SHIELDING CONSIDERATIONS

Since this experiment involved the measurement of very low level signals in a somewhat noisy environment, some remarks about the grounding scheme would be in order. The principles of proper grounding are straightforward, but not so easily optimized in practice. Figure 43 shows the grounding scheme for the low level signal processing circuitry. The power supply, tuned amplifier, phase-lock amplifier and digital multimeter are all isolated from the rack and the grounded neutral of the AC line. The signal ground is connected to the rack and the neutral line only at the oscilloscope. This means the link on the back of the phase-lock amplifier must be disconnected and the position of S_1 doesn't really matter. The 31 Ohm resistor is designed to semi-float the amplifier input from common should the possibility of ground loops exist. The connections as shown embody two rules of practical shielding.[81] Rule One requires that the shield must be tied to the zero-signal reference potential. Rule Two requires that the shield conductor should be connected to the zero signal reference potential at the signal earth connection. Since the oscilloscope is intimately tied to the rack but is not connected to neutral, everything was tied as close as possible to it. A view of the overall grounding scheme can be seen in Figure 44. When grounding instrumentation with widely varying power and noise levels, one should group the leads selectively. The signal ground for low-level

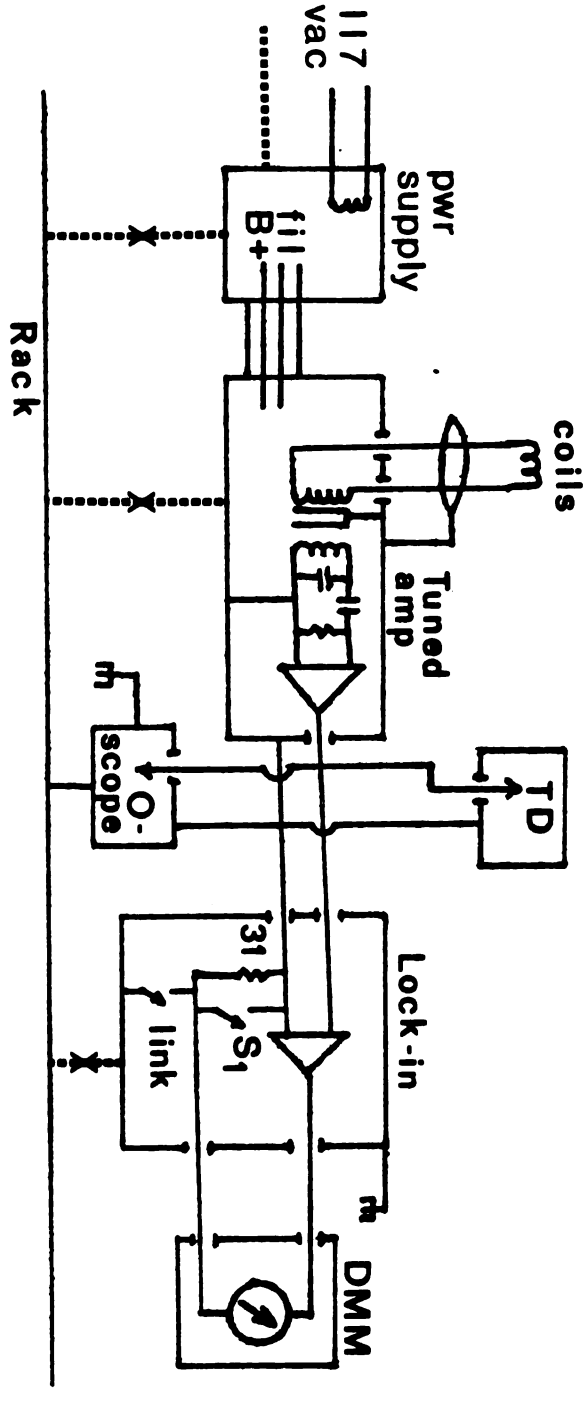

Figure 47. Grounding scheme (low level signal circuitry).

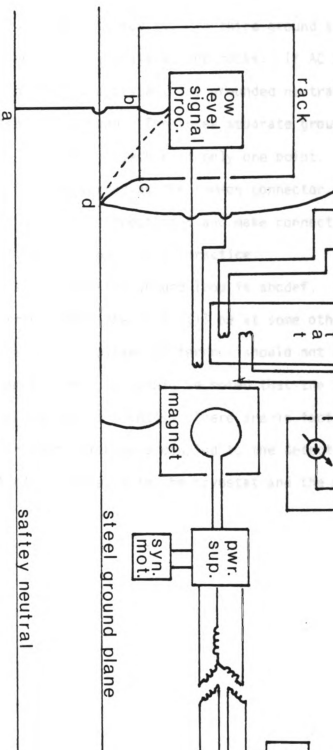

Figure 48. Grounding scheme (overall).

electronic circuits should be separated from the relatively noisy ground of relay and motor circuits. A third ground should be used for mechanical enclosures, chassis, and racks. If AC power is distributed throughout the system, the grounded neutral should be connected to the rack ground. The three separate ground return circuits should be connected together at only one point. In our system, the steel ground plane served as the common connector. It would have been preferable to break connection 5 and make connection 4 (shown dashed) but this wasn't possible in practice.

The only possible massive ground loop is abcdef. If there is a ground loop current, then the rack will be at some other voltage than the ground plane. This voltage difference should not be seen by the phase-lock preamplifier. It should be noted that the previous discussion was directed at dc signals. There are in fact large AC noise signals present which were coupled to the detection coils through mutual capacitances with the cryostat and the magnet.

E. PHASE SHIFT CONSIDERATIONS

Although it is the intention of the author to concentrate most of the experimental discussion to the final, finished magnetometer, some indication of the nature of the problems which can arise should be included. One of the most interesting problems is one I refer to as the phase shift problem. What was observed was the simple fact that when the current through the Domenicali coil was reversed, the phase of the signal did not change by 180°. This implies that there is another signal present (presumably from the holder) which is not collinear with the signal caused by the nulling current. This was indeed the case. One could check this very easily by measuring the strength of the signal along 3 different directions in phase space. In each direction one would measure the magnitude of the signal with some amount of positive nulling current, the same amount of negative nulling current, and with no nulling current at all. Now, two questions must be asked. The first question is how sensitive is the system to quadrature error? The second question is what is the origin of it and can it be eliminated? If one assumes that the true signal from the sample (i.e., that due to its magnetization) has the same phase as the signal from the coil, then presumably one can obtain this correctly by sending a very large current through the Domencaili coil. Then the question becomes, if for some reason or other a phase setting error still exists, how much damage can the

quadrature signal cause? Some idea can be gotten from the graph shown in Figure 45. This diagram refers to a Princeton Applied Research Model 220 Lock-in amplifier, but similar values probably exist for the Ithacio phase-lock amplifier. The residual signal at 4.2°K and 0 KOe has a strength of about $\frac{11}{52}$ x 30 = 6 mA at 6 K6 it is approximately 12 mA. Its quadrature component is roughly 6 mA. What sort of error does this induce? The strength of the Domenicali coil is such that one produces 45 mV of detector output for one mA of current (for some gain settings of the amplifier). Thus, 6 mA of quadrature signal would produce 270 mV of quadrature error. This is approximately 10 times the selected sensitivity of 30 mV. Assuming a worst case phase setting error of 3°, this implies a quadrature induced output of 50% of full scale or 15 mV which is to say approximately 0.33 mA. For most of the data this would be tolerable. But one would like to do better. So some attempt was made to eliminate or reduce it. If one ascribes the quadrature signal to eddy currents, one is a little hard pressed. If one examines the homogeneity curves provided by Harvey-Wells (see Figure 45) one has uniformity to one part in 10^5 over a substantial region. The vibration amplitude of the coil is only several millimeters. This does not appear to be a likely candidate. It turns out that some of the current carrying leads to the holder would vibrate in syne with the holder vibration and the degree of vibration depended on the direction of current flow. By twisting the Domenicali coil current leads together and anchoring them higher up on the holder, this problem was greatly reduced. The amount of metal in the holder was also reduced to minimize eddy currents. The idea of producing a signal with which to

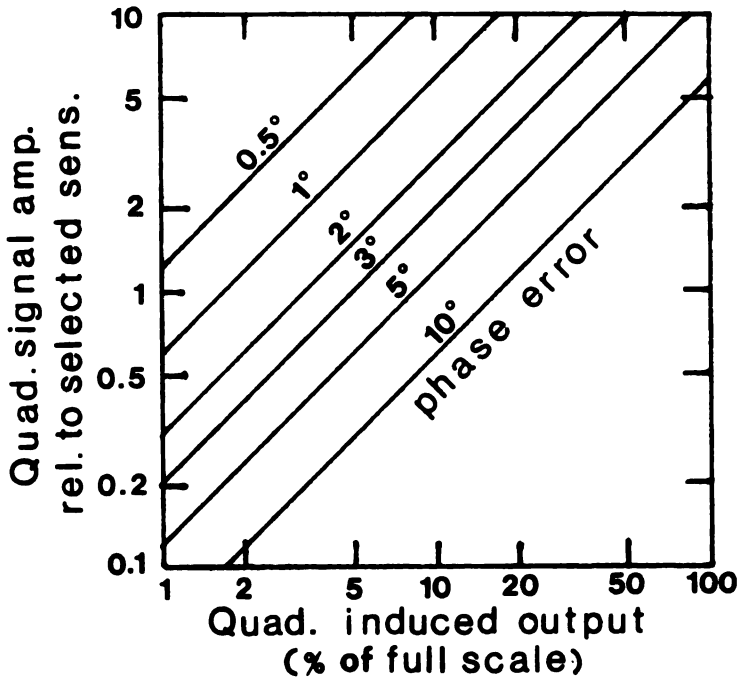

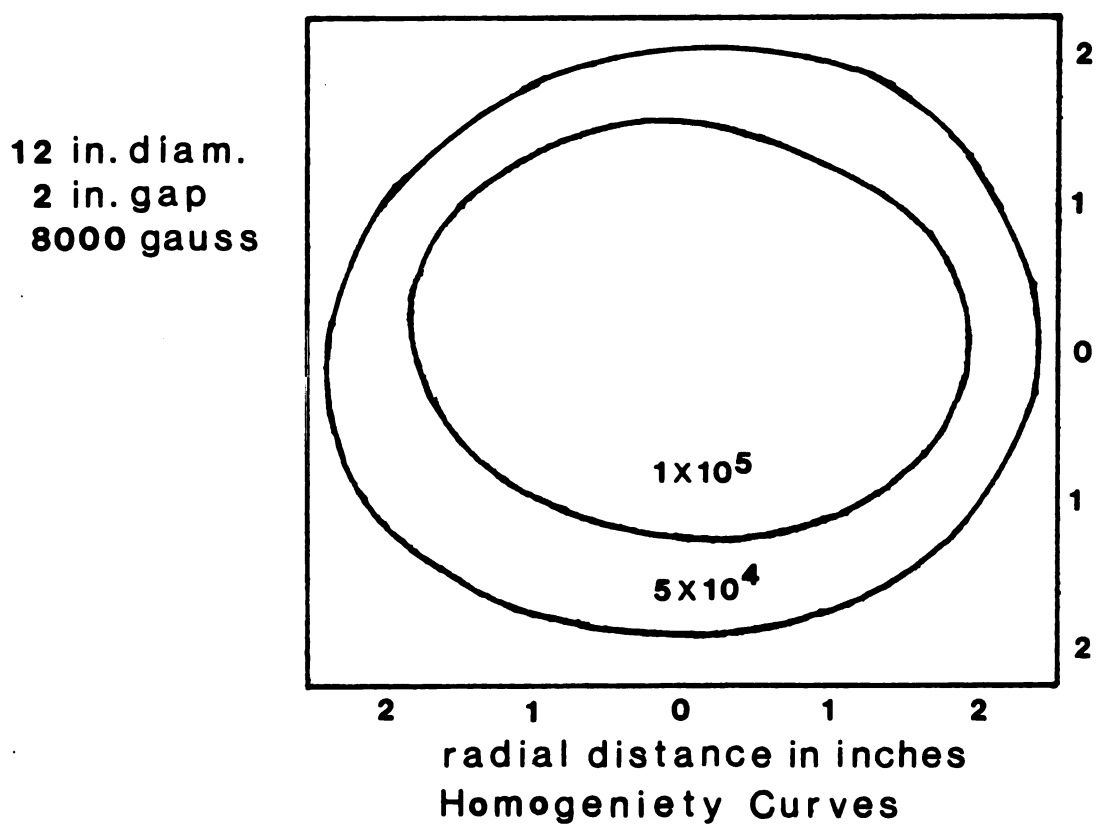

Figure 49. Quadrature sensitivity and homogeneity curves.

cancel the quadrature signal was also considered. A simple phase shifter circuit was constructed. But the quadrature signal was such a strong function of temperature and field that the idea was abandoned. Further testing revealed the cause of the quadrature signal to be one of 3 sources:

(1) a carbon resistor used to heat the sample and holder;

(2) the OFHC copper which held the carbon resistor; or

(3) the stainless steel dewar.

The equipment was redesigned so as to eliminate all three of these.

F. HYSTERESIS AND ANISOTROPY

It is the purpose of this section to give a brief introduction to the hysteresis properties of spin-glasses and discussion of a possible origin. Some very good work in this area has been done by the French[75,76] school and will serve as the basis for most of this discussion. The characteristic hysteresis loop of what I shall refer to as soft spin-glasses is shown in Figure 46 and is typical for CuMn. The conventional way of thinking about this M vs. H plot is to consider the magnetization to be the sum of two parts, a remanent magnetization and a reversible magnetization. That is,

$$M = \sigma_r + \chi(T)\, H$$

where σ_r is the remanent magnetization and $\chi(T)$ is a reversible susceptibility. The value of the magnetization at point A is the remanent magnetization σ_r. So motion along the segment GAB is due to a changing reversible magnetization with $\chi(T)$ and σ_r fixed. At point B there occurs a sudden reversal of σ_r, that is $\sigma_r \rightarrow (-\sigma_r)$. Furthermore motion along the segment DCE is again due to the reversible magnetization with the same $\chi(T)$; but now σ_r has changed sign. At point E the remanent magnetization changes sign once more and the loop is closed. In fact, the amplitude of the reversal can be as great as 95% of the initial remanent magnetization, but can sometimes

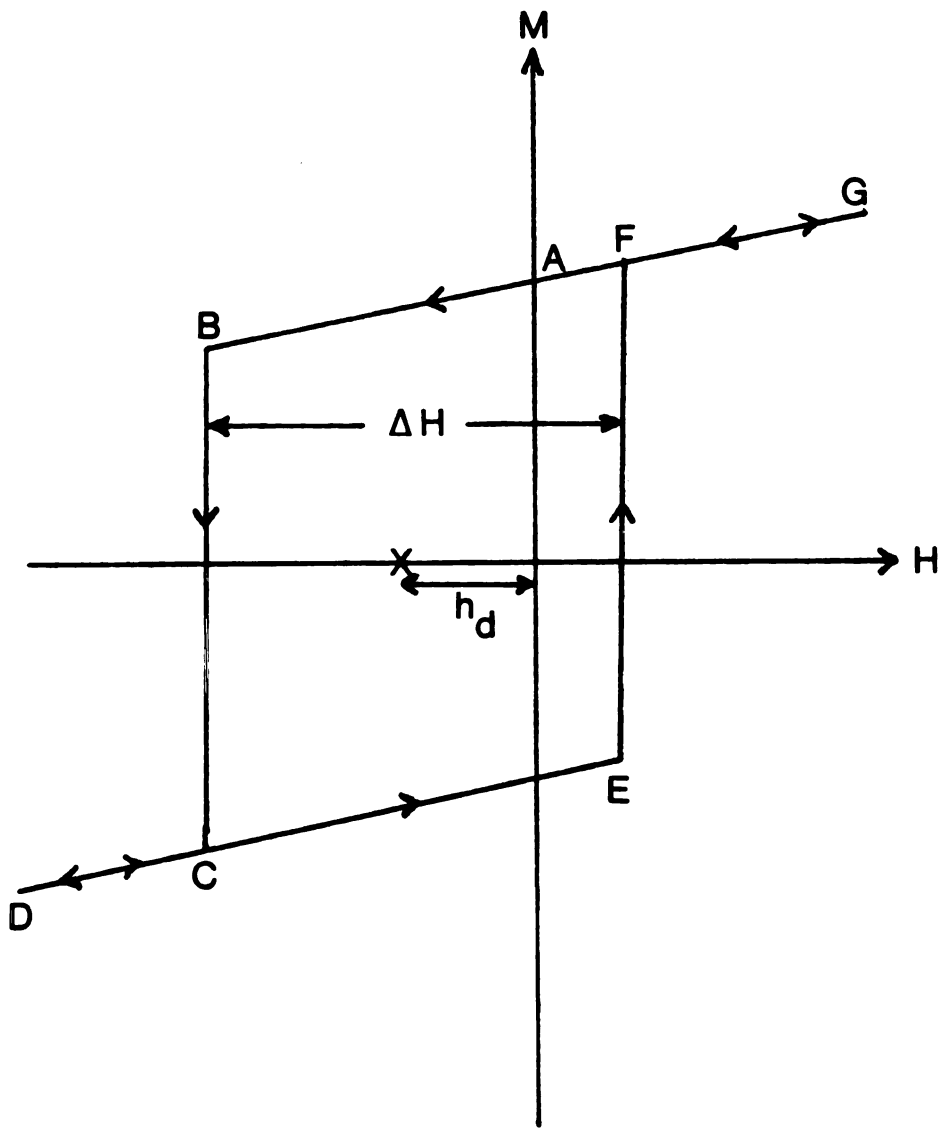

Figure 50. Soft spin-glass hysteresis curve.

be less. This upper bound seems to exist regardless of the value of the reversible magnetization. Most loops don't close exactly, and the transitions from B to C and E to F are not instantaneous, but instead follow a rather complicated time dependence. The reason for the reversal is not known, but it is believed <u>not</u> to be connected with the logarithmic time dependence of the magnetization since this seems to be independent of H even near the reversal field H_r. The strictly dynamic questions are not of interest to us here. We are concerned with the shape of the hysteresis curve. The two parameters of interest are the width of the loop and the displacement of the loop from the origin denoted by ΔH and h_d respectively. These parameters are used to define the anisotropy energy

$$K_a = \frac{1}{4} (\sigma_r)(H)$$

and the elastic energy

$$K_d = \frac{1}{2} (\sigma_r)(h_d)$$

Determination of these parameters is easy if the hysteresis curve has a sharp sudden reversal. This is thought to be due to the whole sample acting like a single domain. The reversals tend to be sharper for the more dilute samples. Evidence of a collective effect is also provided by the sensitivity of the loop geometry to cold working. The cold working changes the loop from a sharp, sudden reversal to one which is broadened and composed of a series of smaller jumps.

It is thought that the defects pin the instability whose propagation is required for magnetization reversal to take place. The spins, although they are locked together, are free to orient themselves as a whole with respect to the lattice.

We should mention that there are other spin-glasses (notably AuFe) whose hysteresis curves are very smooth and symmetrical. They are what I refer to as "hard" spin-glasses since they are thought to be composed of a distribution of magnetically hard microdomains. One of the biggest differences between spin-glasses and ordered magnetic materials lies in the degeneracy of their saturation state. In ordered magnetic materials the degeneracy is very low ($\simeq 1$). In the spin-glass state the degeneracy is very high because the remanent magnetization is composed of at most 2% of the saturation of all spins. Even so, there appears to be very little reshuffling of the spins if one goes around the hysteresis loop completely because the time dependence seems to be a continuous ongoing thing that doesn't seem to get reset. In the midst of this murky situation, attempts have been made to discover the origin of the anisotropy. ESR measurement by Owen, Brown, Arp and Kip showed that in CuMn the anisotropy is not linked to the crystal direction but only to the remanent magnetization direction. Perhaps the most successful approach to this problem has involved doping CuMn with certain non-magnetic impurities in dilute amounts. For example, Prejean et al. added Au, Al, Ag, and Pt impurities to CuMn (1%). They found the remanent magnetization and the reversible susceptibility to be unchanged in all cases. However, the value of the reversal field H_r was found to be

a strong function of the impurity used. The addition of gold and platinum impurities has a large effect on the reversal field whereas the addition of Ag and Al had a much smaller effect. The other effect caused by adding Au and Pt is to considerably lengthen the time constant of the magnetization reversal. Several possibilities come to mind as to the cause of the H_r increase with impurity type. It is probably not connected with impurity valence difference, nor is it likely to be a size effect, although cold work effects might suggest this. The most widely accepted explanation is that the anisotropy field arises from spin-orbit scattering.

G. ANISOTROPIC EXCHANGE INTERACTIONS

Let's consider briefly the origin and form of various types of anisotropic exchange. For our purposes, there are three sources of anisotropy. They are dipolar, crystal field, and spin-orbit interactions. The dipolar anisotropy is clear from the interaction between two magnetic dipoles a distance r apart.

$$H_{ij} = \frac{1}{r_{ij}^3}\left[\vec{\mu}_i \cdot \vec{\mu}_j - 3(\vec{\mu}_i \cdot \hat{r}_{ij})(\vec{\mu}_j \cdot \hat{r}_{ij})\right].$$

Crystal field anisotropy arises from the asymmetrical charge distribution surrounding the magnetic ion. Spin-orbit interactions arise from the interaction of an electron spin with the field produced by its orbital motion in a potential V(r).

It is useful to take the general second order interaction between a spin on lattice site i and a spin on lattice site j and express it in terms of its symmetric and anti-symmetric parts. That is,

$H_{ij} = -\sum_{\alpha\beta} A_{ij}^{\alpha\beta} S_i^{\alpha} S_j^{\beta}$ can be written as

$$H_{ij} = -J_{ij}\, \vec{S}_i \cdot \vec{S}_j + \vec{D}_{ij} \cdot (\vec{S}_i \times \vec{S}_j) + \vec{S}_i \cdot \overleftrightarrow{K}_{ij} \cdot \vec{S}_j \qquad \text{(G1)}$$

where

$$A_{ij}^{\alpha\beta} = A_{ij}^{\alpha\beta}\,(\text{sym}) + A_{ij}^{\alpha\beta}\,(\text{antisym})$$

where

$$A_{ij}^{\alpha\beta}(s) = \frac{1}{2}(A_{ij}^{\alpha\beta} + A_{ij}^{\beta\alpha}) \text{ and } A_{ij}^{\alpha\beta}(a) = \frac{1}{2}(A_{ij}^{\alpha\beta} - A_{ij}^{\beta\alpha}) \text{ and}$$

$$J_{ij} = \frac{1}{3} \text{ tr } A_{ij}^{\alpha\beta}(s); \quad K_{ij}^{\alpha\beta} = J_{ij} - A_{ij}^{\alpha\beta}(s); \quad D_{ij}^{\gamma} = A_{ij}^{\alpha\beta}(a)\, \varepsilon_{\alpha\beta\gamma}$$

The first term in Gl is the usual Heisenberg interaction. The second term is the so-called Dzyaloshinsky-Moriga (DM) exchange.[84] The third term is the anisotropic exchange.

The most common source of the DM exchange interaction is spin-orbit coupling. Its crucial feature is its antisymmetry. See Figure 47. Let the magnetic atoms reside at sites 1 and 2. Let α be the location of the spin-orbit scattering center. Then if we write $H_{DM} = \vec{D}\cdot(\vec{S}_1 x \vec{S}_2)$ it's easy to show that $D(R_{12},-r) = -D(R_{12},r)$. Therefore, in order for D to be nonzero, the distribution of spin-orbit centers around the two spin sites must be of low symmetry. (In other words, if two spin-orbit centers possess an inversion symmetry about the midpoint between the two spin sites then D will be zero unless the spin orbit coupling constants are different.) If the spins themselves carry spin orbit couplings (then $\vec{r} = \frac{1}{2}\vec{R}_{12}$), the two spins must be inequivalent to produce a DM exchange coupling.

Theoretical attempts to generate a macroscopic anisotropy field based on spin-orbit scattering have been made by Smith[85] and Fert and Levy.[86] Fert and Levy using the perturbing potential

$$V = -\Gamma\delta(\vec{r}-\vec{R}_1)\vec{s}\cdot\vec{S}_1 - \Gamma\delta(\vec{r}-\vec{R}_2)\vec{s}\cdot\vec{S}_2 + \lambda(r)\vec{L}\cdot\vec{s}$$

They find the leading term which contains all three scattering centers

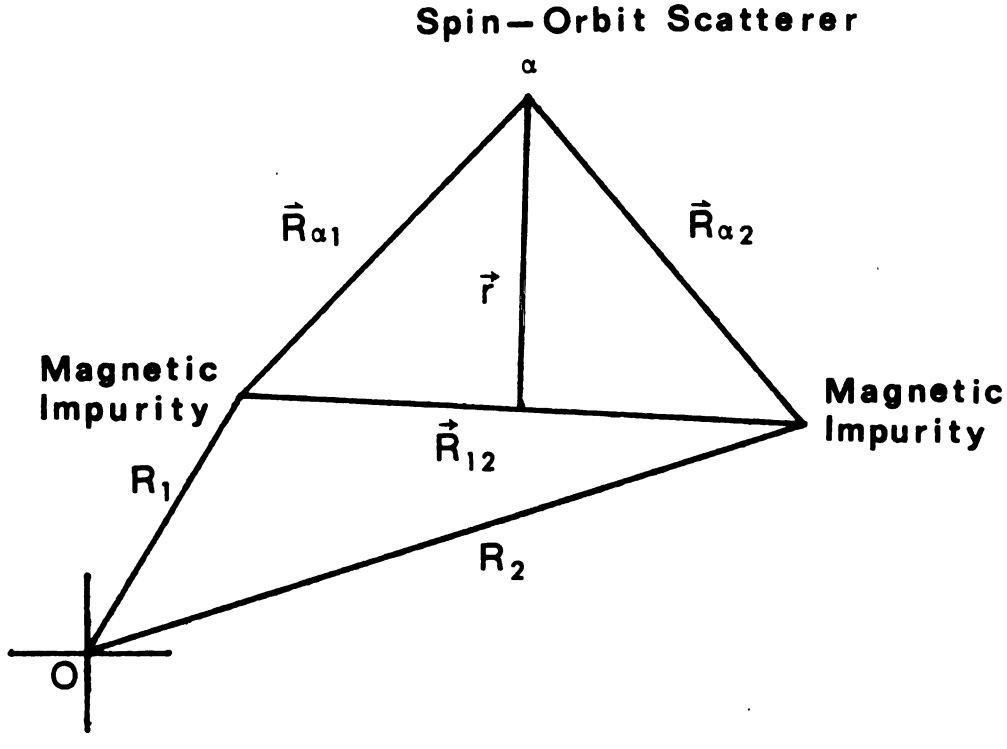

Figure 51. DM interaction vectors.

to be

$$H_{DM} = -V_1 \frac{\sin[k_F(R_1+R_2+R_{12})+(\frac{\pi}{10})Z_d]\ \hat{R}_1\cdot\hat{R}_2(\hat{R}_1 x \hat{R}_2)\cdot(\vec{S}_1 x \vec{S}_2)}{R_1 R_2 R_{12}}$$

with

$$V_1 = \frac{135\pi}{32}\left(\frac{\lambda\Gamma^2}{E_F^2 k_F^3}\right) \sin\left(\frac{\pi Z_d}{10}\right)$$

where E_F is the Fermi energy, Z_d is the number of d electrons and k_F is the Fermi momentum.

The anisotropy stems from the fact that the interaction energy depends on the orientation of $(\vec{S}_1 x \vec{S}_2)$ with respect to the space vector $(\vec{R}_1 x \vec{R}_2)$. Recalling that

$$H(RKKY) = V_o \frac{\cos(2k_F R_{12})}{R_{12}^3}\ \vec{S}_1\cdot\vec{S}_2 \quad \text{where}$$

$$V_o = \frac{9\pi\Gamma^2}{32E_F k_F^3} \quad \text{we see that} \quad \frac{V_1}{V_o} = 15\left(\frac{\lambda}{E_F}\right)\sin\left(\frac{\pi}{10}Z_d\right).$$

Fert and Levy argue that the anisotropy energy per localized spin arising from the DM interactions is $E_{DM}^2/E_{RKKY} = \left(\frac{V_1}{V_o}\right)^2 \frac{V_o S^2}{r^3}$.

H. SHERRINGTON-KIRKPATRICK PHASE DIAGRAM

Since one of the important connections between our data and spin-glass theory is being made through the use of the SK phase diagram, some discussion of its range of applicability to real systems should be made. Several questions can be raised. To what extent is the infinite range aspect of the interaction important? To what extent does the phase diagram depend on the replica mean field solution?

Some light can be shed on the first question through some work of Klein, Schowalter and Shukla.[27] They studied the thermodynamic properties of Ising spin-glasses using non-replica based methods. In particular, one facet of their work included a study of the SK phase diagram within the mean random field approximation as a function of the number of nearest neighbors Z.

Their results are shown in Figure 48. They find that the phase diagram for $Z = 8$ is already very close to the $Z \to \infty$ case. They differ by as little as 10%. The other important point about the work of Klein et al. is the demonstration that in the limit $Z \to \infty$ the mean random field, BPW, and SK solutions give identical magnetic properties. This seems to rule out any special significance to the replica method.

A solution of the spherical model of a spin-glass was obtained[87] using both the replica trick and techniques based on the eigenvalue spectrum of a large random matrix. In the spherical model limit,

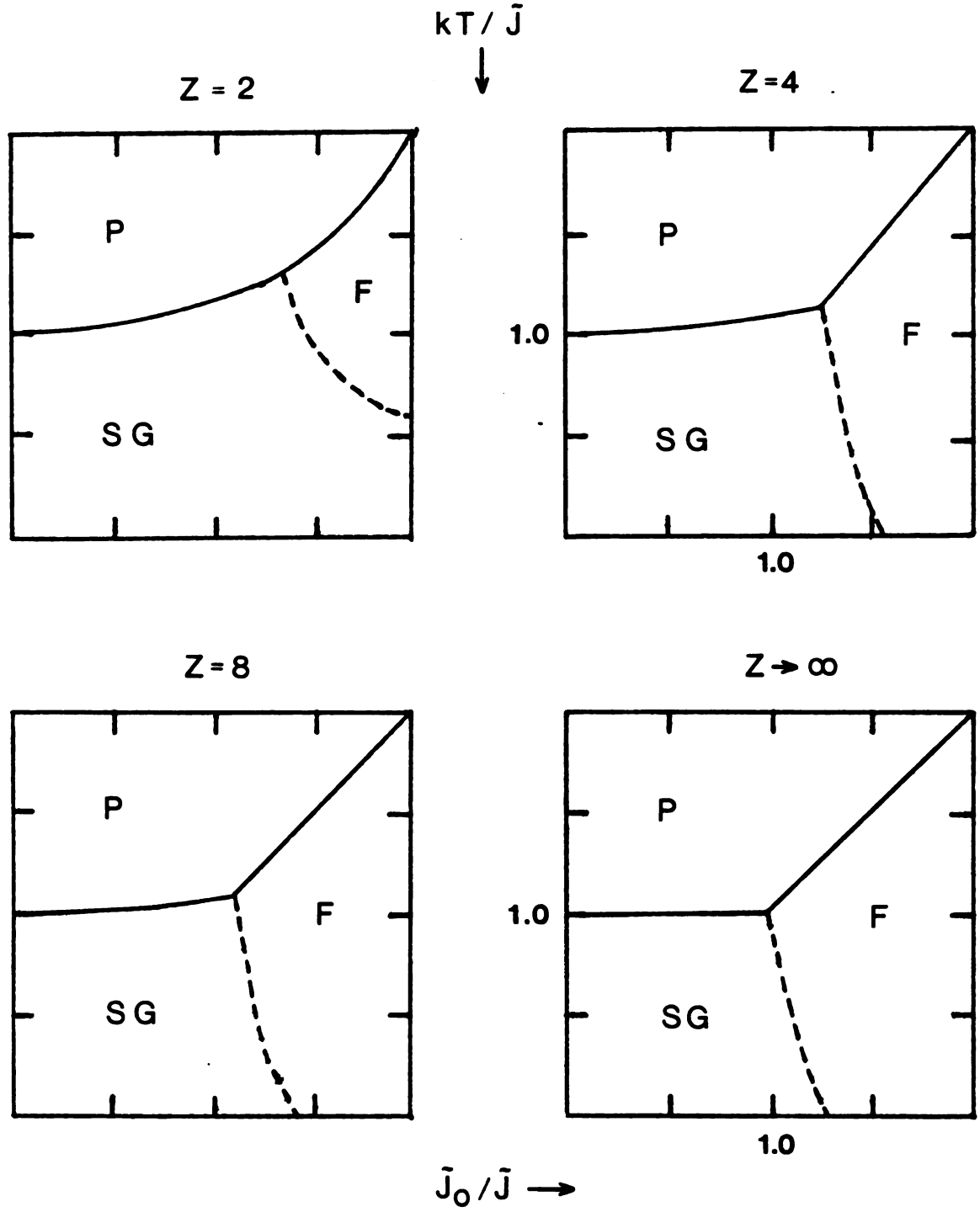

Figure 52. SK phase diagram - BPW approximation.

both methods give the same results. The phase diagram obtained by Kosterlitz et al. is shown in Figure 49 and looks remarkably like the SK phase diagram. Now, the spherical model Hamiltonian has been shown to be equivalent to a standard Heisenberg Hamiltonian where the dimensionality of the spins approaches infinity. This would indicate some insensitivity of the phase diagram to spin dimensionality or quantum spin effects.

The use of Ising model spins in the SK solution should also be addressed. Nature appears to be cooperating with theory in this respect. Even though the manganese impurities are believed to be correctly represented by a Heisenberg Hamiltonian, and the susceptibility is reasonably isotropic, they seem to exhibit Ising-like properties. For example, remanence is an effect which requires the existence of potential barriers in configuration space. Such potential barriers may exist for Ising spins, but are normally not found in normal Heisenberg ferromagnets or antiferromagnets. Also, the linearity of the specific heat with temperature at low temperatures implies Ising spins.

Thereare at least two possible explanations.

(1) There are anisotropic forces which act to reduce the freedom of the spins. The experimental fact that the remanence obeys scaling laws characteristic of a $1/r^3$ interaction suggest that it is due either to the RKKY exchange or dipole interactions. Probably the single-ion cubic anisotropy is most widely accepted.

(2) The Heisenberg system may have potential barriers (or some other form of two level system) which make it appear like an Ising

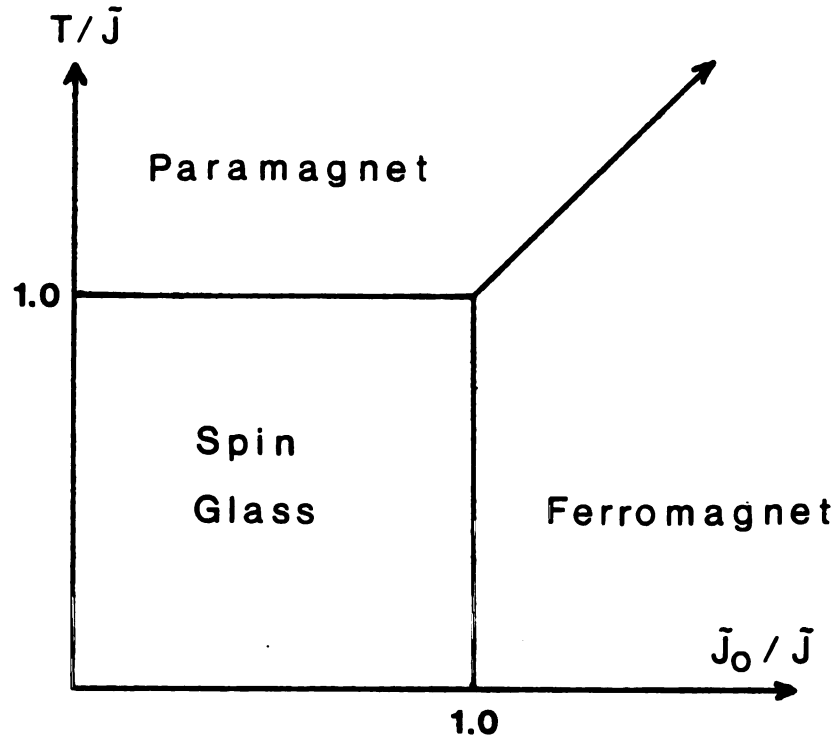

Figure 53. SK phase diagram - spherical model.

spin-glass.[88] One shouldn't concentrate on the energy levels of a spin in a fixed, random, magnetic field. Instead, one should look at the potential energy as a function of the orientation of all the spins. The meta stable states of the spin-glass correspond to local minima in the energy of the spin configurations. Tunnelling between local minima can occur if the separation in configuration space is not too great. Such a system can lead to a linear specific heat.[89]

Another way to approach the problem is to look at the internal field distribution P(H) predicted by Ising and Heisenberg spins and measured by experiment.

Ising model calculations typically give an internal field $P(H=0)\neq 0$. J. Kopp[90] found a similar distribution of internal fields based on nearest neighbor RKKY couplings between spins. The aforementioned agreement between Ising model calculations and observed properties would suggest a non-vanishing P(H=0). However, experiments by Fiory[91] et al. with polarized muons suggest $P(H=0) \rightarrow 0$ which is consistent with a Heisenberg set of spins.[92] So the question is why the Ising model calculations give the correct properties of the system even though the fields are Heisenberg like distributed.[93]

One possible hand-waving argument is the following. In the polarized muon experiment, the internal field distribution is measured relative to a fixed external direction (lab frame) and the randomness of the fields in amplitude and orientation give essentially a Heisenberg-like distribution. Globally there appear to be no constraints and all orientations are equally probable. When the system orders, the local spin at a particular site will not have an

arbitrary direction of orientation. The spin will tend to be frozen in the direction of the local order parameter. The volume element is no longer H^2dH and is closer to an Ising distribution.

There are, however, calculations which predict significant deviations in detail from the SK phase diagram. One of these is a real space rescaling study of spin-glass behavior in three dimensions.(94) They study an S = 1/2 Ising Hamiltonian with nearest neighbor interactions only. The basic idea in rescaling studies is to progressively remove degrees of freedom from the problem and examine the new effective interactions between the remaining spins. In random systems, the interaction probability distribution changes upon rescaling but retains its symmetry. The idea is to follow the distribution through successive rescalings and monitor its width. (We shall characterize the width by J and the mean by J_0). In the paramagnetic phase the interactions decrease under repeated rescalings. This is because the effective interactions give information about correlations at larger and larger distances, but the correlation length is finite in the paramagnetic phase. If the width of the distribution continues to increase (but the mean stays small), one is believed to be in the spin-glass regime. If the exchange distribution has a finite mean ferromagnetic order is possible. In the case of ferromagnetic order the interactions grow under rescaling and the distribution is characterized by $J_0 \to \infty$; $J/J_0 \to 0$. Using these definitions, the phase diagram derived by rescaling techniques is shown in Figure 50. In their model the spin-glass-ferromagnetic transition occurs at a considerably larger value of $\vec{J}_0/\vec{J}$. They predict 1.63 whereas the mean field value is between 1.0 and 1.25. Also, the boundary

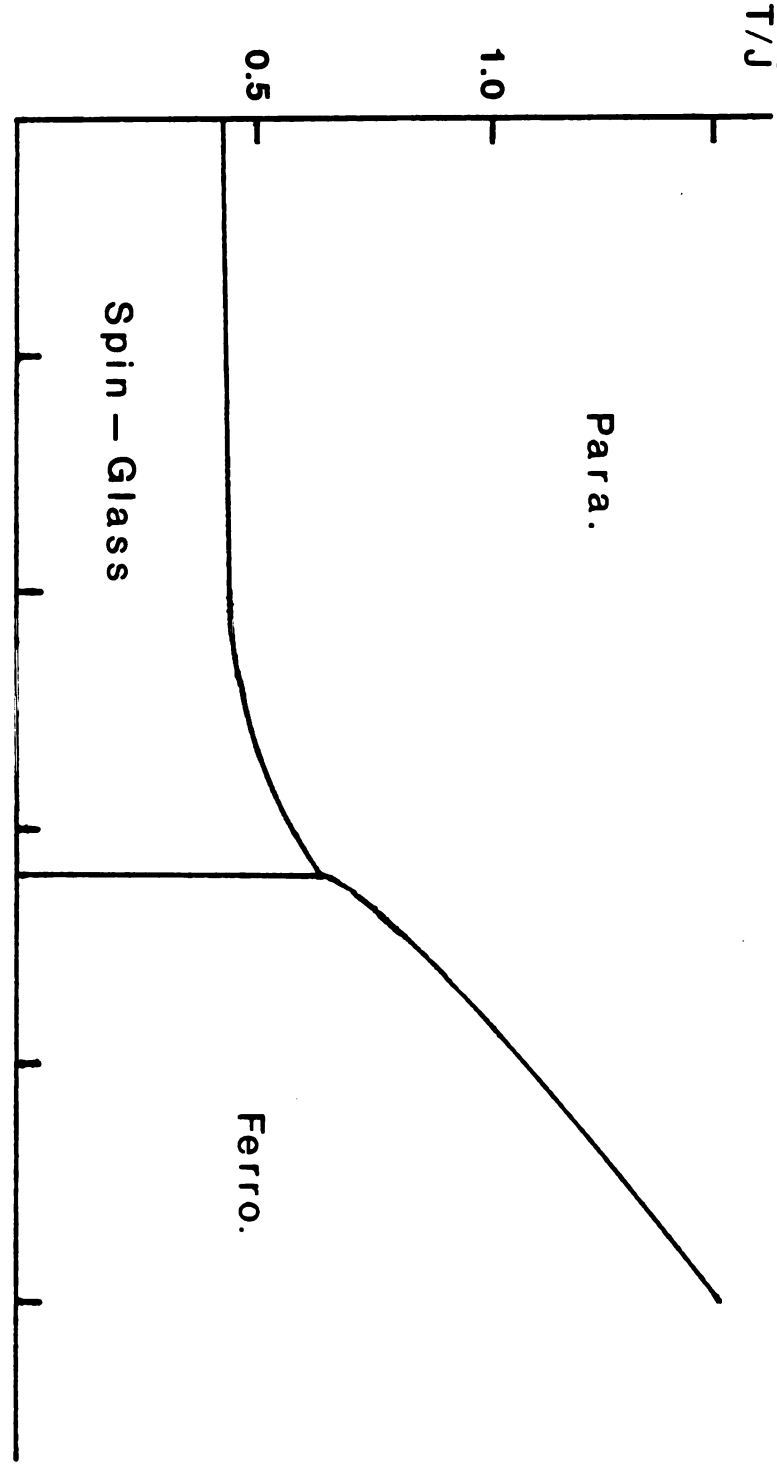

Figure 54. SK phase diagram - rescaling calculation.

between the paramagnetic and spin-glass phases occurs at a lower value of $(T/\vec{J})$. They predict ≤ 0.5 whereas mean field theory predicts 1.0.

I. MEAN RANDOM FIELD

Earlier in the thesis (Section VI.C.2) an attempt was made to extract information from the high temperature magnetic susceptibility of dilute alloys using the mean-random-field approximation.[95] Some of the details leading to equation (6.1) are now presented. The mean random field has as its goal the determination of the temperature dependent probability distribution $P(\bar{H}_o)$ where $\bar{H}_o$ is the random variable corresponding to the effective field at site $\vec{r}_o$. It is given by $\bar{H}_o = \sum_j v_{oj}\bar{\mu}_j$ where $\bar{\mu}_j$ is the thermal average of μ_j. That is,

$$\bar{\mu}_j = \frac{\mathrm{tr}e^{-\beta H}\mu_j}{\mathrm{tr}e^{-\beta H}} ,$$

and v_{oj} is the interaction between the moment at site j and the origin. Once the probability distribution function is known, the thermodynamic function can be obtained by integrating the thermodynamic variables for a single spin in a fixed internal field $\bar{H}$ over all fields. The thermal averages above are for a fixed set of position coordinates. The average over position coordinates must be performed last. The Hamiltonian describing the interaction between the impurities $H = \sum_{i<j} v_{ij}\mu_i\mu_j$ can be rewritten in terms of the effective fields at the sites as

$$H = -\sum_i \mu_i \bar{H}_i = -\sum_i \mu_i \left(\sum_j \bar{\mu}_j\right)$$

where the thermal average uses the effective field

$$\bar{\mu}_j = \frac{\mathrm{tre}^{+\beta\Sigma_i \bar{H}_i \mu_i}\, \mu_j}{\mathrm{tre}^{+\beta\Sigma_i H_i \mu_i}} .$$

For a fixed set of spatial positions, $\bar{H}_o$ and $\bar{H}_j$ are constants. The distribution of the $\bar{H}_o$ arises from the requirement that the positions of the impurities are random variables. The distribution $P(H_o)$ is calculated as follows. Pick an impurity μ_o at site $\vec{r}_o$. Average over an ensemble of systems, each containing N spins, with fixed coordinates, but where each member of the ensemble has a different set of fixed coordinates. This effectively calculates the thermodynamic properties of a single spin in an internal field which is an average over all possible spatial configurations of all spins except that at $\vec{r}_o$.

The essential approximation (which in effect allows one to do the calculation) is that each $P(\bar{H}_j)$ has the same functional form (i.e., $P(\bar{H}_j) = P(\bar{H}o)$).

Also, when calculating the internal field at site 0, all functions of the internal field at sites other than 0 are replaced by their mean values. This allows one to derive an integral equation for $P(\bar{H})$. One finds that

$$P(\bar{H}) = \frac{1}{\pi} \frac{\Delta(\beta)}{\Delta^2(\beta) + \bar{H}^2}$$

where $\Delta(\beta) = \gamma c||\bar{\mu}||$, $\gamma = \frac{2}{3}\pi^2|a|n_o$ and $||\bar{\mu}|| = \int_{-\infty}^{\infty} P(\bar{H})|\bar{\mu}|d\bar{H}$.

This theory is a molecular field theory which is one step better than the Weiss molecular field approximation. Instead of all fields being replaced by a mean field which is the same at all sites, they are replaced by a distribution of fields which is the same at all sites.

J. LARSEN INTEGRAL

$$kT_{sg} = Ac\{\frac{3}{c} I\}^{1/2}$$

where

$$A = \frac{b_s J^2 (2\ell+1)^2}{4E_F}, \quad b_s = \frac{[(2s+1)^4-1]^{1/2}}{12}$$

J = effective s-d coupling constant

ℓ = angular momentum quantum number (for d electrons $\ell = 2$)

s = the magnitude of the spins; and

$$I = \int_1^\infty \frac{dx}{x^4} e^{-rcx} [1 - e^{y^1(1-x^3)}]$$

where

$$r = \frac{4\beta e^2 \rho(T_o)}{a_o h_y} \quad \text{and} \quad y^1 = \frac{y}{1-y}$$

and

ρ = total resistivity at the freezing temperature

$\beta = \sigma/\sigma_{tr}$ (ratio of ordinary cross section/transport cross section) 3.5 to 4 for 3d impurities

e = charge of the electron

a_o = lattice spacing

h = Planck's constant

y = c = impurity concentration

Letting $rc = \omega$,

$$I = \int_1^\infty \frac{e^{-\omega x}}{x^4}\,dx - e^{y^1}\int_1^\infty \frac{e^{-\omega x - y^1 x^3}}{x^4}\,dx = I_1 - e^{y^1} I_2$$

$$I_1 = \frac{e^{-\omega}}{6}(2-\omega+\omega^2) + \frac{\omega^3}{6}\left(0.57722 + \ell n\omega - \omega + \frac{\omega^2}{4} - \frac{\omega^3}{18}\right)$$

$I_2 = \int_0^1 e^{-\omega/x + y^1/x^3}\, x^2 dx$ is integrated using an IMSL library routine called DCADRE (Cautious Adoptive Romberg Extrapolation).

```
Program Temp (Input, Output)
Integer IER
Real DCADRE,F,A,B,AGRR,RERR,ERROR,C
External F
A = 1.0 E-5
B = 1.0
REER = 0.0
AERR = 1.0 E-4
C = DCADRE (F,A,B,AGRR,RERR,ERROR,IER)
Print 10,c
FORMAT (E11.5)
END
REAL FUNCTION F(X)
REAL X,W,YP
W = 6.1553 E-3 (or 4.9096 E-2)
YP = 0.8166 E-2
F = X**2*EXP(-(W/X)-(YP/X**3))
RETURN
End
```

Output C = 0.31630 (or 0.29766)

K. Cu_3AuMn Data

We mention the preliminary results for Cu_3AuMn (1%) data because we have data which suggests that the ordered state alloy has a large spin-glass temperature than the disordered state alloy. This is in direct contrast with Cu_3PtMn and CuPd(17)Mn alloys. Figure 51 shows high temperature χ^{-1} vs T data and Figure 52 shows the χ vs T data used to determine the spin-glass temperatures. However, a word of caution is in order here. It is a difficult task to obtain good quality ordered state samples of Cu_3Au. The magnetic parameters for these samples are:

	DOS	OS
θ	+3.31	+3.82
T_{sg}	5.75	6.2

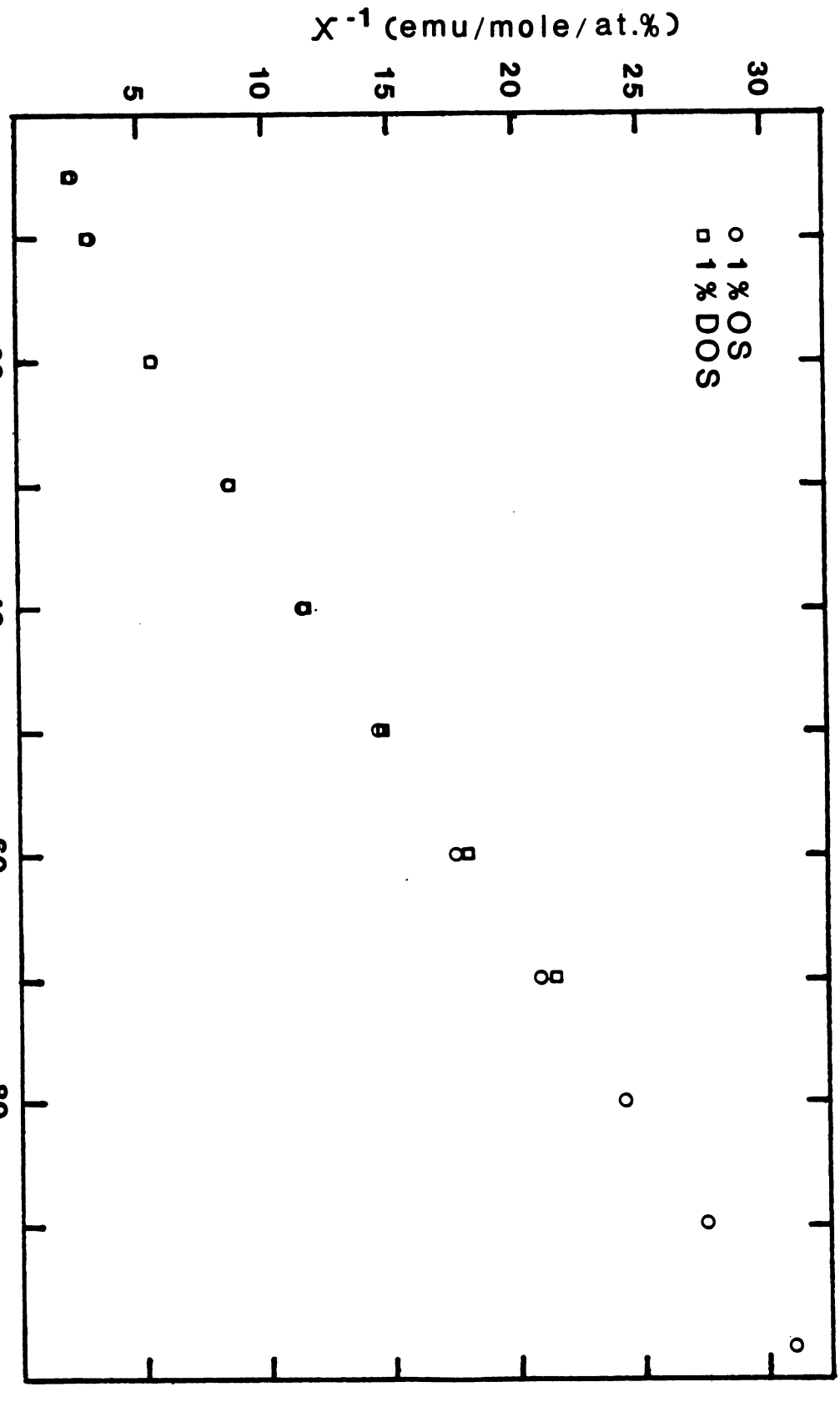

Figure 55. $\underline{Cu_3AuMn}$ (1%) - inverse susceptibility vs temperature - (Squid).

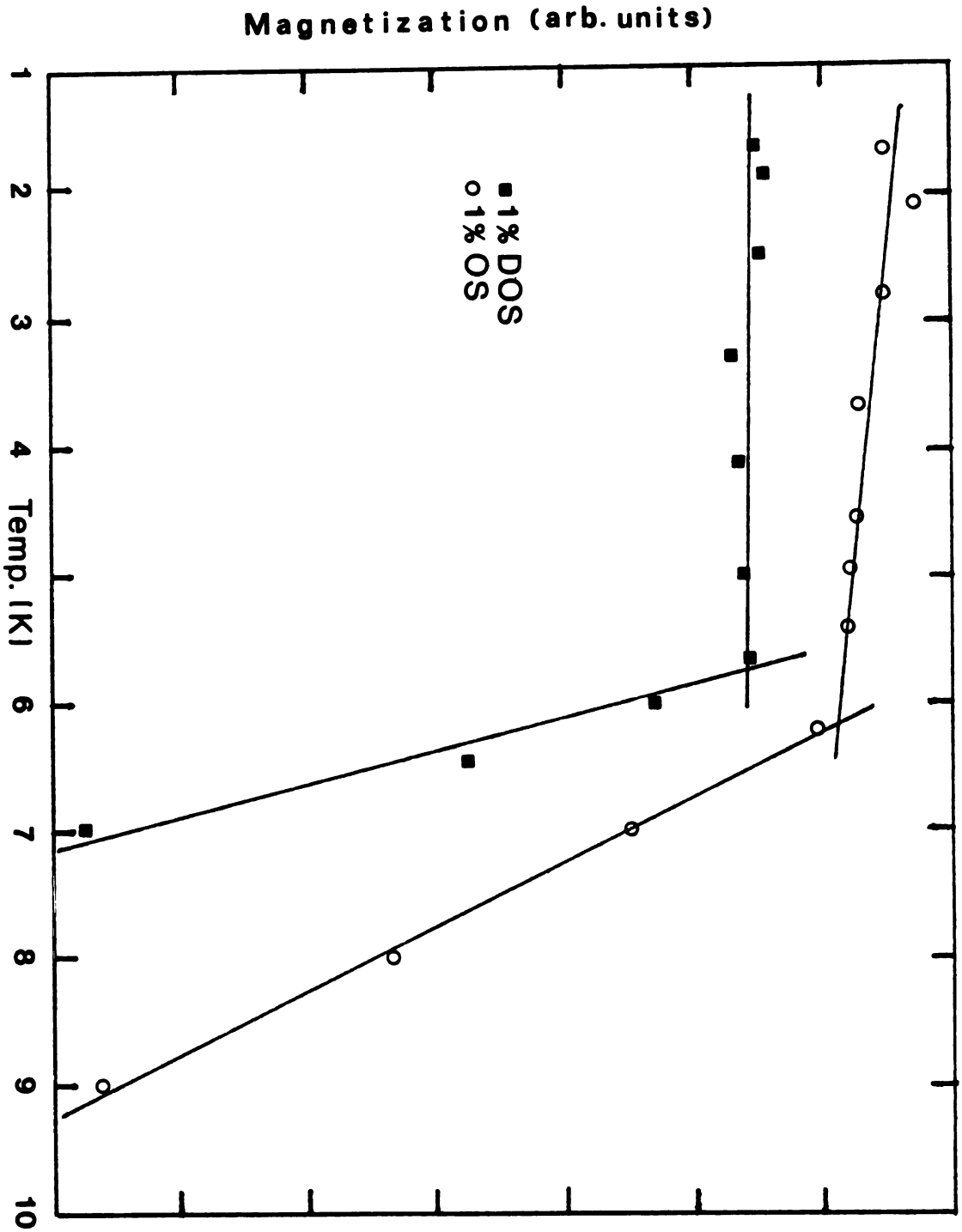

Figure 56. Cu_3AuMn (1%) - susceptibility vs. temperature - (Squid).

LIST OF REFERENCES

LIST OF REFERENCES

1. K. G. Wilson, Reviews of Modern Physics, 47, p. 773 (1975).
2. Physics Today, May 1981, p. 21.
3. P. W. Anderson, Phys. Rev. 86, p. 694 (1952); Phys. Rev. 130, p. 439 (1963).
4. L. Onsager, Phys. Rev. 65, p. 117 (1944).
5. J. Kogut, Reviews of Modern Physics, 51, p. 659 (1979).
6. C. A. M. Mulder, Phys. Rev. B; 23, p. 1384 (1981).
7. R. E. Behringer, J. of Chem. Phys. 29, p. 537 (1958).
8. M. M. Kreitman and F. Hanaker, J. of Chem. Physics, 45, p. 2396 (1966).
9. T. W. McDaniel, Ph.D. Thesis, Michigan State University (1973) unpublished.
10. F. W. Jones and C. Sykes, J. Institute of Metals, 65, p. 419 (1939).
11. W. B. Pearson, Handbook of Lattice Spacings and Structures of Metals, Pergammon Press, International Series of Monographs on Metal Physics and Physical Metallurgy, Vol. 4 (1958).
12. T. W. McDaniel and C. L. Foiles, Solid State Comm., 14, p. 835 (1974).
13. W. C. Kok and P. W. Anderson, Phil. Mag. 24, p. 1141 (1971).
14. P. G. DeGennes, Phys. Rad. 23, p. 630 (1962).
15. R. Brout, Phys. Rev., 115, p. 824 (1959); 118, p. 1009 (1960).
16. G. Horwitz and H. B. Callen, Phys. Rev. 124, p. 1757 (1961).
17. F. Englert, Phys. Rev. 129, p. 567 (1963).
18. M. W. Klein and R. Brout, Phys. Rev. 132, p. 2412 (1963).
19. R. G. Palmer and C. M. Pond, J. Phys. F. Metal Phys. 9, p. 1451 (1979).

20. M. W. Klein, Phys. Rev. 188, p. 933 (1969).

21. S. F. Edwards, P. W. Anderson, J. Phys. F. 5, p. 965 (1975), 6, p. 1927 (1976).

22. S. Kirkpatrick, D. Sherrington, Phys. Rev. B, 17, p. 4384 (1978).

23. D. J. Thouless, P. W. Anderson, R. G. Palmer, Phil. Mag. 35, p. 593 (1977).

24. J. L. VanHemmen and R. G. Palmer, J. Phys. A, 12, p. 563 (1979).

25. A. Blandin, M. Gabay, T. Barel, J. Phys. C, 13, p. 403 (1980).

26. H. J. Sommers, Z. Physik B, 31, p. 301 (1978); 33, p. 173 (1979).

27. M. W. Klein, L. J. Schowalter, P. Shukla, Phys. Rev. B, 19, p. 1492 (1979).

28. J. R. L. deAlmeida, D. J. Thouless, J. Phys. A, 11, p. 983 (1978).

29. A. J. Bray and M. A. Moore, J. Phys. C, 12, p. 79 (1979); 13, p. 419 (1980).

30. G. Parisi, Phys. Rev. Lett. 43, p. 1754 (1979).

31. A. F. J. Morgownik and J. A. Mydosh, Phys. Rev. B (1981).

32. A. I. Larkin and D. E. Khmelnitskii, Soviet Physics JETP 31, p. 958 (1970).

33. A. I. Larkin, et al., Soviet Physics JETP, 33, p. 458 (1971).

34. B. Southern, J. Phys. C, Solid State Phys. 8, (1975).

35. K. Matho, Physica 86-88B, p. 854 (1977).

36. A. Arrot and J. E. Goldman, Rev. of Sci. Inst., 28, p. 99 (1957).

37. R. Reeves, J. of Phys. E, 5 (1972).

38. D. O. Smith, Rev. of Sci. Instruments, 27, p. 261 (1956).

39. C. W. Fairall, Ph.D. Thesis, Michigan State University, unpublished.

40. S. Nagata, P. H. Keesom, and H. R. Harrison, Phys. Rev. B19, p. 1633 (1979).

41. R. P. Giffard, R. A. Webb, and J. C. Wheatley, J. of Low Temp. Physics, 6, p. 533 (1972).

42. S. Foner, Rev. Sci. Inst., 30, p. 548 (1959).

43. R. P. Reed, R. P. Mikesell, Adv. in Cryogenic Engineering, 4, p. 84 (1960).

44. D. C. Larbalestier and H. W. King, Cryogenics, p. 160, March 1973.

45. E. M. Forgan, Cryogenics, April 1974.

46. C. L. Foiles, T. W. McDaniel, Rev. Sci. Inst. 45, p. 756 (1974).

47. J. E. Noakes et al., Rev. of Sci. Inst. 39, p. 1436 (1968).

48. C. L. Foiles, AIP Conference Proceedings, No. 34, p. 358 (1976).

49. C. L. Foiles, Phase Transitions, Vol. 1, p. 351, Gordon and Breach (1980).

50. D. E. Larch, Thesis, Michigan State University (1978), unpublished.

51. R. W. Walstedt and L. R. Walker, Phys. Rev. Lett., 47, p. 1624 (1981).

52. R. Harris and D. Zobin, AIP Conference Proc., 29, p. 156.

53. P. W. Anderson, J. Appl. Physics, 49, p. 1599 (1978).

54. C. L. Foiles, AIP Conf. Proceedings, No. 34, p. 17; Thermal Conductivity (Eds. P. G. Klemens, T. K. Chu) 14, p. 97 (1976).

55. G. Borehius, C. H. Johnsson, J. O. Linde, Ann. Physik 86, p. 291 (1928).

56. H. P. Myers and R. Westin, Phil. Mag. 8, p. 669 (1963).

57. J. Owen, M. Browne, V. Arp, A. F. Kip, J. Phys. Chem. Solids, 2, p. 85 (1957).

58. L. Andersson et al., Solid State Comm. 7, p. 319 (1969).

59. D. Sherrington and S. Kirkpatrick, Phys. Rev. Lett., 35, p. 1792 (1975).

60. S. Geschwind et al., J. Phys. (Paris) 41, C5-105 (1980).

61. B. Southern, J. Phys. C, 8, p. L213 (1975).

62. D. Sherrington and B. W. Southern, J. Phys. F, 5, p. L49 (1975).

63. C. Held and M. Klein, Phys. Rev. Lett., 35, p. 1783 (1975).

64. D. C. Mattis, The Theory of Magnetism, p. 275 Harper & Row (1965).

65. A. Freudenhammer, Phys. Stat. Sol. B, 86, p. 579 (1978).

66. I. Y. Dakhtyar, et al., Soviet Physics Doklady 7, p. 1135 (1963).

67. P. F. deChatel, J. Mag. and Mag. Mat. 23, p. 28 (1981).

68. C. M. Srivastava, et al., J. Mag. and Mag. Mat. 25, p. 147 (1981).

69. N. F. Mott and H. Jones, The Theory of the Properties of Metals and Alloys, Dover (1936).

70. S. Ogawa, et al., J. Phys. Soc. Japan, 34, p. 384 (1973).

71. H. Sato and R. Toth, Phys. Rev. 124, p. 1833 (1961), Phys. Rev. 127, p. 469 (1962).

72. J. C. Slater, Phys. Rev. 84, p. 179 (1951).

73. J. F. Nicholos, Proc. Phys. Soc. (London) A66, p. 201 (1953).

74. C. A. Domenicali, Rev. of Sci. Instr., 21, p. 327 (1950).

75. K. Matho, J. of Low Temp. Phys. 35, p. 165 (1979).

76. E. E. Bragg and M. S. Seehra, J. of Phys. E, 9, p. 216 (1976).

77. G. J. Bowden, J. of Phys. E, 5, p. 1115 (1972).

78. C. N. Guy and W. Howarth, J. of Phys. C, 11, p. 1635 (1978).

79. J. Mallinson, J. of Appl. Phys. 37, p. 2514 (1966).

80. R. Reeves and J. Reeves, Proc. IEE, 118, p. 1307 (1971).

81. Ralph Morrison, Grounding and Shielding Techniques in Instrumentation, John Wiley and Sons (1977).

82. P. Monod, J. J. Prejean, B. Tissier, J. of Appl. Phys., 50, p. 7324 (1979).

83. J. J. Prejean, M. J. Joliclerc, P. Monod, J. Physique, 41, p. 427 (1980).

84. T. Nagamiya, R. Kubo, K. Yosida, Phil. Mag. Supp. 4, 1 (1955).

85. D. A. Smith, J. Mag. and Mag. Mat., 1, p. 214 (1976).

86. A. Fert, P. M. Levy, Phys. Rev. Lett., 44, p. 1538 (1980).

87. J. M. Kosterlitz, D. J. Thouless, R. C. Jones, Phys. Rev. Lett. 36, p. 1217 (1976).

88. P. W. Anderson et al., Phil. Mag., 25, p. 1 (1972).

89. P. W. Anderson, Amorphous Magnetism, eds. Hopper and deGraaf, p. 1 (1972).

90. J. Kopp, J. Phys. F, 3, p. 1994 (1973).

91. D. E. Murnick, et al., Phys. Rev. Lett., 36, p. 100 (1974).

92. R. G. Palmer and C. M. Pond, J. Phys. F, 9, p. 1451 (1979).

93. B. Fischer and M. W. Klein, Phys. Rev. B, 14, p. 5018 (1976).

94. B. W. Southern, A. P. Young, J. Phys. C, 10, p. 2179 (1977).

95. I. Souletie and R. Tournier, J. Low Temp. Phys. 1, p. 95 (1969).

96. U. Larsen, Solid State Comm., 22, p. 311 (1977).

97. M. W. Klein and L. Shen, Phys. Rev. B, 5, p. 1174 (1972).

98. R. A. Klemm, J. Phys. C, 12, p. L735 (1979).